

Developing a Generic Software-Defined Radar Transmitter using GNU Radio

A thesis submitted in partial fulfilment of the requirements for the degree of
Master of Sciences (Defence Signal Information Processing)

by

Michael Maxwell Hill

November 2012

The University of Adelaide
School of Electrical and Electronic Engineering

Declaration

This work contains no material which has been accepted for the award of any other degree or diploma in any university or other tertiary institution and to the best of my knowledge and belief, contains no material previously published or written by another person, except where due reference has been made in the text.

I give consent to this copy of my thesis, when deposited in the University Library, being available for loan and photocopying.

<Author: Michael Hill>



CEI Minor Thesis Clearance Form

Instructions

It is a requirement that employees seek approval from DSTO prior to commencing their Minor Thesis: this process also reiterates that the topic selected and thesis content must be unclassified. Employees should also subsequently seek approval from DSTO to submit their CEI Minor Thesis for examination by their university. Please complete the employee declaration then attach the form to a draft copy of your thesis and forward through your DSTO thesis (or workplace) supervisor to your Chief of Division. A copy of the completed form must be attached to all copies of the thesis that are submitted for assessment, or to the university and DSTO libraries.

Employee Declaration

Name: Michael Hill Division: EWRD Date: 2/11/2012

Thesis Title:
 Developing a Generic Software-Defined Radar Transmitter using GNU Radio

CEI Stream: SIP Award Title: Master of Sciences (DSIP)

Conferring University: University of Adelaide

I acknowledge that ownership of all IP developed as part of my CEI Minor Thesis vests in the Commonwealth and cannot be transferred without prior permission from DSTO.

Signature:

Declaration by DSTO Thesis (or Workplace) Supervisor

This document is suitable to be released for examination and into the public domain. It contains no security classified material, encumbered background IP, third party proprietary information or IP that is expected to have a commercial application.

Comments:

Signature Name: Dr. Bevan Bates Division: EWRD Date: 2/11/12

Approval by DSTO Chief of Division

I approve the release of this thesis and confirm that security, IP and industry considerations have been addressed. It may be submitted for examination by the university and released into the public domain.

Comments:

Signature: Name: Position: *Chief* EWRD Date: 8/11/12

Abstract

Research into the development of software defined radars (SDRs) often combines the GNU Radio software toolkit, with the Universal Software Radio Peripheral (USRP) hardware platform.

Studies have already demonstrated that these tools can be combined to develop and implement versatile, low-cost, SDR systems. These studies focus on the question as to whether or not a GNU Radio and USRP based SDR can address a specific set of requirements for a particular radar application; but do not explore the characteristic behaviour of the technology.

Understanding the characteristic behaviour of this technology, more specifically its limitations and accuracy, is critical to radar designers considering using these tools to achieve SDR design requirements.

This thesis examines how effectively GNU Radio and the USRP can be combined to create a software-defined radar transmitter. A SDR transmitter has been developed using these tools as a subject for experimentation and implemented to produce a set of generic radar waveforms at a frequency of 5.8GHz. This set consists of continuous wave, 1 μ s pulsed waveforms and frequency modulated continuous waveforms with sweep ranges from 0.5 to 25MHz.

Characterisation tests thoroughly investigated and verified limitations of the USRP performance, and identified many others that were unknown at the time or did not match expected values. Waveform verification tests demonstrated that these tools can be used to accurately transmit CW, pulsed and frequency modulated waveforms with characteristics similar to those in this study.

GNU Radio and the USRP can be combined to effectively produce a generic radar transmitter, however some imperfections such as intermodulation products and poor local oscillator suppression may be unacceptable for some radar transmission applications.

Acknowledgements

I would like to express my gratitude to all whose support has made this thesis possible. Firstly, thanks to my supervisors Dr. Said Al-Sarawi and Dr. Bevan Bates for all their guidance and input over the course of the year. Thanks to Brian Reid for arranging funding to make this project possible. To the staff of Electronic Warfare & Radar Division (EWRD) who allowed me to borrow their equipment, lab space, and gave up their time to assist with my queries; particularly Dr. Rohit Naik, Marcus Varcoe and Chris Pitcher I owe thanks to you all for your help and support!

Finally, thanks goes to Aleksandra Golat for her love and patience throughout this year, and to the 'Midnight Study Sessions at the Hub' group who provided motivation and energy at hours where there was none.

Contents

1. INTRODUCTION.....	14
1.1 Thesis Problem Statement.....	14
1.2 Thesis Outline	15
1.3 Background	16
1.3.1 Software Defined Radio.....	16
1.3.2 GNU Radio	18
1.3.3 Introduction to the Universal Software Radio Peripheral	19
1.4 Literature Review.....	20
1.4.1 Previous Work	20
1.4.2 Existing Documentation on System Behaviour.....	20
1.4.3 Primary Factors Limiting USRP Radar Performance	21
2. TRANSMITTER DESIGN.....	23
2.1 Requirements.....	23
2.2 Hardware Selection	24
2.2.1 USRP	24
2.2.2 RF Daughterboard.....	26
2.2.3 GPSDO Reference Clock.....	27
2.2.4 GPS Antenna	27
2.2.5 Host Computer	27
2.3 Software Selection	28
2.3.1 Operating System.....	28
2.3.2 GNU Radio	28
2.3.3 UHD Firmware	28
2.4 System Description.....	30
2.4.1 Transmit Signal Path.....	30
2.4.2 Receive Signal Path	31
2.5 Configurable Variables.....	32
2.5.1 Sample Size.....	32
2.5.2 Sampling Rate	32
2.5.3 Number of Samples per Period	33
2.5.4 Amplitude Variable.....	33
2.5.5 Gain Request Variable	33
2.5.6 Local Oscillator Tuning	34
2.5.7 Baseband Filter.....	34
2.6 Design Summary.....	35
3. EXPERIMENT METHODOLOGY.....	36
3.1 Test Setup.....	37
3.1.1 Spectrum Analyser	38
3.1.2 Oscilloscope.....	38
3.1.3 Signal Analyser	39
3.2 Characterisation Test Methodology	40
3.2.1 Test Waveform 1: Single Tone Waveform	41

3.2.2	Test Waveform 2: Two Tone Waveform	43
3.2.3	Test Waveform 3: Wideband Gaussian Noise	45
3.3	Waveform Verification Test Methodology	47
3.3.1	Radar Waveform 1: Continuous Waveform	49
3.3.2	Radar Waveform 2: Pulsed Waveform.....	51
3.3.3	Radar Waveform 3: Frequency Modulated Continuous Waveform	53
4.	EXPERIMENTATION & RESULTS	56
4.1	Characterisation Testing.....	56
4.1.1	Sampling Rate Testing	56
4.1.2	Modulation Bandwidth Limit Testing.....	57
4.1.3	Frequency Limit Testing.....	60
4.1.4	Effects of the Amplitude Variable.....	61
4.1.5	Effects of the Gain Request Variable.....	69
4.1.6	Power versus Gain Request and Amplitude Variables.....	75
4.1.7	Power versus RF Frequency.....	77
4.1.8	Effects of the Baseband Filter	79
4.1.9	Third Order Output Intercept Point	85
4.1.10	Local Oscillator Suppression	91
4.1.11	Phase Noise Measurements	92
4.2	Waveform Verification Testing.....	97
4.2.1	Continuous Waveform	98
4.2.2	Pulsed Waveform	101
4.2.3	Frequency Modulated Continuous Waveform	106
4.3	Experimentation Summary	113
5.	CONCLUSIONS.....	117
6.	APPENDIX	118
6.1	Appendix A - Matlab FFT Function from GNU Radio	118
6.2	Appendix B - Tabulated Phase Noise Measurements.....	119
7.	REFERENCES	122

List of Figures

Figure 1: Block diagram of a generic software defined radio system.....	17
Figure 2: Screenshot of GNU Radio Companion	18
Figure 3: USRP Networked Series N210 Model.....	19
Figure 4: Block diagram showing the main functions of a typical USRP	20
Figure 5: Block diagram of the USRP N210 with XCVR2450 daughterboard, modified from a block diagram of the functionally similar National Instruments USRP-2921 [30].....	29
Figure 6: Block diagram of a digital up converter from the AD9777 module in the transmit path. Selectable filters offer interpolation factors of 2, 4 or 8 [34].	30
Figure 7: Block diagram of a digital down converter from the ADS62P4X module in the transmit path. Selectable filters offer decimation factors of 2, 4 or 8, and may function as low, high or pass band filters.....	32
Figure 8: GNU Radio Companion GUI windows highlighting some of the key variables .	34
Figure 9: System block diagram of experiment test setup.....	37
Figure 10: Laboratory experiment test setup.....	37
Figure 11: GRC flow graph for generating the single tone waveform.....	42
Figure 12: Diagram of the two tone test waveform showing frequencies F1, F2 and intermodulation products IM1 and IM2 at the frequencies indicated.	43
Figure 13: GRC flow graph for generating the two tone waveform	44
Figure 14: GRC flow graph for generating wideband Gaussian noise	46
Figure 15: Data collected and compared in this study	48
Figure 16: GRC flow graph for generating the continuous waveform	50
Figure 17: GRC flow graph for generating the pulsed waveform.....	52
Figure 18: Triangle signal output used to control the FMCW behaviour	53
Figure 19: GRC flow graph for generating the FMCWs	55
Figure 20: GNU Radio response to an unachievable sampling rate	56
Figure 21: Frequency response for a single tone waveform with a 7.5 MHz baseband frequency	58
Figure 22: Frequency response for a single tone waveform with a 12.5 MHz baseband frequency	59
Figure 23: Frequency response for a single tone waveform with a 15 MHz baseband frequency	59
Figure 24: Frequency response for a single tone waveform modulated above 6000 MHz..	60
Figure 25: Single tone waveform response to various amplitude values (low band)	63
Figure 26: Single tone waveform response to various amplitude values (high band).....	64
Figure 27: Two tone waveform response to various amplitude values (low band)	67
Figure 28: Two tone waveform response to various amplitude values (high band)	68
Figure 29: Expected gain response for the two individual gain sources in the XCVR2450 .	69
Figure 30: Stepped gain test results for a single tone waveform (low band).....	71
Figure 31: Stepped gain test results for a single tone waveform (high band)	71
Figure 32: Single tone waveform response to various gain values (low band).....	73
Figure 33: Single tone waveform response to various gain values (high band).....	74
Figure 34: Gain and amplitude test results for a single tone waveform (low band)	76
Figure 35: Gain and amplitude test results for a single tone waveform (high band)	76

Figure 36: Transmit power plots for the low band (left) and high band (right) from the MAX2829 Transceiver datasheet [39]	77
Figure 37: Peak power vs. frequency test results for a single tone waveform (low band) ..	78
Figure 38: Peak power vs. frequency test results for a single tone waveform (high band) .	79
Figure 39: Baseband frequency offset test results – Response of unfiltered single tone waveforms (low band).....	81
Figure 40: Baseband frequency offset test results – Response of filtered and unfiltered single tone waveforms (low band).....	81
Figure 41: Baseband frequency offset test results - Comparison of low band and high band single tone responses for offsets up to 25 MHz	83
Figure 42: Baseband frequency offset test results – Comparison of low band and high band responses for offsets over 25 MHz	83
Figure 43: Baseband frequency offset test results – Response of wideband Gaussian noise (low band).....	84
Figure 44: Representation of the OIP3 [40]	86
Figure 45: OIP3 results using the graphical method at 2450 MHz.....	87
Figure 46: OIP3 results using the graphical method at 5400 MHz.....	87
Figure 47: OIP3 results using the rapid calculation method for selected low band frequencies.....	89
Figure 48: OIP3 results using the rapid calculation method for selected high band frequencies.....	89
Figure 49: Phase noise plots from the MAX2829 Transceiver datasheet [34]	92
Figure 50: Phase noise plot for a single tone at 2450 MHz (Gain = 0 dB, Amplitude = 0.25)	93
Figure 51: Phase noise plot for a single tone at 5400MHz (Gain = 0 dB, Amplitude = 0.25)	94
Figure 52: Phase noise plot for a single tone at 5400 MHz (Gain = 35 dB, Amplitude = 0.25)	94
Figure 53: Phase noise plot for a single tone at 5400 MHz (Gain = 0 dB, Amplitude = 1) ...	95
Figure 54: Phase noise measurements at various low band frequencies.....	96
Figure 55: Phase noise measurements at various high band frequencies	96
Figure 56: Time scope plot of the baseband CW input to the USRP.....	98
Figure 57: Modelled normalised power spectrum of the baseband CW input to the USRP	98
Figure 58: Measured power spectrum of the CW output from the USRP.....	99
Figure 59: Measured time scope plot of the non-interpolated CW output from the USRP (500 ps/div, 5 ns span)	100
Figure 60: Measured time scope plot of the interpolated CW output from the USRP (500 ps/div, 5 ns span).....	100
Figure 61: Time scope plot of the baseband pulsed waveform input to the USRP.....	101
Figure 62: Modelled normalised power spectrum of the baseband pulsed waveform input to the USRP.....	102
Figure 63: Modelled normalised power spectrum (close up view) of the baseband pulsed waveform input to the USRP.....	102
Figure 64: Measured power spectrum of the pulsed waveform output from the USRP ...	103
Figure 65: Measured power spectrum of the pulsed waveform output from the USRP ...	104
Figure 66: Measured time scope plot of the non-interpolated pulsed waveform output from the USRP (5 μ s/div, 50 μ s span).....	105

Figure 67: Measured time scope plot of the non-interpolated pulsed waveform output from the USRP (200 ns/div, 2 μ s span)	105
Figure 68: Time scope plot of the 2 MHz sweep FMCW input to the USRP	107
Figure 69: Time scope plot of the 5 MHz sweep FMCW input to the USRP	107
Figure 70: Time scope plot of the 10 MHz sweep FMCW input to the USRP	107
Figure 71: Measured time scope plot of the 2 MHz sweep FMCW output from the USRP (2 μ s/div, 20 μ s span).....	108
Figure 72: Measured time scope plot of the 5 MHz sweep FMCW output from the USRP (2 ns/div, 20 μ s span).....	108
Figure 73: Measured time scope plot of the 10 MHz sweep FMCW output from the USRP (2 ns/div, 20 μ s span)	108
Figure 74: Modelled normalised power spectrum of the 2 MHz sweep FMCW input to the USRP.....	110
Figure 75: Modelled normalised power spectrum of the 5 MHz sweep FMCW input to the USRP.....	110
Figure 76: Modelled normalised power spectrum of the 10 MHz sweep FMCW input to the USRP.....	110
Figure 77: Measured power spectrum of the FMCW output from the USRP, for a range of Triangular FM sweeps at 20 MSps.....	111
Figure 78: Measured power spectrum of the FMCW output from the USRP, for a range of Triangular FM sweeps at 50 MSps.....	112

List of Tables

Table 1	Acronyms Table	13
Table 2	USRP models currently available from Ettus Research [1]	25
Table 3	RF daughterboard models currently available from Ettus Research [29]	26
Table 4	Characteristics of a range of Low Cost GPS Antennas	27
Table 5	Summary of selected software components	28
Table 6	Spectrum analyser measurement resolution settings	38
Table 7	Oscilloscope acquisition settings	38
Table 8	Signal analyser acquisition settings	39
Table 9	Default parameters for the single tone waveform	41
Table 10	Default parameters for the two tone waveform	43
Table 11	Default parameters for the wideband Gaussian noise signal	45
Table 12	Parameters for the continuous waveform	49
Table 13	Parameters for the pulsed waveform	51
Table 14	Key parameters for applying various frequency modulation values	54
Table 15	Parameters for FMCW A	54
Table 16	Parameters for FMCW B	54
Table 17	Summary of results for sampling rates testing	57
Table 18	Amplitude reduction test results for a single tone waveform (low band)	62
Table 19	Amplitude reduction test results for a single tone waveform (high band)	62
Table 20	Amplitude reduction test results for a two tone waveform (low band)	66
Table 21	Amplitude reduction test results for a two tone waveform (high band)	66
Table 22	Characteristics of unfiltered power curves for various modulation bandwidths 84	
Table 23	LO and Image Suppression Summary for a Single Tone Test	91
Table 24	Summary of characterisation test findings (Part A)	114
Table 25	Summary of characterisation test findings (Part B)	115
Table 26	Summary of waveform verification test findings	116
Table 27	Summary of general test findings	116
Table 28	Single tone waveform response to various amplitude values with gain values of 0 and 10dB (high band)	119
Table 29	Single tone waveform response to various amplitude values with gain values of 20 and 35dB (high band)	120
Table 30	Single tone response to stepped changes in the RF signal frequency across the low and high bands	121

Table 1 Acronyms Table

Acronym	Term
ADC	Analogue-to-Digital Converter
API	Application Programming Interface
BB	Baseband
COTS	Commercial-Off-The-Shelf
CW	Continuous Wave
DAC	Digital-to-Analogue Converter
DDC	Digital Down Converter
DSP	Digital Signal Processor
DSTO	Defence Science and Technology Organisation
DUC	Digital Up Converter
EWRD	Electronic Warfare and Radar Division
FAQ	Frequency Asked Question
FFT	Fast Fourier Transform
FIFO	First-In, First Out
FMCW	Frequency Modulated Continuous Waveform
FPGA	Field Programmable Gate Array
GPL	General Public License
GPS	Global Positioning System
GPSDO	GPS Disciplined Oscillator
GRC	GNU Radio Companion
GUI	Graphical User Interface
IC	Integrated Circuit
IF	Intermediate Frequency
IM	Inter-modulation
LO	Local Oscillator
MBW	Modulation Bandwidth
MIMO	Multiple-Input Multiple-Output
MMIC	Monolithic Microwave Integrated Circuit
NCO	Numerically Controlled Oscillator
OIP3	Third Order Output Intercept Point
OS	Operating System
PC	Personal Computer
PLL	Phase Locked Loop
PPM	Parts per million
PRF	Pulse Repetition Frequency
PRI	Pulse Repetition Interval
RBW	Resolution Bandwidth
RF	Radio Frequency
SDR	Software-Defined Radar
SFDR	Spurious Free Dynamic Range
SNR	Signal to Noise Ratio
UHD	'Universal Software Radio Peripheral' Hardware Driver
USRPN	Universal Software Radio Peripheral
VBW	Video Bandwidth
VCO	Voltage Controlled Oscillator
VGA	Voltage Gain Amplifier

1. Introduction

1.1 Thesis Problem Statement

Software defined radars (SDRs) are an attractive concept since they enable radar systems with highly flexible operating parameters, that can be reconfigured for different purposes and that can be produced at lower costs than traditional radar systems.

Research into the development of software defined radars often combines the GNU Radio software toolkit, with the Universal Software Radio Peripheral (USRP) hardware platform [1].

Studies have already demonstrated that these tools can be combined to develop and implement versatile, low-cost, software defined radar systems [2-7]. These studies focus on the question as to whether or not a GNU Radio and USRP based SDR can address a specific set of requirements for a particular radar application, but do not explore the characteristic behaviour of the technology.

The purpose of this thesis is to determine how effectively GNU Radio and the USRP can be combined to create a software-defined radar transmitter. This will be achieved by developing a SDR transmitter, examining its characteristic behaviour to identify performance limitations, and verifying the accuracy of output waveforms.

A set of generic waveforms are defined in this study. The accuracy with which the SDR can produce these waveforms will serve as the measure of how effectively GNU Radio and the USRP can be combined to create a SDR transmitter.

1.2 Thesis Outline

The thesis problem was addressed by first combining GNU Radio and the USRP to implement a software-defined radar transmitter that can produce basic test waveforms. Characterisation tests were then conducted to determine the performance limitations of the system. More specifically, to understand exactly 'what' is being transmitted from the device and under what operating conditions the transmitted output starts to differ from what the radar designer is expecting.

Next a set of target radar waveforms with signal parameters representative of common radar signals was defined. These target waveforms were then produced using the USRP transmitter, which were then measured and assessed to determine the accuracy of the output waveforms, hence answering how effectively these tools can be combined to develop a SDR transmitter.

- **Section 1** expands this introduction by discussing key background concepts such as software defined radio, GNU Radio, providing an introduction to the USRP, and reviewing the related topic literature.
- **Section 2** details the design and hardware selection of the generic radar transmitter, and the configurable variables that impact the system output.
- **Section 3** defines the experimental setup, test methodology and parameters of the waveforms to be used during characterisation tests and waveform verification tests.
- **Section 4** discusses the experimental testing and results. The characterisation tests conducted are discussed along with comparisons between the expected results and measured results. The waveform accuracy tests follow where the measurements of the output waveforms are compared to modelled data to verify their accuracy.
- **Section 5** concludes this work by summarising the overall achievements and outcomes.

1.3 Background

1.3.1 Software Defined Radio

Software defined radar is an application of the same technology and concepts used for software-defined radio, thus we begin with a discussion on software-defined radio.

A software-defined radio is a radio system that performs some or all signal processing using software, ideally operating on a reprogrammable processor, such as a personal computer (PC) or embedded system [8, p.1]

There is no defined criteria as to what type or amount of signal processing must be performed by software for a radio to be considered software-defined [9], however the ideal system will implement as much of the radio frequency (RF) chain in software as is possible (given technology limitations) leading up to the antenna.

Moving the challenge of radio engineering design from the hardware domain to the software domain provides several key advantages [8, p.2] [10, p.1]:

- **Flexibility:** Since the operating characteristics of a software-defined radio are mainly defined by the software running on the system, this enables highly flexible radio systems that can provide a different signal processing functionality or set of behaviour with a simple software modification or upgrade, (within the hardware limitations of the RF transceiver.)
- **Common Hardware:** The ability to use commercial-off-the-shelf (COTS) or general-purpose hardware removes the need for application specific analogue hardware, and allows the reuse of existing hardware.
- **Reduced System Costs:** A combination of the above two factors result in simplified architectures, and reduces system costs.

Nonetheless, software defined radio performance is still bound by hardware limitations such as the following key factors [2, p.5] [8, p.3]:

- **ADC Sampling Rates:** Sampling rates should ideally be twice the maximum frequency of the signal to be digitized, as required by the Nyquist theorem [11, p.40]. Since many RF applications use frequencies in the GHz region, the required sampling rates are not achievable by most (COTS) analogue-to-digital converters (ADCs).
- **Antenna Bandwidth:** Antennas are designed to operate within specified frequency bands, limiting the operating frequency ranges of software-defined radios.
- **Processor Speed:** COTS processors do not have the processing speed to perform real-time processing of signals with GHz frequencies.

To address these limitations, current software defined radios adopt a design similar to that of the generic software defined radio presented in Figure 1.

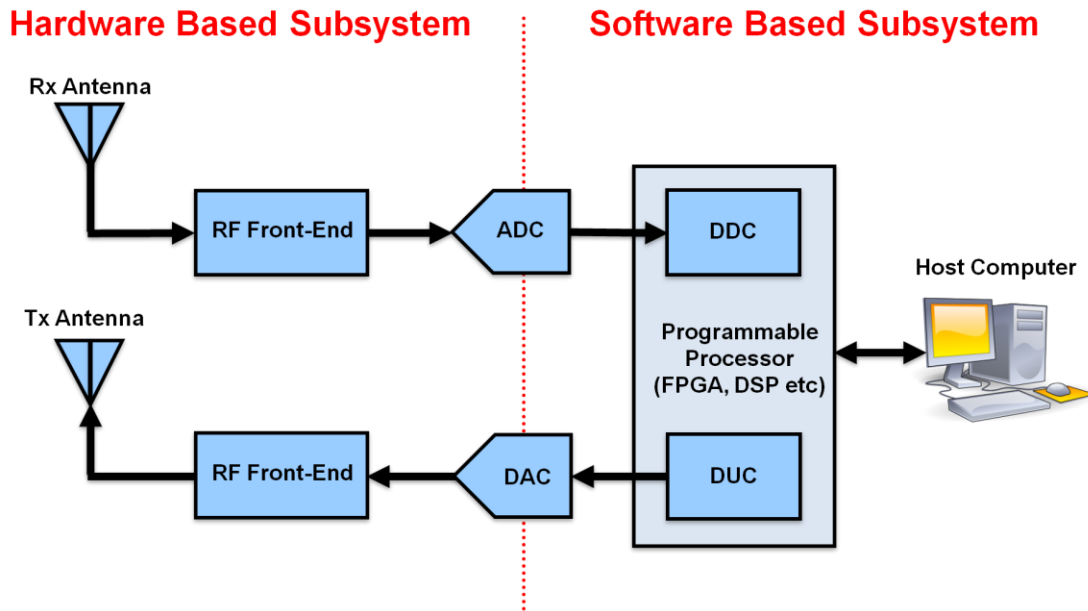


Figure 1: Block diagram of a generic software defined radio system

This design includes a device called a RF front-end which mixes signals between the carrier RF and lower frequencies suitable for the sampling rates of the ADC / digital-to-analogue-converter (DAC) components. These lower frequencies may either be an intermediate frequency (IF) or baseband (BB).

As a result the ADC / DAC components are only required to achieve sampling rates sufficient to handle the modulation bandwidth (MBW) of the signal rather than the carrier frequency bandwidth.

A programmable processor is used to perform modulation, demodulation or other computationally expensive digital signal processing tasks that would present a significant burden on the host computer. This processor may consist of a field programmable gate array (FPGA), digital signal processor (DSP) or other type of programmable processor.

This subsystem also digitally down/up converts the signal between IF and BB (unless direct conversion to baseband is performed by the RF-Front End.) The digital down/up conversion may be performed by the processor itself or by separate digital-down-converters (DDCs) or digital-up-converters (DUCs).

1.3.2 GNU Radio

GNU Radio consists of a toolkit of signal processing blocks for implementing software-defined radios on external RF hardware. GNU Radio Companion (GRC) extends the toolkit by providing a Graphical User Interface (GUI) that allows flow graphs and signal visualisers¹ to be built out of signal processing blocks in a manner similar to Matlab Simulink. A screenshot of GNU Radio Companion is shown in Figure 2.

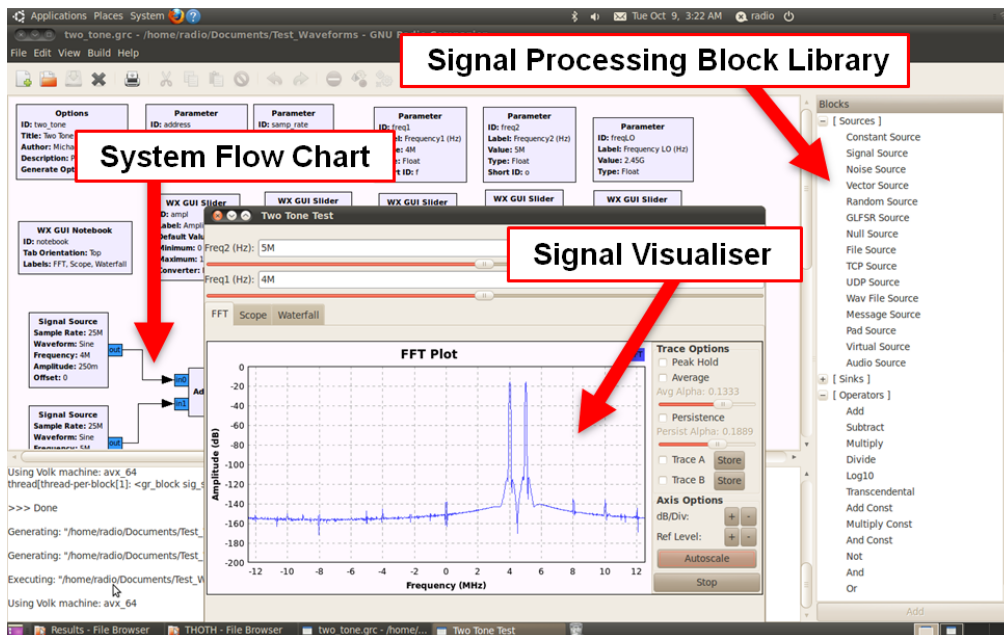


Figure 2: Screenshot of GNU Radio Companion

Applications are written in Python and C++ programming languages. Performance-critical signal processing blocks are written in C++ whilst Python is used to create flow graphs, scripts and combine signal processing blocks [12].

GNU Radio is primarily used with the USRP hardware but is compatible with a number of other available RF hardware devices. Although not intended as a simulation tool, it can be used stand-alone to provide simulated results.

All codes for GNU Radio are copyright of the Free Software Foundation and distributed as open-source [12] under the GNU General Public Licence (GPL). It provides the public domain with a powerful, free, modifiable toolkit for software-defined radio development.

¹ GNU Radio Companion offers a range of useful GUIs for visualising signal data, however the output from the Fast Fourier Transform (FFT) visualiser is an artificially generated 'realistic' output based upon a combination of real data values and modelled imperfections such a noise. Since these artificially generated artefacts are undesired, the output from the GRC FFT visualiser was not used in this study for data analysis.

Although initially created to run on Linux based operating systems (OS) for which there is currently more installation support, installation packages have now been developed for Windows and Mac operating systems.

1.3.3 Introduction to the Universal Software Radio Peripheral



Figure 3: USRP Networked Series N210 Model

The Universal Software Radio Peripheral products are a line of hardware platforms for hosting software defined radios. Designed initially to support GNU Radio, the USRP can now be used with other GUI control software such as Matlab and LabView, or can be run from a computer command line. The USRP products are sold by Ettus Research and their parent company National Instruments.

The two core Ettus Research products required to provide the functionality of a software-defined radio are a USRP (with internal motherboard), and a RF daughterboard that mounts onto the motherboard. The USRP (see Figure 3) then connects to a host computer with GNU Radio (or other software), via USB 2.0 or Gigabit Ethernet cable. Alternatively, some USRP models utilise an embedded computing device and may be run stand-alone after instructions have been downloaded from a host computer.

In the context of the generic software defined radio discussed in Section 1.3.1, the USRP motherboard consists of an FPGA with components to provide the ADC, DAC, DUC and DDC functionality, whereas the RF daughterboard provides the RF-Front-End functionality. A block diagram illustrating this is shown in Figure 4. A range of RF daughterboards exist to address different frequency ranges, and can be easily interchanged. Similarly, different series of USRP models exist with additional features to meet different application requirements.

Due to the comparatively low cost of the Ettus Research hardware products [13] (e.g. USRP motherboards are available for less than 1700 USD), the open-source specifications of their sub components, and their synergy with the free GNU Radio software the two platforms are often combined for the development of low cost software defined radios by research and hobby groups [14].

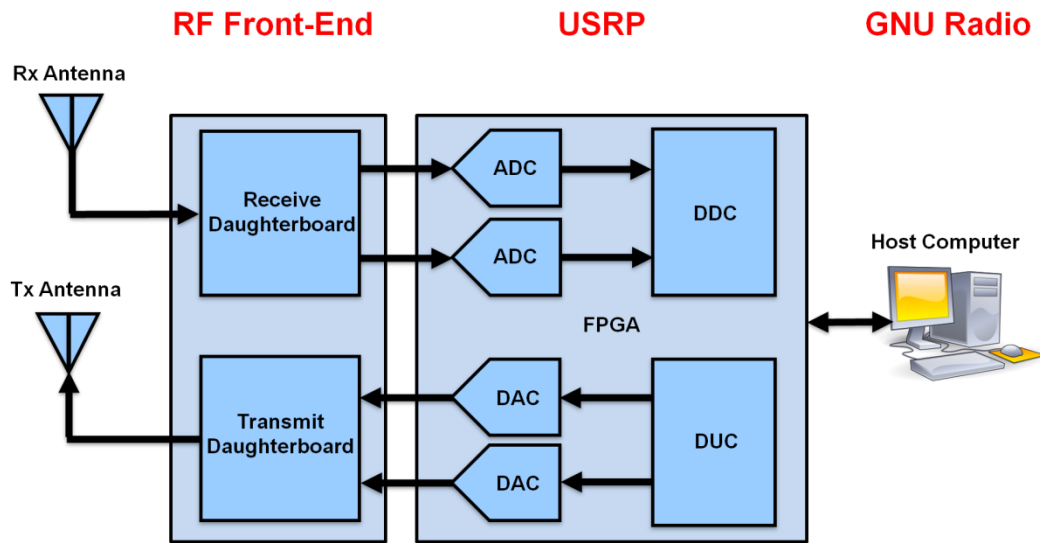


Figure 4: Block diagram showing the main functions of a typical USRP

1.4 Literature Review

1.4.1 Previous Work

Numerous studies have demonstrated that GNU Radio software and USRP hardware can be combined to develop software-defined radars for a variety of active and passive radar applications. These applications include (but are not limited to) networked radars and sonars [4], weather surveillance [7], aircraft or ship detection radars [15], measurement of indoor human movement [16], SDR test beds, temperature sensing [17] etc .

These studies are often feasibility or demonstrator projects that illustrate the implementation of a SDR design using these tools for a specific application. They measure and evaluate the performance of the SDR for that application and may discuss the limiting design factors; but often do not measure or explore in a more general sense - the characteristic behaviour of the SDR, such as performance limitations or accuracy.

1.4.2 Existing Documentation on System Behaviour

A wealth of open-source information on GNU Radio and the USRP is available on the internet [12]. However this knowledge is poorly documented. In most cases the information resides on community wikis / forums, is inconsistent due to contributions from multiple authors, or out of date due to the rapid rate of software defined radio development. The main sources of documentation and information include the following:

- Schematics of the USRP motherboards and RF daughter-boards can be accessed through the Ettus Research website [18], whilst datasheets of subcomponents are made available on the internet by manufacturers [19].

- A limited number of guides exist that provide a detailed discussion of the internal architecture of the USRP hardware [20-22] along with its implementation with GNU Radio, however these apply to the original USRP 1 model and do not apply to the hardware of the subsequent USRP models.
- The GNU Radio Discussion list archives answers regarding specific questions on the behaviour, limitations and implementation of GNU Radio and the USRP. Often the core developers and pioneers directly answer questions relating to these tools.

These resources provide a useful starting point and resource for understanding the internal architecture of the USRP along with data on the limitations of its subcomponents. However these do not provide a compiled (or well documented) examination of the behaviour and performance limitations of the USRP hardware as a whole system that can be directly leveraged for radar design.

1.4.3 Primary Factors Limiting USRP Radar Performance

The limitations encountered in developing USRP based radars may vary depending upon the application requirements, however the primary factors affecting the performance of USRP transmitters are the computer processor speed, host connection bandwidth and the choice of antenna as summarised in a 2010 study examining the current state of the software-defined radar technology [8, pp.1-5] and as is apparent in many SDR design studies. The low transmit power of the Ettus Research RF daughter-boards is also worth addressing.

Processor Speed

A USRP based transmitter must have sufficient processor resources to maintain the desired throughput rate from the host computer to the USRP. A failure to maintain this is referred to as a transmit under-run (indicated by “U” outputs in the GNU Radio GUI). The demands on the processor will vary depending upon the application, however GNU Radio discussion list comments from Eric Blossom (founder of the GNU Radio Project) indicates that from his experience it takes at least an Intel Core 2 Duo running at 3 GHz or more to transmit at full speed to the latest USRP models [23]. Due to the small transmit buffer size, the average transmit rate over a very small window needs to be reliable. If the CPU is focussing processor resources on other tasks, transmit under-runs will occur.

This particularly applies if the radar is mono-static, in which case if the processing required on the receiver side dominates resources it could cause transmit under-runs. In some studies [3, pp.69-70] the high processor and resource requirements hindered the performance of the radar system, causing difficulties in obtaining real time performance and minimising packet losses during transmit and receive. If processor resources are insufficient to balance both transmit and receive functions on a single host computer, optimising processor resources may require performing transmission and receive on two separate dedicated host computers.

Host Connection Bandwidth

The host connection bandwidth refers to the connection throughput between the USRP and the host computer. Although the newer models of the USRP offer a Gigabit Ethernet connection surpassing the USB 2.0 interface of earlier models, the host connection bandwidth is still the core 'bottle-neck' limiting USRP system performance as shown in many studies [2, 3, 8]. The host connection bandwidth not only limits the maximum sampling rate achievable, but also the MBW of the system, and the samples per period for a given intermediate frequency. This will be discussed further in 2.5.3.

Antennas

Software-defined radars that perform basic functions such as operation within a narrow frequency range will be able to use most types of antenna. Multi-function software-defined radars will require antennas that fulfil specific needs or functionality requirements, e.g. that offer wideband or multi-band capacity, specific directional performance, or even fully digital array functionality. The antennas available by Ettus Research are low-cost antennas compatible with their RF daughterboard range and may not meet the frequency band or signal-to-noise ratio (SNR) performance required of multi-function SDRs. Higher performance antennas can be obtained via other suppliers but will likely exceed a low cost budget.

Radar Transmit Power

The radar transmit power is a primary factor affecting the signal to noise ratio (SNR) at the receiver, and hence the maximum detection range. This may be up to a typical value of 200mW depending upon the RF daughterboard model. Depending upon the performance requirements this may require careful selection of waveform parameters to ensure adequate SNR is maintained.

Some designs [2] have used Barker codes to increase SNR with the drawback that increasing the Barker code size increases the pulse width; lowering the range resolution performance and increasing the radar dead zone. Other designs have adopted Frequency Modulated Continuous Waveforms (FMCWs) [24, 25] which can offer high performance using low transmit power [26].

A low transmit power may also require resource intensive processing at the receiver end to obtain the desired SNR [27]. As discussed earlier, in the case of mono-static radars this may in turn hinder transmit performance causing transmission under-runs.

2. Transmitter Design

This section addresses the SDR transmitter used in this thesis. It begins with a discussion of the design requirements, then the hardware and software components selected in implementing the transmitter.

Following this is a detailed system description of the combined hardware selected, along with the configurable variables in GNU Radio that are used to influence the behaviour of radar transmitter.

2.1 Requirements

As the purpose of this work is to examine how effectively the USRP and GNU Radio can be combined to create a generic radar transmitter, this study is concerned with investigating the achievable radar transmitter performance of the technology rather than meeting a specific set of performance requirements such as carrier frequency etc. Radars typically operate at frequencies, ranging from 1GHz potentially up to 100 GHz or more [28, pp.83-85]. As such it is desirable to explore the highest frequency limits achievable. As experiments will be conducted in a laboratory environment, an antenna will not be addressed as part of this design.

As such the following requirements of the transmitter design are set:

- **Hardware Performance:** The transmitter should incorporate the highest performing USRP hardware available.
- **Transmit Frequency:** The transmitter should explore operation at the highest frequency band achievable using the USRP hardware.
- **Operating System:** A self imposed constraint was to use a Debian based Linux distribution, as it is a widely used and well supported in the public domain.
- **Processor Requirements:** Intel Core 2 Duo @ 3GHz (Minimum)
- **Waveform Functionality:** The transmitter should be capable of transmitting continuous waveforms (CW), pulsed waveforms, and frequency modulated waveforms.

2.2 Hardware Selection

2.2.1 USRP

As identified in the literature review, the host connection bandwidth is the key bottleneck in USRP performance. The Networked series (N210/N200) models offer the highest host connection bandwidth out of the available USRP range as shown in Table 2.

The USRP N210 connects to a host computer using a high speed Gigabit Ethernet cable. Although theoretically this could allow 1000 Mbps data throughput, a maximum of 800 Mbps is utilised. Signal processing functions from the host computer are loaded onto the FPGA for faster execution. Although the Embedded series (E100/E110) allows for all processing to occur on an embedded computing device on a standalone USRP, the data throughput between the embedded computing device and the FPGA is limited to 40 MB/s (e.g. 320 Mbps) and further limited by the processor which can only process 16-bit samples at 8 MSps. As such, the Networked series provides the highest host connection bandwidth.

Additionally the Networked Series offers faster DAC sampling rates and hence a higher dynamic range than the other models. The N210 model was selected over the N200 models since it offers a larger FPGA than the N200 model. The model received was an N210 revision 4.0.

Some of the key features of the N210 are:

- Gigabit Ethernet Interface
- Xilinx Spartan 3A-DSP 3400 FPGA, with onboard processing
- Dual ADCs: 14-bits at 100 MSps
- Dual DACs: 16-bits at 400 MSps
- Frequency Accuracy ~ 2.5 ppm with onboard clock reference
- Optional internal GPSDO locked reference oscillator provides 0.01ppm
- Multiple-input multiple-output (MIMO) capable - (Requires two or more N210s)

Table 2 *USRP models currently available from Ettus Research [1]*

NOTE:
This table has been removed due to copyright.
Alternatively, the item is available from the referenced links

2.2.2 RF Daughterboard

The range of RF daughterboards available at the time of writing is shown in Table 3. The XCVR2450 model was selected so that operation at the highest possible frequency band could be achieved.

The XCVR2450 operates within a frequency range of 2400 to 2500 MHz, and a frequency range of 4900 to 5900 GHz. The Ettus product information is inconsistent, with some documents claiming its high frequency band extends to 6000 MHz rather than 5900 MHz.

This daughterboard is a half-duplex transceiver, thus it cannot transmit and receive at the same time. Since this study is only concerned with the transmit side of operation this limitation is not an issue.

Table 3 RF daughterboard models currently available from Ettus Research [29]

<p style="text-align: center;">NOTE: This table has been removed due to copyright. Alternatively, the item is available from the referenced links</p>

2.2.3 GPSDO Reference Clock

The standard onboard reference clock of the USRP N210 is specified to an accuracy of 2.5 parts per million (ppm), meaning that for a maximum clocking rate of 100 MHz², the frequency of the clock could theoretically deviate by up to a maximum of 250 Hz.

To achieve a higher clocking accuracy, the optional Ettus Research GPS Disciplined Oscillator (GPSDO) was purchased. This internal reference oscillator connects to the USRP board and provides a GPS referenced accuracy of 0.01 ppm, thus reducing the maximum theoretical deviation to 1 Hz.

2.2.4 GPS Antenna

As Ettus do not provide GPS antennas for their GPSDO kit, a range of generic, low-cost GPS antennas were investigated (see Table 4). The ROJONE Low Cost Antenna was selected on the basis that it had low noise, and provided the largest gain and frequency coverage when compared to the other antennas.

Table 4 Characteristics of a range of Low Cost GPS Antennas

Manufacturer	Model	Gain	Noise Figure (dB)	Frequency (MHz)
GPSOZ	MK76	≥ 26 dB	≤ 2	1575.42 ± 1.023
GPSOZ	SM76	≥ 28 dB	≤ 2	1575.42 ± 1.023
GPSOZ	RV16	≥ 26 dB	≤ 2	1575.42 ± 1.023
RFI	GPS 1-28 dBi	28 dBi	~2.575	1575.42
ROJONE	GPS 1575 MHz, Low Cost Antenna	~27 dBi	~1.5	1575 ± 5
ROJONE	A-IGPSA83-24C18C-MAG (Dual Band Iridium / GPS)	18 dB	~1.5	1575 ± 2
ROJONE	L1 & Dual L1-L2	50 dB	≤ 0.7	1530 to 1580, 1220 to 1230

2.2.5 Host Computer

The host computer was loaned from DSTO, and offered the fastest processor performance out of those available. The computer had the following performance specifications which met the minimum recommended processor performance identified in the literature review (Section 1.4.3).

- Intel Core 2 (Quad) CPU Q9650 @ 3 GHz
- Front Side Bus (FSB) Speed 1998 MHz
- 2 x 6144 kB, L2 Cache

² This calculation refers to 8-bit (non-complex) samples

2.3 Software Selection

The process of installing GNU Radio onto a host computer and achieving communication with a USRP device can be complicated. Many frequently asked questions (FAQ) pages are devoted to addressing difficulties faced by users during the installation process. As such, this installation attempted to use the most stable software components available at the time to minimize installation problems. A summary of these settings is provided in Table 5.

Table 5 Summary of selected software components

Software Component	Version
Operating System	Ubuntu version 10.04 (Lucid Lynx) 64-bit
GNU Radio	GNU Radio version 3.6
UHD Firmware	UHD_003.004.001-23

2.3.1 Operating System

As mentioned earlier, a self imposed constraint was to use a Debian based Linux distribution. Ettus Research only provides firmware releases using officially supported and maintained Linux distributions. This limited the selection to a version of Ubuntu. A 64-bit installation of Linux Ubuntu version 10.04 (Lucid Lynx) was selected on the basis that it was an earlier release and has more support available.

2.3.2 GNU Radio

At the time of selection, GNU Radio version 3.6 was the latest stable release of GNU Radio available and supports Ubuntu 10.04.

2.3.3 UHD Firmware

The ‘Universal Software Radio Peripheral’ Hardware Driver (UHD) provides a host driver and API for Ettus Research products. A variety of USRP Hardware Driver (UHD) firmware releases are available for download from the Ettus Research website. At the time of selection, UHD_003.004.001-23 was the latest version of the UHD driver rated as stable by Ettus Research and is compatible with GNU Radio version 3.6, and Ubuntu 10.04.

NOTE:
This figure has been removed due to copyright.
Alternatively, the item is available from the referenced links

Figure 5: Block diagram of the USRP N210 with XCVR2450 daughterboard, modified from a block diagram of the functionally similar National Instruments USRP-2921 [30]

2.4 System Description

This section provides a discussion of the signal transmit path through the subcomponents of the USRP system and the signal processing steps performed [31]. A detailed block diagram illustrating the core signal processing steps is provided in Figure 5 that should be examined in conjunction with this description.

Although the focus of this thesis is on the behaviour of the radar transmitter, the receive behaviour is described as well to provide a full understanding of the hardware.

2.4.1 Transmit Signal Path

The host computer running GNU Radio is used to develop the signal processing software, which is transmitted and loaded onto the FPGA'S volatile memory prior to operation via the Gigabit Ethernet interface. Samples for transmit are produced at baseband frequency in a complex valued format (i.e. in phase and quadrature). This is termed 'complex baseband'. The user selects to use either 16-bit or 8-bit complex samples.

These are collected in a first-in first-out (FIFO) buffer, then interleaved into data packets which are transmitted from the host computer to the FPGA via the Ethernet cable. The FPGA collects received packets in a FIFO buffer, which are then de-interleaved and transmitted to the AD9777 module [32].

The AD9777 module receives 16-bit complex samples across dual channels. It applies a DUC process (see Figure 6) that involves filtering and interpolating the input to a user-specified factor, then complex mixing the input with a complex modulator. By default the complex modulator does not mix the signal up to an IF unless specified by the user (as the XCVR2450 RF-daughterboard can shift signals up to the carrier RF directly from baseband) [33]. Dual DACs convert the signal to analogue at 400 MSps, before passing it to the MAX2829 integrated circuit (IC).

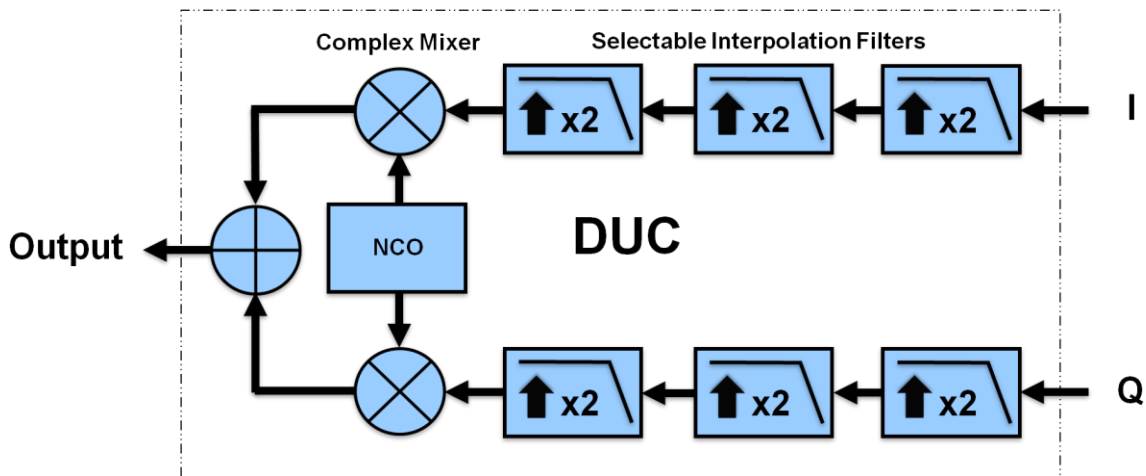


Figure 6: Block diagram of a digital up converter from the AD9777 module in the transmit path. Selectable filters offer interpolation factors of 2, 4 or 8 [34].

The MAX2829 transceiver IC is the main component of the XCVR2450 RF-daughterboard. The analogue signal received is sent through a low-pass filter, before branching off to both the low band (2.4 to 2.5 GHz) and high band (4.9 to 6 GHz) signal paths, which are almost identical. These paths are indicated in Figure 5 by the numbers '2450' and '5' respectively. Next, the signal is mixed to the desired RF using a voltage controlled oscillator (VCO) with a phase locked loop (PLL) [34]. As the MAX2829 is a direct conversion transceiver it is capable of direct conversion between baseband and the desired RF without requiring an IF stage. The signal then passes through a Monolithic Microwave Integrated Circuit (MMIC) power amplifier.

At this point one variation in the transmit paths occurs; a signal travelling along the high band path enters a bandpass filter, whereas a transmit signal on the low band path doesn't. The signal then undergoes power amplification based upon a user specified gain value at which point both paths converge at a diplexer which determines the frequency band used for transmission. The daughterboard may transmit the signal through either of the two RF ports as specified by the user.

2.4.2 Receive Signal Path

The receive path is, with a few exceptions, the reverse of the transmit path. The input received from the RF port passes through a diplexer then branches off to the low band or high band path as appropriate. The signal progressing along the low band path passes through a band pass filter whereas a signal on the high band path does not.

The signal on either path enters the MAX2829 IC, where it undergoes power amplification. It is then mixed down to a baseband frequency (or user specified IF) and passed through a low pass filter and passed to the ADS62P4X module.

The ADS62P4X ADCs digitise the analogue input at 100 MSps using 14-bit samples across dual channels. A DDC process (see Figure 7) is then applied that involves mixing the signal with a complex modulator down to baseband frequency if not done so already, then decimating the signal by a user-specified factor. The complex valued signal is then passed to the FPGA.

The FPGA collects the received samples in a FIFO buffer then interleaves them in data blocks that are transmitted via a Gigabit Ethernet cable to the host computer. These are then collected in a FIFO buffer on the host computer, de-interleaved and processed as required.

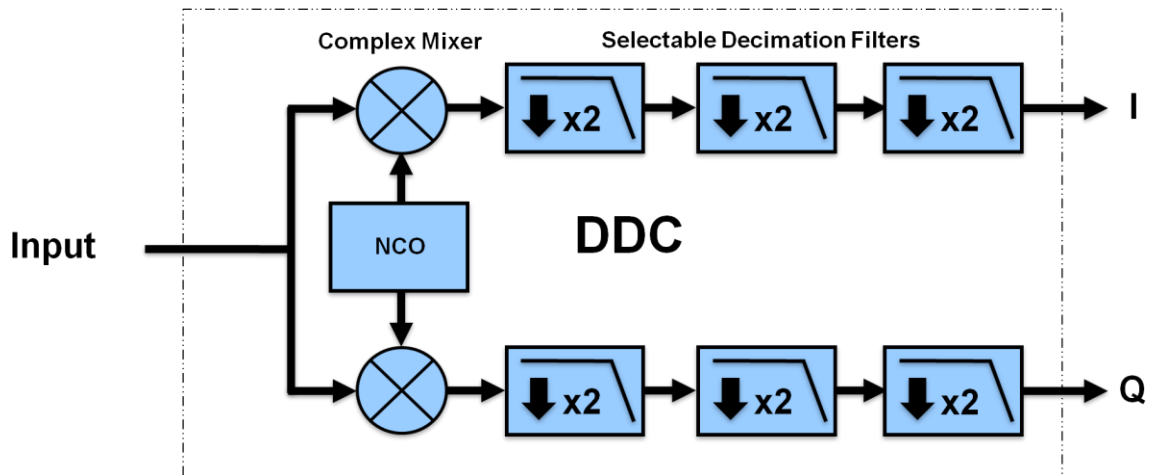


Figure 7: Block diagram of a digital down converter from the ADS62P4X module in the transmit path. Selectable filters offer decimation factors of 2, 4 or 8, and may function as low, high or pass band filters.

2.5 Configurable Variables

In addition to the signal waveform itself, which is discussed later this study, many other selectable variables influence the behaviour of the radar transmitter. These variables are discussed here along with their anticipated impact on the USRP system output.

2.5.1 Sample Size

The user can select between signed 16-bit complex samples (32-bits total) and signed 8-bit complex samples (16-bits total). The implementation for 8-bit samples involves only taking the 8 most significant bits of each sample. The use of 8-bit complex samples trades off dynamic range to achieve a higher sampling rate.

2.5.2 Sampling Rate

Despite the USRP N210 incorporating a Gigabit Ethernet connection a maximum data throughput of 800Mbps is used. Therefore during half-duplex operation 16-bit complex samples and 8-bit complex samples can be transmitted at a maximum sampling rate of 25 MSps³ and 50 MSps⁴ respectively.

According to Nyquist criteria, the maximum frequency that avoids aliasing is equal to half the sampling frequency f_s . As we are using complex samples, our range of non-aliased frequencies extends to from $-f_s/2$ to $f_s/2$ centred at zero. This range is our MBW, and limits our frequency modulation of complex samples to a maximum of Δf_s from one end of the MBW to the other.

³ $800 \text{ Mbps} / (16\text{-bits}/I\text{-Sample} + 16\text{-bits}/Q\text{-Sample}) = 25 \text{ MSps} = 25 \text{ MHz}$

⁴ $800 \text{ Mbps} / (8\text{-bits}/I\text{-Sample} + 8\text{-bits}/Q\text{-Sample}) = 50 \text{ MSps} = 50 \text{ MHz}$

The minimum sample time is also a factor of the sample frequency, and is limited to a minimum of 0.02 μ s, occurring with 8-bit complex samples at 50MSps.

2.5.3 Number of Samples per Period

Further consideration must be given to the desired number of samples per period of the signal. Although a high value will maintain signal structure it will further limit the MBW and the maximum baseband frequency f_{BB} achievable.

$$f_{BB} = \frac{f_s}{\text{No. of Samples per period}}$$

For this SDR transmitter design it was decided to maintain a minimum of four complex samples per period. This will limit the f_{BB} to a useable modulation range of $-f_s/4$ to $f_s/4$; which equates to an effective range of -6.25 MHz to 6.25 MHz ($\Delta f_{BB} = 12.5$ MHz) for 16-bit complex samples, and -12.5 MHz to 12.5 MHz ($\Delta f_{BB} = 25$ MHz) for 8-bit complex samples.

2.5.4 Amplitude Variable

The amplitude parameter in GNU Radio impacts both the voltage and the amplitude of the digital signal sent to the DAC. Signal amplitude is expected to be in the range from -1.0 and +1.0. The UHD driver then normalises this into the range expected by the DAC of the USRP. Amplitudes exceeding a magnitude of 1, will saturate the DAC causing the signal to clip digitally. The amplitude value needs to be selected carefully since even values lower than 1 may still cause the power output from the RF daughterboard to be compressed. The amplitude should ideally remain at a suitably low value so the output voltage avoids a region of non-linear output for that daughterboard [35, p7].

2.5.5 Gain Request Variable

The XCVR2450 offers a range of 0 to 35 dB implemented by its MAX2829 transceiver component during transmit. According to the hardware specifications obtained from the command line output, 5 dB of this gain is implemented through baseband gain control and 30 dB through a variable gain amplifier.

As the user only specifies a single gain parameter using the GRC interface (Figure 8), it is unclear at the time of writing as to how that gain request is assigned between these two gain sources to achieve the full 35 dB gain range available. This process became clearer during testing.

2.5.6 Local Oscillator Tuning

The frequency of the daughter-board's local oscillator (LO) can be tuned in two ways. It may be set automatically by the USRP, where the LO is tuned as close as possible to the target RF with the remaining difference digitally compensated for by the DUC or DDC. Alternatively the user can manually tune the LO by specifying the frequency that the LO is tuned to as shown in Figure 8. As this provides greater control over the frequency selection, the distance between the LO and the RF, and the placement of the image frequencies this method was used in all testing.

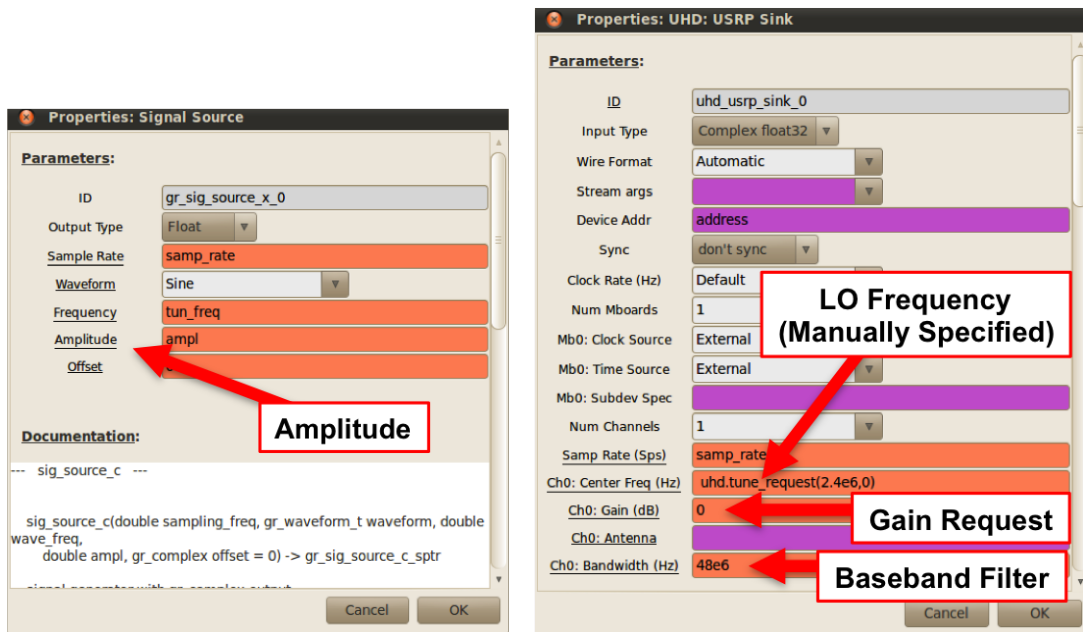


Figure 8: GNU Radio Companion GUI windows highlighting some of the key variables

2.5.7 Baseband Filter

The bandwidth variable adjusts the size of the baseband bandpass filter implemented by the USRP hardware. The filter size applies to both positive and negative sides of the complex baseband signal, thus a size of $f_{baseband_filter}$ covers a range of $-f_{baseband_filter}/2$ to $f_{bandwidth_filter}/2$. The XCVR2450 offers filter sizes of 24 MHz (default), 36 MHz and 48 MHz for transmission. This variable may impact the output if it is set to a value lower than that of the MBW (i.e. the sample rate).

2.6 Design Summary

This section detailed the SDR transmitter design produced using GNU Radio and the USRP. A detailed system overview of the hardware has provided, along with an understanding of the GNU Radio variables that control the system output. Analysis of the system's behaviour is the subject of the next section of this thesis, and will be addressed there.

The total SDR transmitter design cost roughly 3000 USD⁵ plus shipping costs. A successfully working system was achieved, however it is worth highlighting that combining GNU Radio and the USRP to obtain a working system state was not a trivial exercise. Significant trial and error was involved despite the setup guides made available through colleagues and the GNU Radio forums. In most cases the guides were not thorough enough to address troubleshooting, or applied to an out of date or previous version of GNU Radio.

⁵ Total Cost = 1700 USD (N210) + 400 USD (XCVR2450) + 750 USD (GPSDO) + 27 AUD (GPS Antenna) + Customs Fees + Shipping Costs

3. Experiment Methodology

Experiments were divided up into characterisation tests and waveform verification tests. The characterisation tests utilised three basic test waveforms to explore the response of the USRP over a series of tests. The overall aim of this test series was to examine aspects of the USRP's characteristic behaviour to determine performance limitations.

The waveform verification tests involved transmitting three defined radar waveforms, then analysing the measured results with the aim of assessing the accuracy achievable by the SDR transmitter.

This section covers the experimental methodology used to assess the effectiveness of the GNU Radio and USRP based SDR transmitter designed in Section 2. First, the test setup applied throughout this thesis is discussed along with the measurement devices used to collect data, and their configuration settings.

Secondly, the characterisation tests are discussed along with the single tone, two tone and Gaussian noise signals used to explore the characteristic behaviour of the USRP so that performance limits could be identified.

Finally the waveform verification tests are discussed along with the continuous waveform, pulsed waveform, and frequency modulated continuous waveforms transmitted to assess the accuracy of the SDR.

In each test section the GNU Radio flowgraphs used to generate the various waveforms are provided for future use.

3.1 Test Setup

A block diagram of the experiment setup is shown in Figure 9, along with a photo of the setup in Figure 10. Measurement devices consisted of a spectrum analyser, oscilloscope and signal analyser. The spectrum analyser was used to collect data for the majority of tests, with a few exceptions. During the Characterisation Testing, the phase noise measurements were obtained used the signal analyser⁶ instead of the spectrum analyser. During the Waveform Verification Testing the oscilloscope was as a secondary source of data collection to support spectrum analyser measurements.

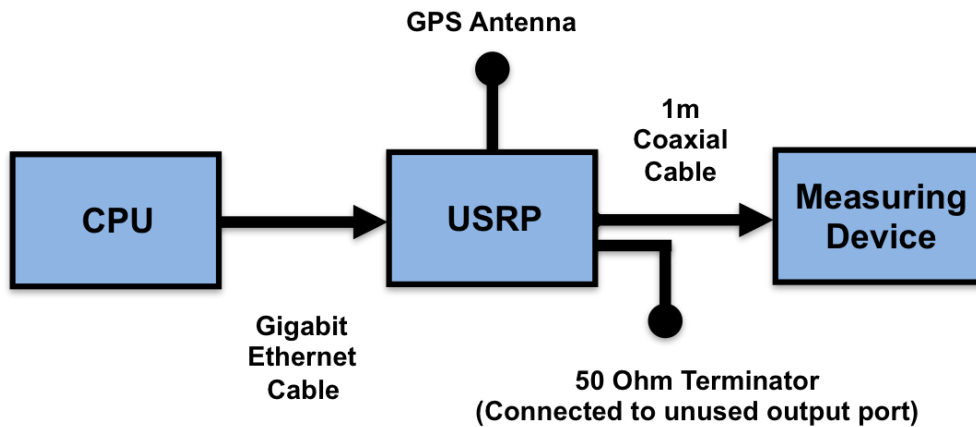


Figure 9: System block diagram of experiment test setup



Figure 10: Laboratory experiment test setup

⁶ Due to laboratory layout, accessing the signal analyser for the phase noise measurement tests required the use of a 10m coaxial cable running along the ceiling instead of a 1m coaxial cable.

3.1.1 Spectrum Analyser

Measurements of the power spectrum as a function of frequency were recorded using a digital spectrum analyser. The default device settings were used, however measurement resolution settings such as the resolution bandwidth (RBW) and video bandwidth (VBW) were varied from test to test. The RBW and VBW selected for each test depended upon the measurement resolution desired, and practicalities such as the corresponding sweep time that would be required to obtain measurements at that resolution for the span of interest. The measurement resolution settings used for each test involving this device are summarised in Table 6.

Table 6 Spectrum analyser measurement resolution settings

Agilent N9344C Handheld Spectrum Analyser (Frequency Range: 1 MHz to 20 GHz)		
Test	RBW	VBW
Modulation Bandwidth Limit Testing	100Hz	100Hz
Frequency Limit Testing	100Hz	100Hz
Effects of the Amplitude Variable	30Hz	30Hz
Effects of the Gain Request Variable	100Hz	100Hz
Power versus Gain and Amplitude Variables	30Hz	30Hz
Power vs RF Frequency	30Hz	30Hz
Effects of the Baseband Filter	300Hz	300Hz
Third Order Output Intercept Point	100Hz	100Hz
Continuous Waveform Testing	100Hz	100Hz
Pulsed Waveform Testing	100Hz	100Hz
Frequency Modulated Continuous Waveform Testing	100Hz	100Hz

3.1.2 Oscilloscope

Measurements of the waveform in the time domain were recorded using a digital oscilloscope. The default settings were used, with adjustments summarised in Table 7, which remained constant for all tests. The device includes an auto-measurement function for obtaining data on the frequency and period of signals.

Table 7 Oscilloscope acquisition settings

Agilent Infiniium DSO-X 92004A Oscilloscope (Frequency Range: Up to 20 GHz)	
Parameter	Setting
Sampling Mode	Real Time
Averaging	Not Enabled
Memory Depth	Automatic (1 kpts)
Sample Rate	20 GSps
Acquisition Mode	Normal
Filtering	Non Interpolated Data: 'None' Interpolated Data: 'Sin(x)/x Interpolation'
Acquisition Bandwidth	Manual: 8 GHz

3.1.3 Signal Analyser

A digital signal analyser was used to take phase noise measurements since the available model was equipped with a mode specifically for this function. Phase noise measurements are referenced to the phase noise of the signal analyser. The device was set to use its default settings for this mode, with adjustments presented in Table 8.

Table 8 *Signal analyser acquisition settings*

Rohde & Schwarz FSV Signal Analyser (Frequency Range: 9 kHz to 30 GHz)	
Parameter	Setting
Acquisition Range	1 kHz to 10 MHz offset
Reference Noise Floor	-140 dBm

3.2 Characterisation Test Methodology

The characterisation tests were exploratory in nature and aimed to identify and investigate limitations in the USRP's performance. This provides an understanding of exactly 'what' is being transmitted from the device and under what operating conditions the transmitted output starts to differ from what the radar designer is expecting.

This was achieved by observing how the output and behaviour of test signals changed in response to the adjustment of individual input variables. These tests investigated the following characteristics and parameters by examining the power spectrum:

- Sample Rate Testing
- Modulation Bandwidth Limit Testing
- Frequency Limit Testing
- Effects of the Amplitude Variable
- Effects of the Gain Request Variable
- Power versus Gain and Amplitude Variables
- Power versus RF Frequency
- Effects of the Baseband Filter
- Third Order Output Intercept Point
- Local Oscillator Suppression
- Phase Noise Measurements

Three types of test waveforms were used during characterisation tests. The purpose of these test waveforms was to define basic waveforms with well known response characteristics, so that the impact of varying individual parameters would be easily observable. Unlike the radar waveforms defined during waveform verification testing, the test waveforms are tools to investigate the USRP behaviour, and are not themselves the subject of testing.

The test waveforms are described in the following section with their standard parameters. Variations that occur to these parameters are described in the section for that test.

Details relating to the aim, method and expected results specific to each sub-test are discussed in the respective test section. Since the XCVR2450 encompasses both a low and high band, tests were conducted in both bands where time was available.

3.2.1 Test Waveform 1: Single Tone Waveform

The single tone waveform consists of a sine wave. The parameters selected (see Table 9) position the RF signal in the centre of the frequency band of operation. The GRC flow graph used to generate this waveform is shown in Figure 11.

Table 9 Default parameters for the single tone waveform

Single Tone Waveform		
Parameter	Low Band Testing	High Band Testing
BB Frequency	6.25 MHz	6.25 MHz
LO Frequency	2443.75 MHz	5393.75 MHz
RF Frequency	2450 MHz	5400 MHz
Sample Rate	25 MSps (16-bit I&Q)	25 MSps (16-bit I&Q)
Baseband Filter	24 MHz	24 MHz
Amplitude	0.25	0.25
Gain	0 dB	0 dB

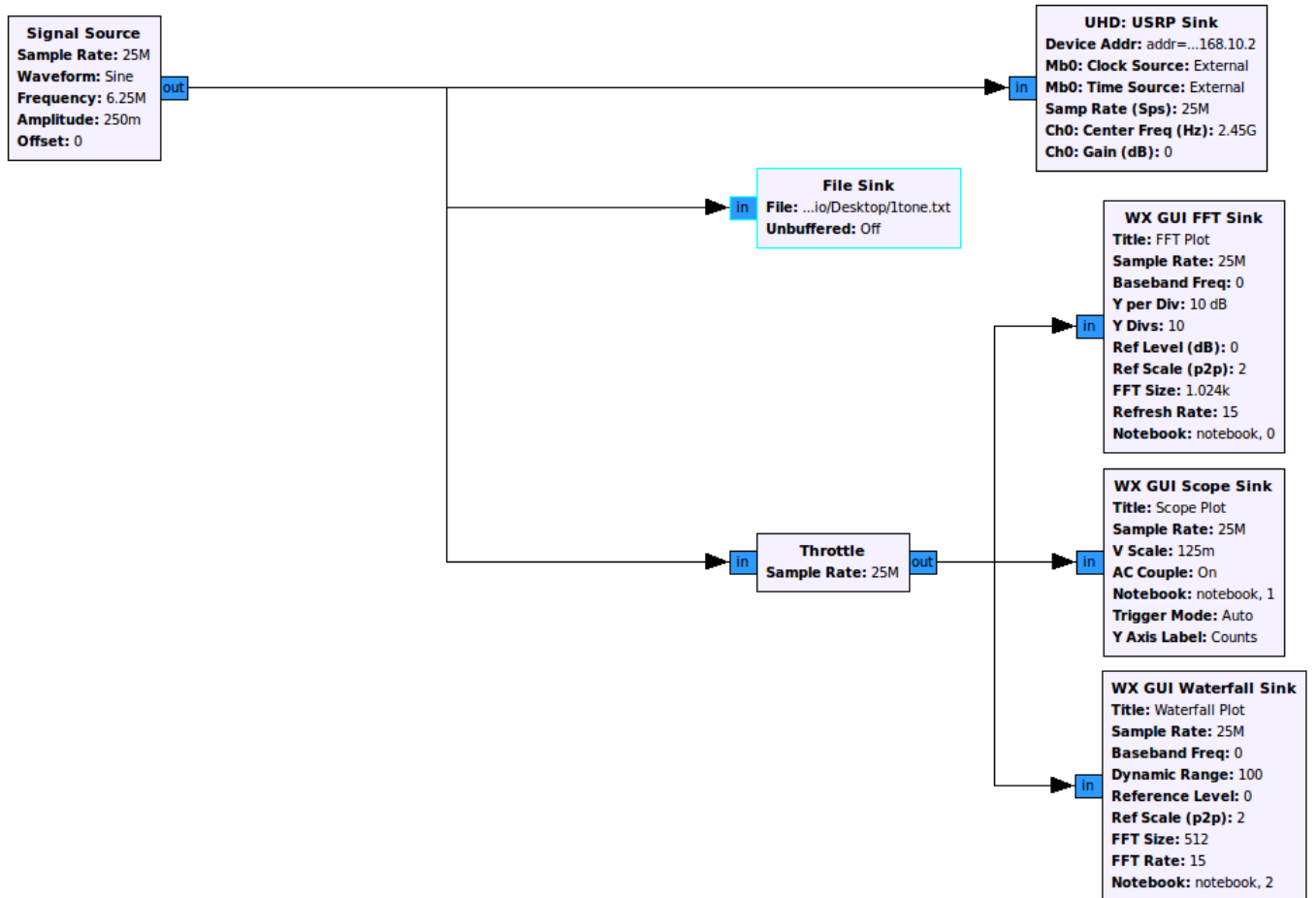
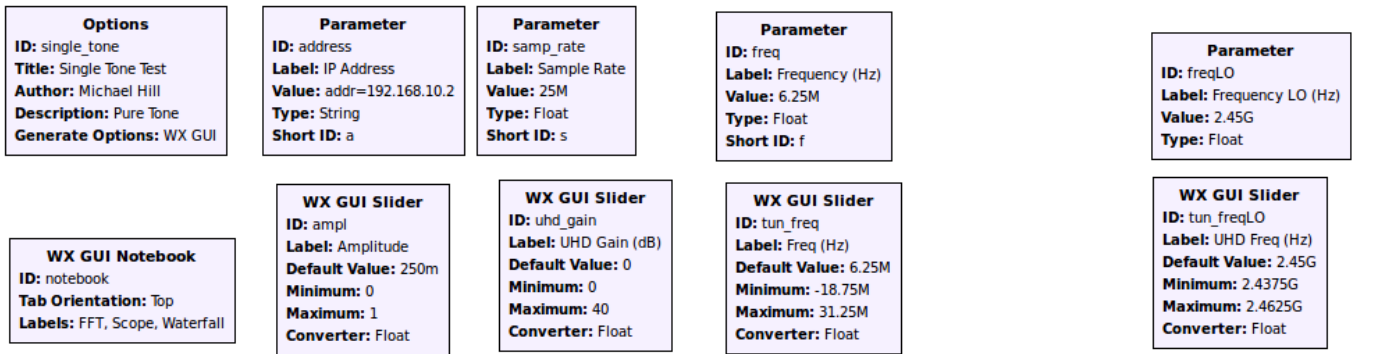


Figure 11: GRC flow graph for generating the single tone waveform

3.2.2 Test Waveform 2: Two Tone Waveform

The two tone waveform consists of two sine waves summed together and transmitted to the USRP. This creates two tones at frequencies $F1$ and $F2$, along with a number of inter-modulation (IM) products. The inter-modulation products at frequencies $IM1$ and $IM2$ shown in Figure 12 can be used to provide a measure of the system's non-linearity, such as the Third Order Output Intercept point (OIP3).

For simplicity during testing, the LO was positioned in the centre of the frequency band tested such that the two tones were offset to the right. Although the placement of the LO signals differs from that of the Single-Tone tests (where the RF signal is positioned in the centre of the band) the resulting frequencies are deemed sufficiently close to the centre of each band for examining the characteristic response. The parameters selected are shown in Table 10. The GRC flow graph used to generate this waveform is shown in Figure 13.

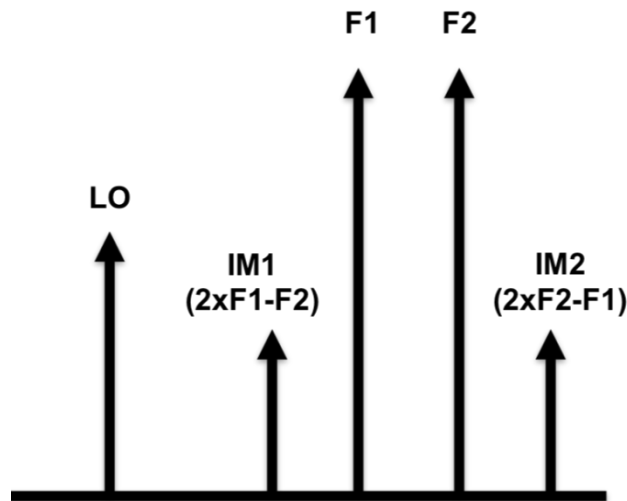


Figure 12: Diagram of the two tone test waveform showing frequencies $F1$, $F2$ and inter-modulation products $IM1$ and $IM2$ at the frequencies indicated.

Table 10 Default parameters for the two tone waveform

Two Tone Waveform		
Parameter	Low Band Testing	High Band Testing
BB Tone 1	4 MHz	4 MHz
BB Tone 2	5 MHz	5 MHz
LO Frequency	2450 MHz	5400 MHz
RF Frequencies	F1=2454 MHz, F2=2455 MHz	F1=5404 MHz, F2=5405 MHz
Sample Rate	25MSps (16-bit I&Q)	25MSps (16-bit I&Q)
Baseband Filter	24 MHz	24 MHz
Amplitude	0.25	0.25
Gain	0 dB	0 dB

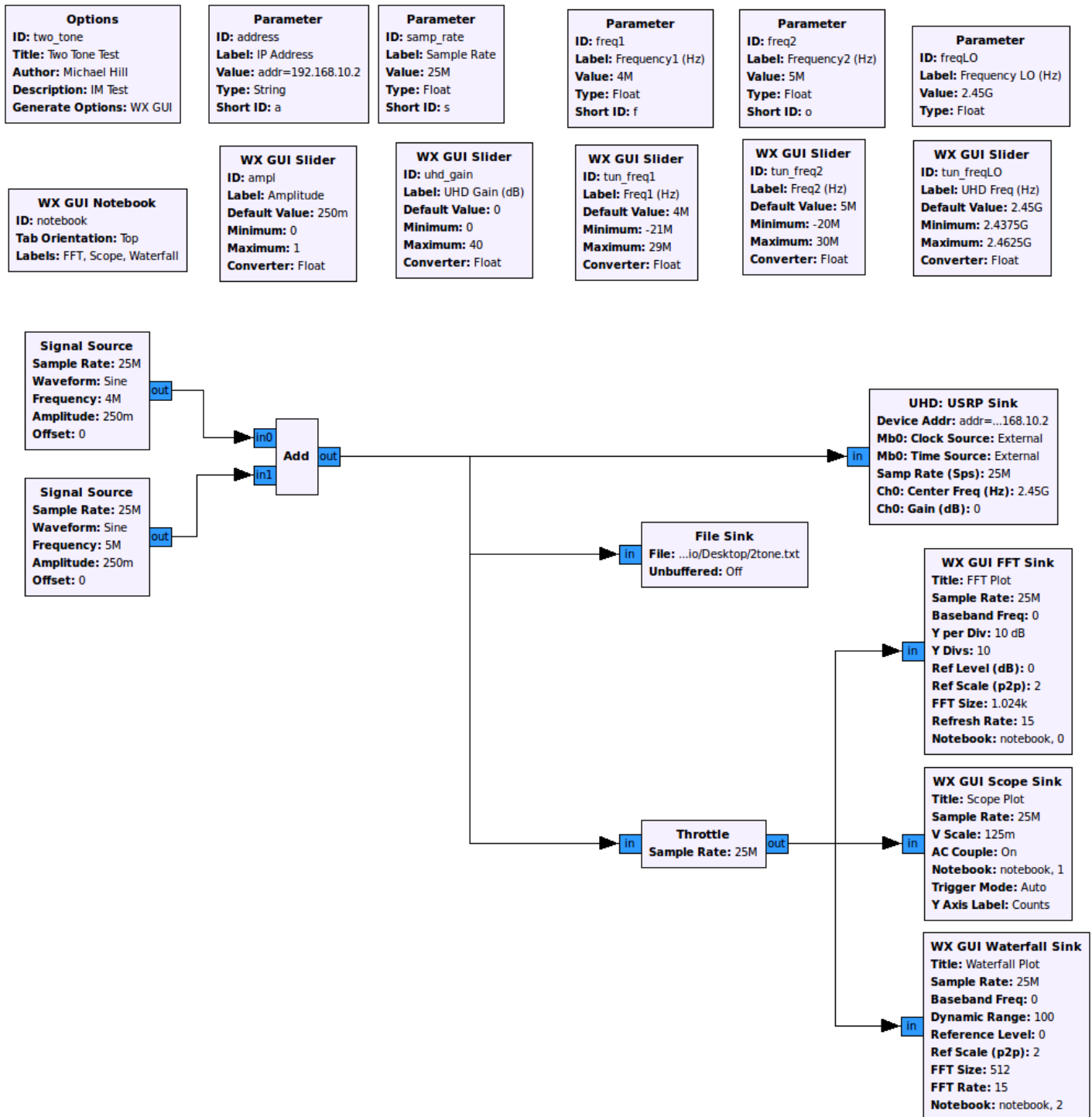


Figure 13: GRC flow graph for generating the two tone waveform

3.2.3 Test Waveform 3: Wideband Gaussian Noise

The third test waveform consists of Gaussian noise spread across the frequency band. The parameters selected (see Table 11) position the LO signal at the centre of the frequency band tested, with the Gaussian noise distributed around the Local Oscillator as the centre. This waveform is intended specifically for examining the baseband filter response. The GRC flow graph used to generate this waveform is shown in Figure 14.

Table 11 Default parameters for the wideband Gaussian noise signal

Wideband Gaussian Noise		
Parameter	Low Band Testing	High Band Testing
BB Frequency	n/a	n/a
LO Frequency	2450 MHz	5400 MHz
RF Frequency	2450 MHz	5400 MHz
Sample Rate	50 MSps (8-bit I&Q)	50 MSps (8-bit I&Q)
Baseband Filter	48 MHz	48 MHz
Amplitude	1	1
Gain	0 dB	0 dB

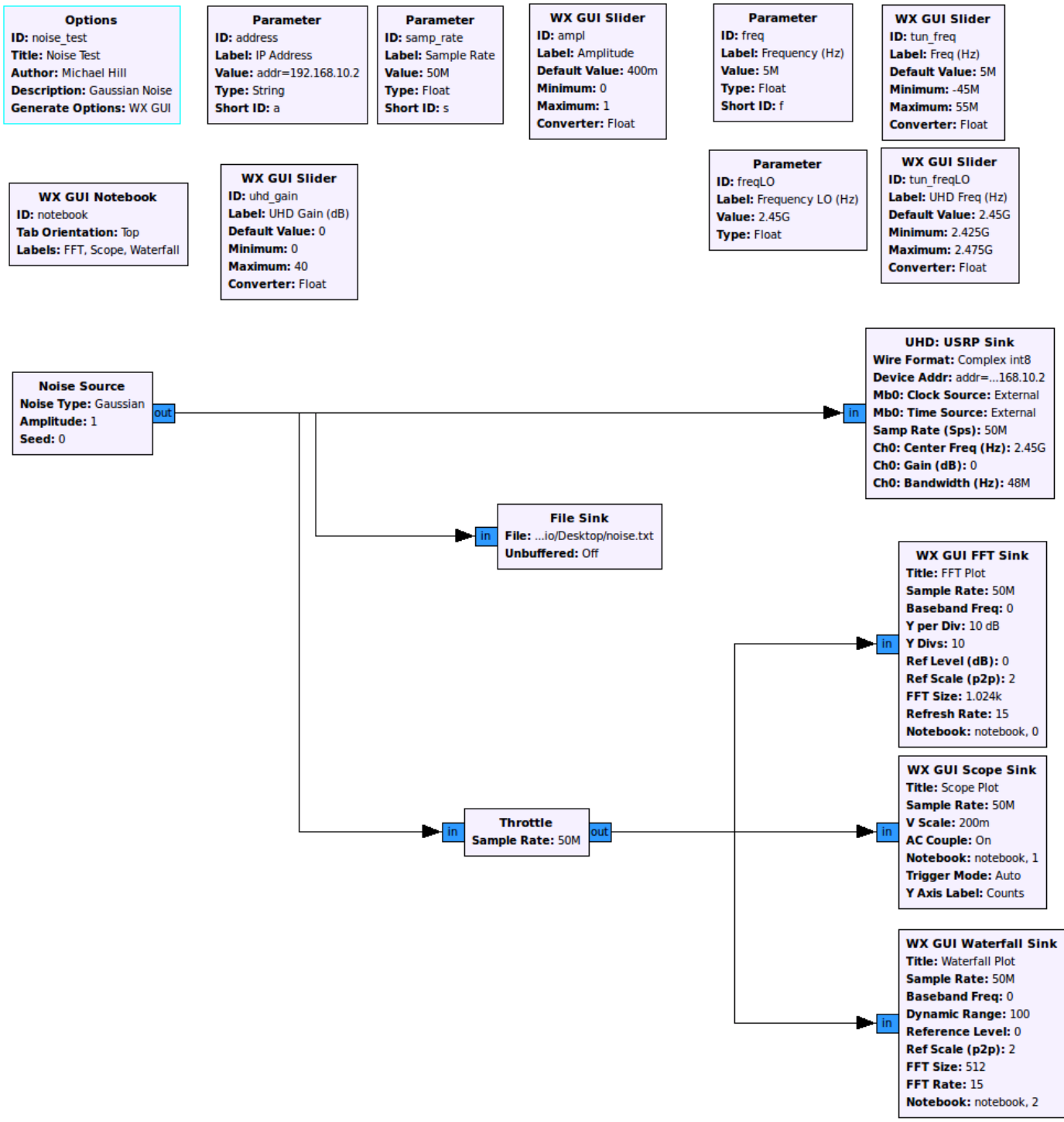


Figure 14: GRC flow graph for generating wideband Gaussian noise

3.3 Waveform Verification Test Methodology

To assess the accuracy of the waveforms output from the radar transmitter, a set of waveforms was defined to be produced, transmitted and recorded for analysis. The set consisted of three different waveform types commonly used by radars, with parameters selected to reflect typical parameters for radar waveforms of that type, and are described in this section.

Since these tests aimed to examine the accuracy of the waveforms generated, the USRP parameters were selected such that the waveforms would not be subject to conditions known to cause distorted behaviour or degraded performance as determined during characterisation tests. This involved the following general settings:

- The amplitude parameter was set to 0.25 and the gain request parameter to 20dB to avoid regions of non-linear behaviour.
- The sampling rate was lowered to 20 MSps to reduce the load on the processor and reduce the likelihood of obtaining sample underrun errors, which were occasionally observed during setup for signals requiring more complex flow graphs and processing.
- The baseband frequency was set to a maximum magnitude of 5 MHz to maintain a minimum of 4 samples per period at the 20 MSps sample rate.
- The baseband filter was set to a maximum width of 48 MHz, so that the signal response could be observed with minimum filtering.
- The RF frequency was set to 5.8 GHz. This frequency was selected since it was at the high end of the available frequency range and is situated in a Defence RF band [36, p.100], enabling free space tests to be conducted in future work.

Unlike the characterisation testing that focused on the limits of the USRP performance to identify unexpected behaviour and regions where it occurred, the waveform testing focused on the performance of the USRP under ideal conditions to examine how accurately it can produce radar waveforms.

The following data output from the USRP was collected:

- Time scope measurements using the oscilloscope
- Power spectrum measurements using the spectrum analyser

The following data input to the USRP was collected:

- Time scope data recorded using GNU Radio

Since GNU Radio Companion does not record data in the frequency domain, time scope data was converted into the frequency domain using an FFT⁷ in Matlab, and used to produce a model of the expected power spectrum within the MBW.

This enabled a frequency domain comparison between the power spectrum data obtained from the spectrum analyser and a model of the expected power spectrum obtained from the input data. The time domain data output to the oscilloscope was compared to the input data as a secondary source of data to support spectrum analyser measurements. A chart summarising the data collected is shown in Figure 15.

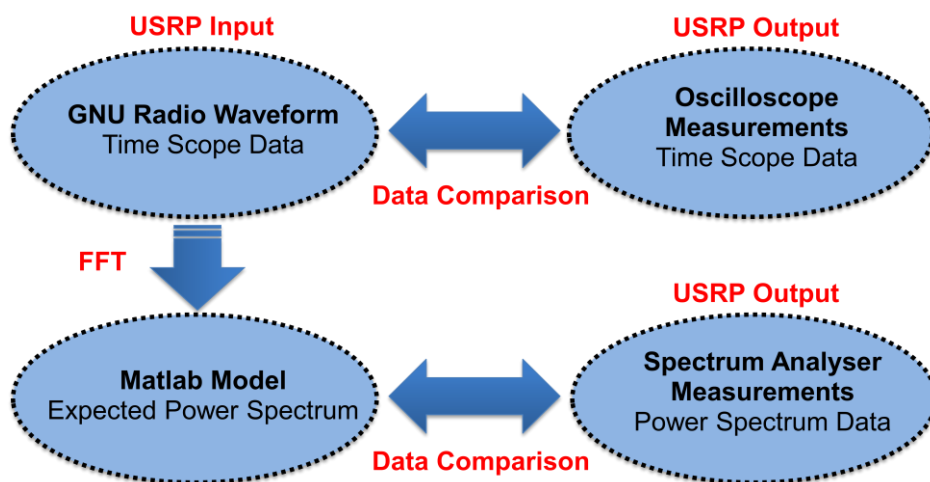


Figure 15: Data collected and compared in this study

⁷ The FFT algorithm used consists of a Matlab script released as part of the GNU Radio package. The script is provided in Appendix A (Section 6.1) and incorporates a Kaiser Window, with a Beta value of 5.

3.3.1 Radar Waveform 1: Continuous Waveform

The continuous waveform consisted of a cosine wave with the parameters provided in Table 12. These were implemented in GRC using the flow graph provided in Figure 16.

Table 12 Parameters for the continuous waveform

Continuous Waveform	
Parameter	Value
BB Frequency	5 MHz
LO Frequency	5795 MHz
RF Frequency	5800 MHz
Sample Rate	20MSps
Baseband Filter	48 MHz
Amplitude	0.25
Gain	20 dB

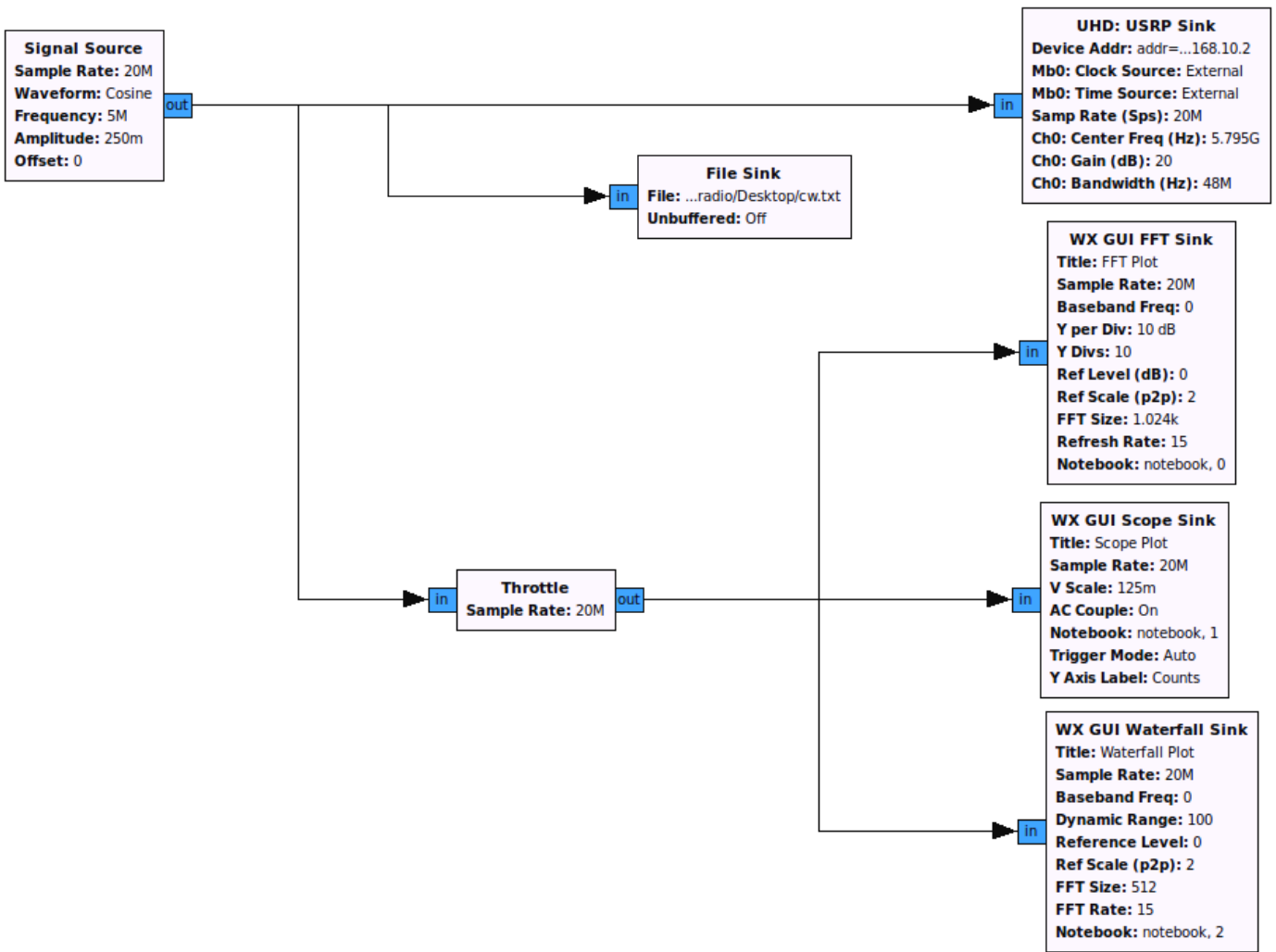
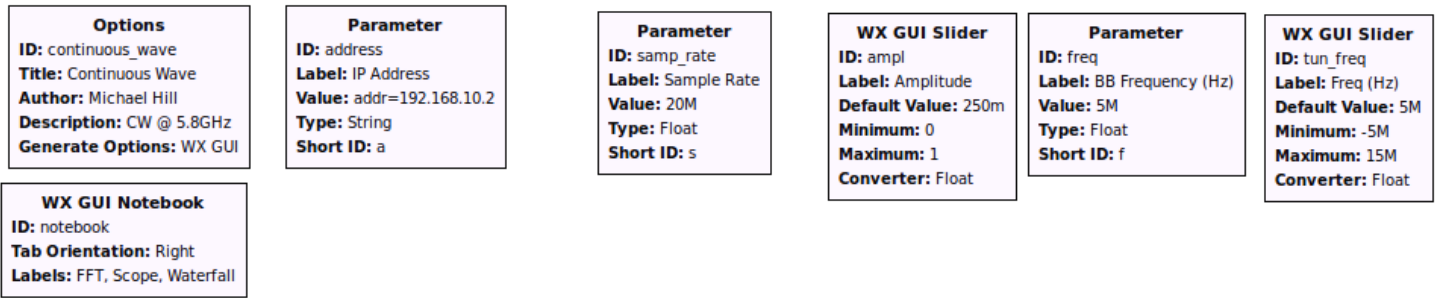


Figure 16: GRC flow graph for generating the continuous waveform

3.3.2 Radar Waveform 2: Pulsed Waveform

The pulsed waveform was implemented in GRC by first creating a rectangular wave vector of 1's and 0's representing the duty cycle on and off time periods of the desired signal. The elements of this vector were then multiplied by samples from a cosine wave source block to 'chop' the cosine wave into pulses of the desired sizes. The vector was set to repeatedly transmit. The parameters are provided in Table 13. The flow graph used is provided in Figure 17.

Table 13 Parameters⁸ for the pulsed waveform

Pulsed Waveform	
Parameter	Value
BB Frequency	5 MHz
LO Frequency	5795 MHz
RF Frequency	5800 MHz
PRI	10 μ s
PRF	100 kHz
Duty Cycle	10%
PW	1 μ s
Sample Rate	20 MSps (16-bit I&Q)
Baseband Filter	48 MHz
Amplitude	0.25
Gain	20 dB

⁸ PRI = Pulse Repetition Interval, PRF = Pulse Repetition Frequency, PW = Pulse Width

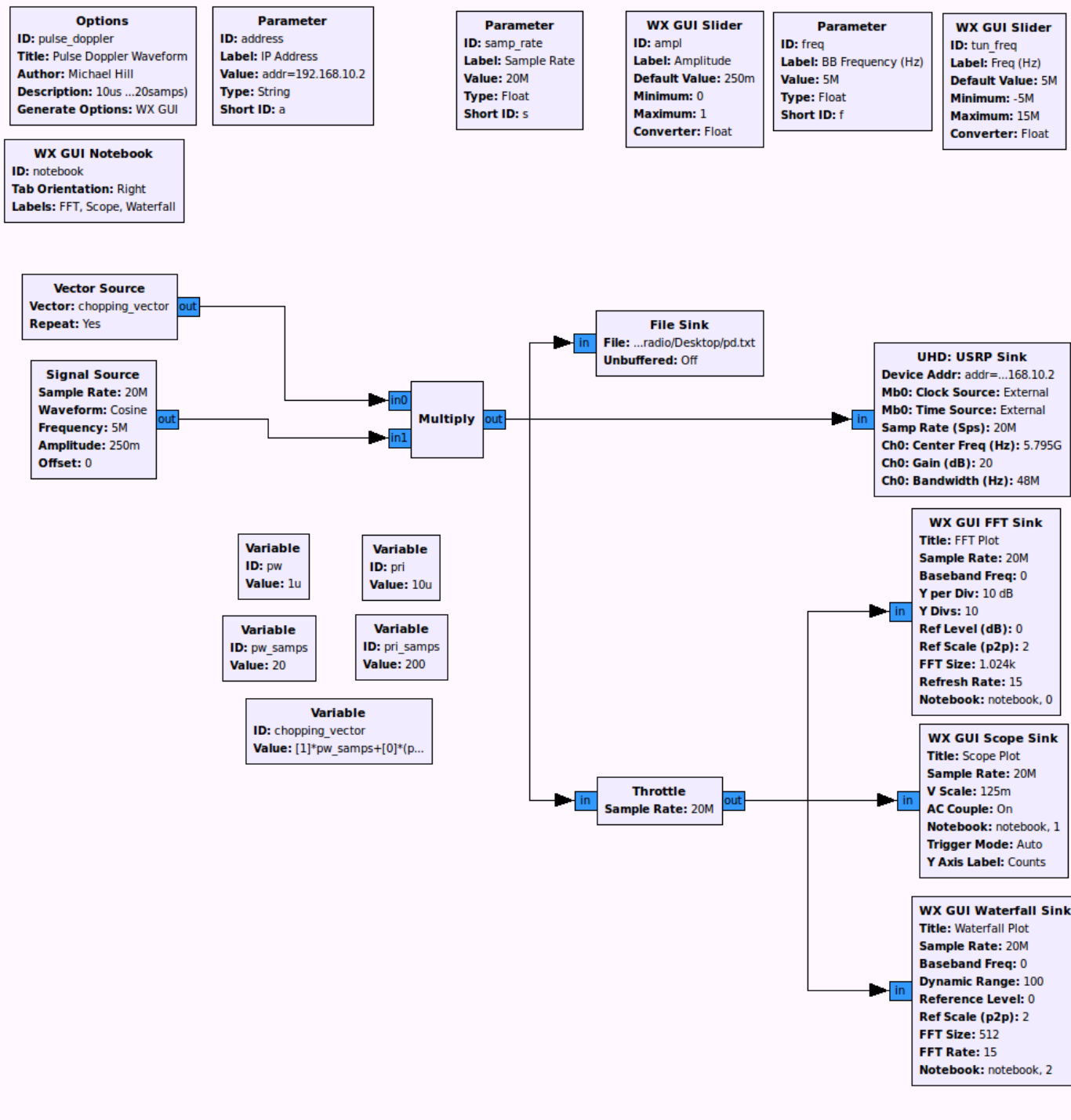


Figure 17: GRC flow graph for generating the pulsed waveform

3.3.3 Radar Waveform 3: Frequency Modulated Continuous Waveform

Frequency modulation sweeps of 0.5, 1, 2, 5, 10, 12.5 and 25 MHz were investigated over a 20 μs cycle, where the sweep included both a 10 μs up sweep followed by a 10 μs down sweep. To implement this in GRC, output from a triangle signal-source block (Figure 18) was used to control the frequency shift required from a frequency modulation block. The signal output from the frequency modulation block was then multiplied by the output from a cosine wave signal source block.

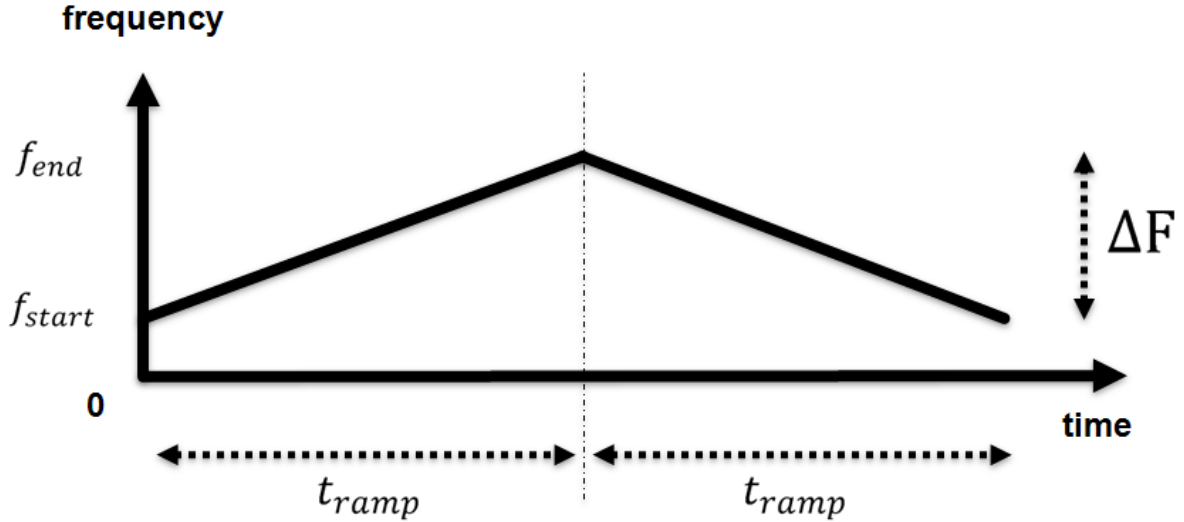


Figure 18: Triangle signal output used to control the FMCW behaviour

The frequency modulation block in GRC uses a sensitivity parameter f_{sens} that defines the rate at which the signal undergoes frequency modulation. This value is defined using the following formula (as determined in the GRC source code), where f_s refers to the sampling frequency and ΔF refers to the total shift in frequency that must occur over the time period t_{ramp} which is the time required to sweep the frequency one way (i.e. 10 μs).

$$f_{sens} = \Delta F \times \left(\frac{2 \times \pi}{f_s} \right)$$

Key modulation parameters are shown in Table 14. The full parameters for the Frequency Modulated Continuous Waveforms tested are shown in Table 15 and Table 16. In these tests the LO has undergone high side injection, with sweeps that keep the magnitude of the f_{BB} during the sweep greater than or equal to $\frac{1}{4}$ of the sampling rate, thus maintaining a number of samples per period equal to or greater than or equal to 4 samples.⁹ The flow graph used is provided in Figure 19.

⁹ Minimum No. of samples per period = $f_s/f_{BB} = f_s/(0.25 \times f_s) \geq 4$

Table 14 Key parameters for applying various frequency modulation values

Key Modulation Parameters for applying FM over a 10 μs ramp time			
ΔF (MHz)	ΔF / Ramp Time (MHz/ μ s)	Sampling Rate (MSps)	f_{sens} ($f_s=20$ MSps)
0.5	0.05	20	0.157079633
1	0.1	20	0.314159265
2	0.2	20	0.628318531
5	0.5	20	1.570796327
10	1	20	3.141592654
12.5	1.25	50	1.570796327
25	2.5	50	3.141592654

Table 15 Parameters for FMCW A

Frequency Modulated Continuous Waveform A	
Parameter	Value
BB Frequency	-5 MHz
LO Frequency	5805 MHz
RF Start Frequency	5800 MHz
Sweep Frequency	0.5 / 1 / 2 / 5 / 10 MHz
RF End Frequency	5800 + Sweep Frequency MHz
Sample Rate	20 MSps (16-bit I&Q)
Baseband Filter	48 MHz
Amplitude	0.25
Gain	20 dB

Table 16 Parameters for FMCW B

Frequency Modulated Continuous Waveform B	
Parameter	Value
BB Frequency	-12.5 MHz
LO Frequency	5805 MHz
RF Start Frequency	5800 MHz
Sweep Frequency	12.5 / 25 MHz
RF End Frequency	5800 + Sweep Frequency MHz
Sample Rate	50 MSps (8-bit I&Q)
Baseband Filter	48 MHz
Amplitude	0.25
Gain	20 dB

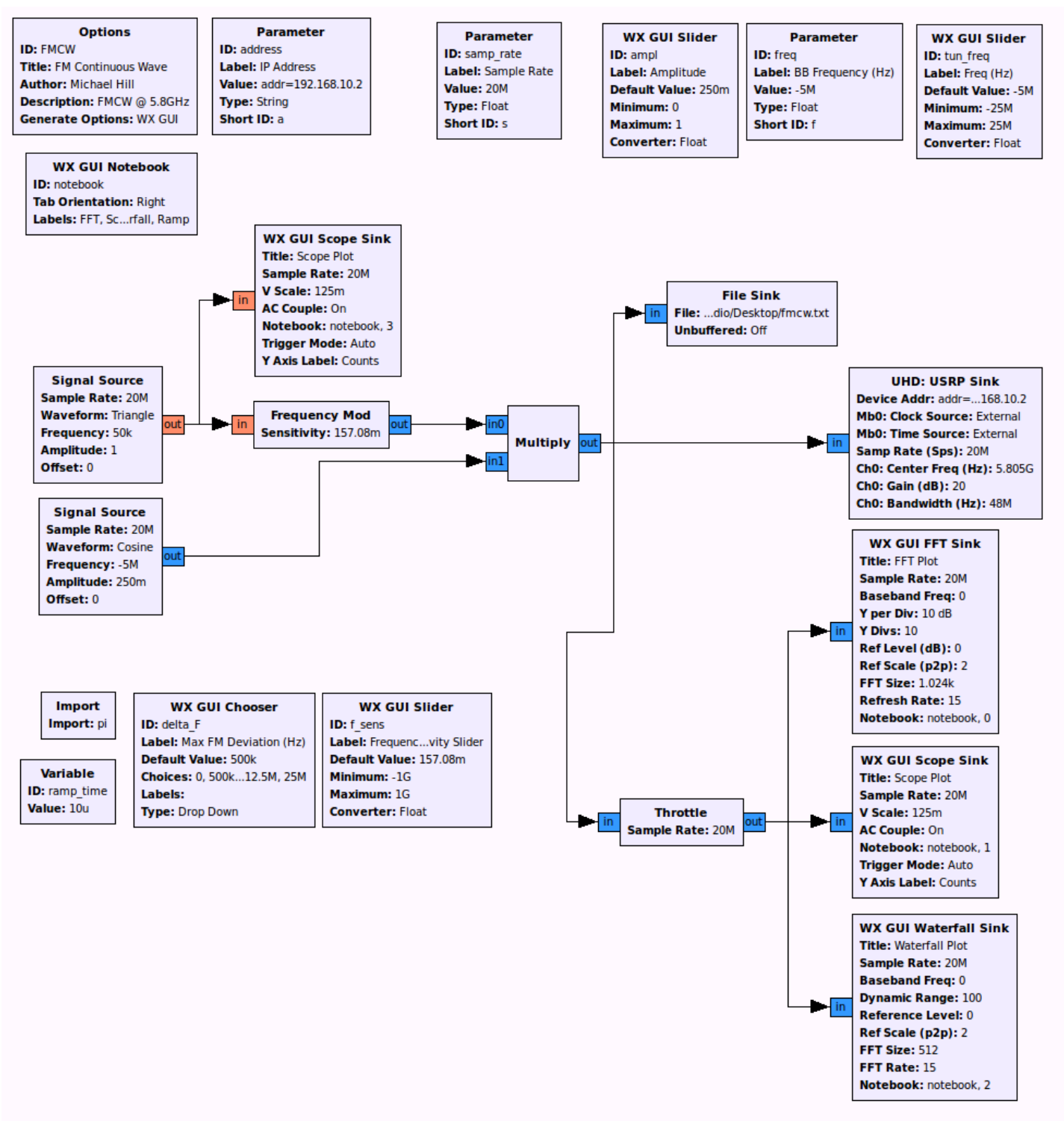


Figure 19: GRC flow graph for generating the FMCWs

Table 17 Summary of results for sampling rates testing

Requested Sampling Rates and Actual Sampling Rates Received (MSps) applicable to 16-bit complex and 8-bit complex samples sizes								
Request	Actual	Request	Actual	Request	Actual	Request	Actual	
0.000001	0.195312	15	14.285714	30	33.333333*	42	50*	
1	1	16	16.66666	31		43		
2	2	17		32		44		
3	3.030303	18		33		45		
4	4	19	20	34		46		
5	5	20		35		47		
6	5.882353	21		36		48		
7	7.142857	22		37		49		
8	7.692308	23	25	38		50		
9	9.090909	24		39		51		
10	10	25		40		52		
11	11.111111	26		41		53		
12	12.5	27				54		
13		28				55		
14	14.285714	29			55+ etc.			

*Causes sample under runs and GNU Radio to cease operation if using 16-bit complex samples

4.1.2 Modulation Bandwidth Limit Testing

The modulation bandwidth testing aimed to confirm the behaviour of the RF signal as the baseband frequency increases and approaches the limits of the MBW.

The MBW limits for the complex valued signal should theoretically be $-f_s/2$ to $f_s/2$, which equates to limits of -12.5 MHz and 12.5 MHz away from the LO frequency for a 25 MSps sample rate using 16-bit complex samples, and -25 MHz and 25 MHz for a 50 MSps sample rate using 8-bit complex samples. As the baseband frequency increases in magnitude, and crosses these boundaries the RF signal should undergo aliasing.

Tests used a single tone waveform with the baseband frequency initially set to 0, then gradually increased past the theoretical limit to 25 MHz. The initial baseband filter width was set to a maximum value of 48 MHz to ensure that any limits observed were due to the 25 MHz MBW, rather than the baseband filter. As the baseband frequency increased from 0 to 12.5 MHz the image frequency on the opposite side of LO frequency moved from 0 to -12.5 MHz from the LO. As the baseband frequency approached 12.5 MHz the RF signal decreased in power whilst the image signal power increased until the baseband frequency reached 12.5 MHz, at which point the signals were of the same power and symmetrical around the LO frequency. As the baseband frequency increased further, the signal power dropped off rapidly after passing 12.5 MHz, whilst an image signal of increasing power was observed folding back from -12.5 MHz approaching 0. Images showing these results are presented in Figure 21, Figure 22 and Figure 23.

The reverse behaviour was observed for a RF signal with a baseband frequency decreasing from 0 to -25 MHz. The tests were repeated for a 50 MSps sample rate using 8-bit samples with the same behaviour observed at limits of -25 MHz and 25 MHz.

These results confirm the measured MBW limits for 25 MSps and 50 MSps sample rates match the theoretical values and that the USRP signal responds as expected whilst the baseband frequency approaches these limits.

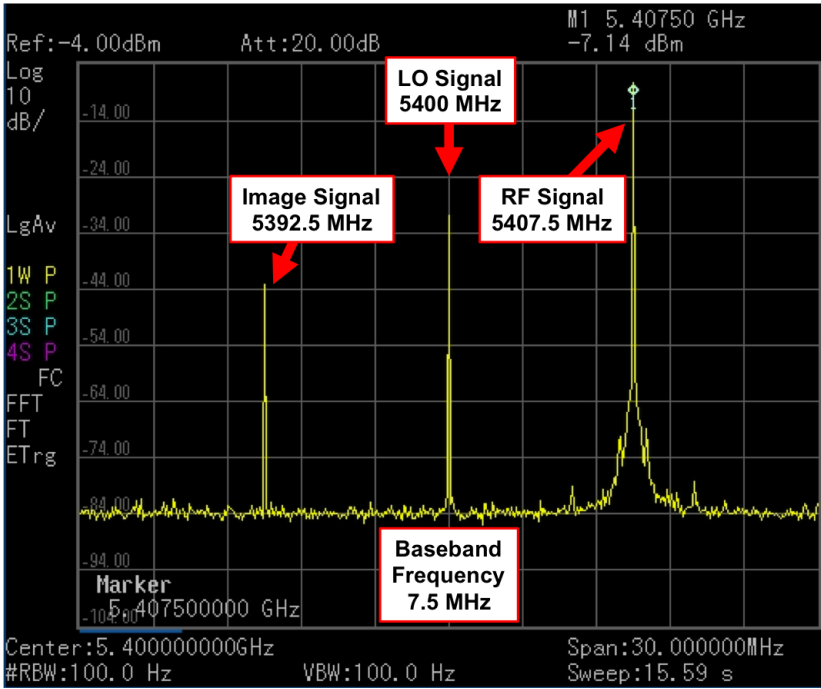


Figure 21: Frequency response for a single tone waveform with a 7.5 MHz baseband frequency

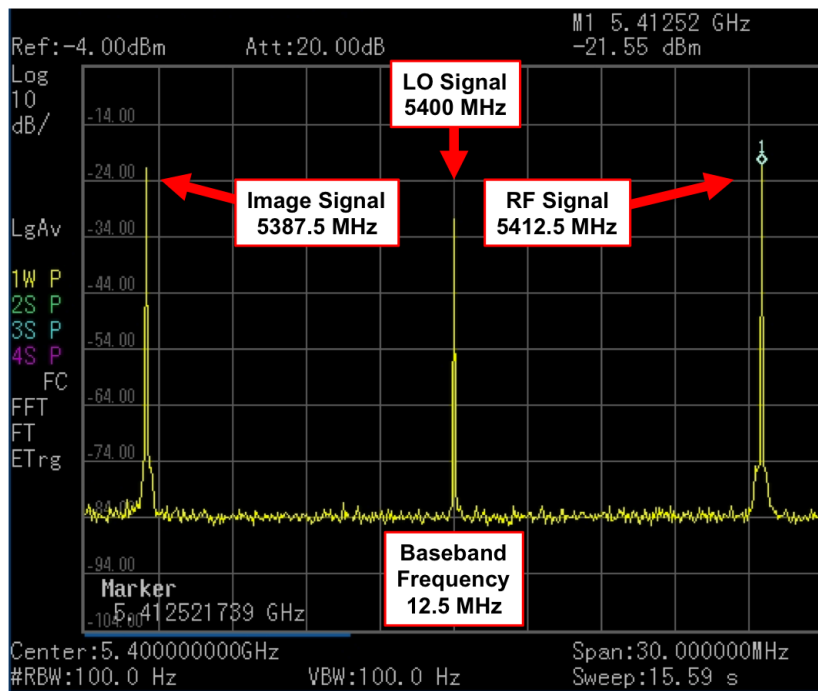


Figure 22: Frequency response for a single tone waveform with a 12.5 MHz baseband frequency

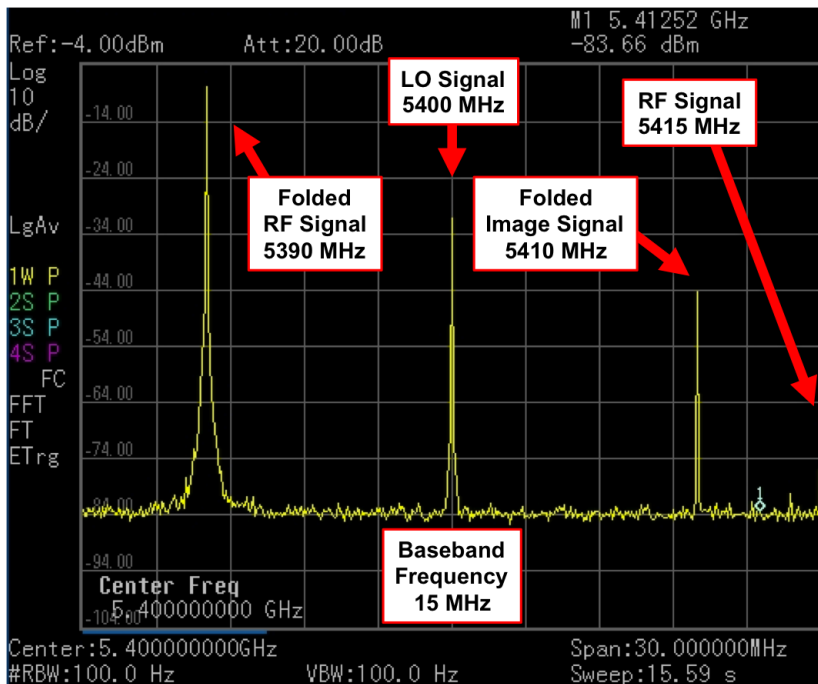


Figure 23: Frequency response for a single tone waveform with a 15 MHz baseband frequency

4.1.3 Frequency Limit Testing

The frequency limit testing aimed to confirm the frequency limits of the XCVR2450 daughter-board. As discussed in the Transmitter Design section, the XCVR2450's low band frequency range is expected to cover 2400 to 2500 MHz, whilst the high band range is expected to cover 4900 to either 5900 or 6000 MHz.

Low and high band testing began with the LO frequency of a single tone waveform placed in the centre of that band (e.g. 2450 or 5400 MHz respectively), with a baseband frequency of zero. The LO frequency was then gradually increased to identify the upper limit of that band. The experiments were repeated with the LO frequency decreasing to identify the lower band limits.

These tests show that the low band covers a frequency range of 2400 to 2500 MHz and that the high band covers a frequency range of 4900 to 6000 MHz. Further testing involved shifting the LO frequency to these limits, then increasing the magnitude of the baseband frequencies. This clarified that the quoted frequency limits applied to the LO frequencies only, and that through modulation, signals can be effectively modulated beyond these boundaries, within MBW constraints as shown in Figure 24.

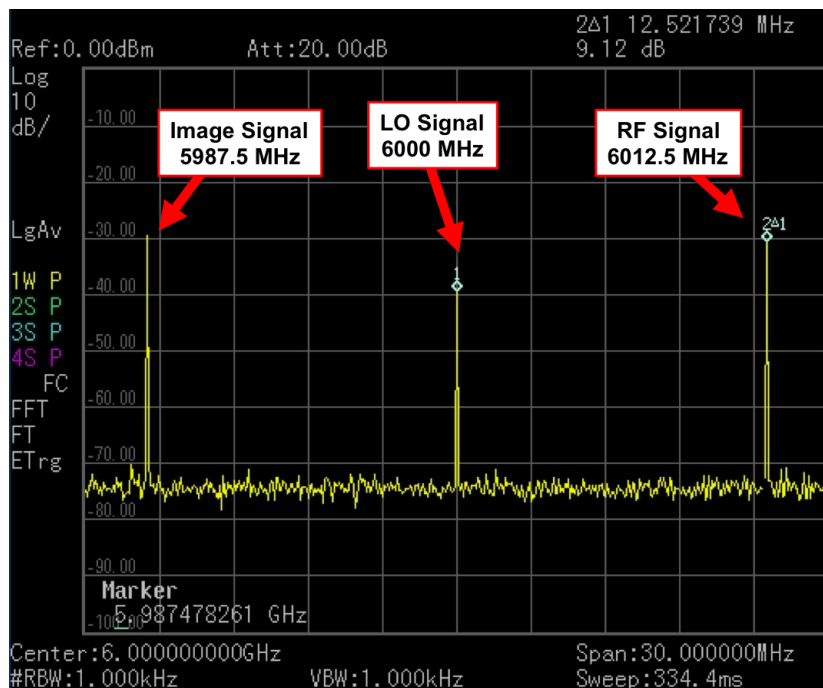


Figure 24: Frequency response for a single tone waveform modulated above 6000 MHz

4.1.4 Effects of the Amplitude Variable

The amplitude parameter impacts both the voltage and amplitude of signals sent to the DAC. Amplitude tests aimed to examine the effects of its behaviour on the system, and more specifically address the following:

- How do changes in the amplitude variable impact the output power of the signal?
- What amplitude values are suitable to avoid generating non-linear responses in the signal output?
- To verify that the signal undergoes distortion for amplitude values above 1, and observe the extent of the distortion.

It was expected that since the amplitude parameter directly impacts the voltage of the DAC, theoretically the output power should change by around -6 dB (i.e. a factor of four) each time the amplitude value is halved¹¹ [28, p.77].

Secondly, it was anticipated that as the amplitude parameter increased from 0 to 1, that the peak power will increase linearly until crossing a threshold, at which point the power response would become non-linear due to compression. Regions below this amplitude value should provide linear behaviour.

Thirdly, as stated earlier it was expected that signals above with an amplitude value above 1 will clip digitally, although the extent of the distortion caused will need to be examined in testing.

Single Tone Tests

These tests involved taking samples of the peak power of a single tone waveform at varying amplitudes to verify the predicted behavioural characteristics, and observe any anomalous behaviour.

As anticipated, each time the amplitude parameter was halved, the peak power dropped by approximately 6 dB in both the low band and high band. See Table 18 and Table 19 respectively. The exact power drop varied depending upon the RF frequency tested. The results at 5.6 GHz (see Table 19) almost perfectly matched the -6.02 dB theoretical response for each amplitude shift, whereas results at other frequencies showed greater fluctuation. This suggests that the power amplifier for the high band path, maybe optimised at LO frequencies around 5.6 GHz. No such optimal region was noticeable in the low band during these tests.

For amplitudes closer to 1, the change in peak power compressed to about 4 or 5 dB. Similarly, the RF noise skirt was significantly higher at these amplitudes as shown in

¹¹ Gain (dB) = $20\log(V2/V1)$, hence by halving the voltage the gain changes by approximately -6.0206 dB

Figure 25 and Figure 26. For the high band the noise skirt had notably increased by around 10 dB as the amplitude shifted from 0.5 to 1.

Raising the amplitude above 1 to 1.0001 caused the signal to distort significantly as predicted. The noise floor increased by around 5 to 20 dB, with harmonic noise spikes occurring approximately every 70 kHz. Additionally the Spurious Free Dynamic Range (SFDR) lowered from 49 dB to 33 dB for the low band, and from 51.5 dB to 35 dB for the high band.

Based on these observations the amplitude parameter for the XCVR2450 should be kept at a value well below 0.5 to optimise its impact on the signal to noise ratio, and to avoid non-linear output from the RF daughterboard. For single tone signals, 0.25 appears to be a suitable value.

Table 18 Amplitude reduction test results for a single tone waveform (low band)

Amplitude Reduction	RF Frequency (GHz)				
	2.40625	2.425	2.45	2.475	2.5
	Step Change in Output Power (dB) with Amplitude Reduction				
1 to 0.5	-4.74	-4.69	-4.69	-3.68	-4.72
0.5 to 0.25	-5.67	-5.76	-5.67	-5.68	-5.75
0.25 to 0.125	-5.95	-5.94	-5.96	-6.01	-5.87
0.125 to 0.0625	-5.98	-5.96	-5.96	-6	-6.09
0.0625 to 0.03125	-6.08	-6.02	-6.07	-6.01	-6.02

Table 19 Amplitude reduction test results for a single tone waveform (high band)

Amplitude Reduction	RF Frequency (GHz)						
	4.90625	5	5.2	5.4	5.6	5.8	6
	Step Change in Output Power (dB) with Amplitude Reduction						
1 to 0.5	-4.7	-4.8	-4.85	-4.81	-6.01	-4.77	-4.71
0.5 to 0.25	-6.02	-6.03	-5.94	-5.99	-6.01	-6.04	-6.03
0.25 to 0.125	-6.09	-6.03	-6.05	-6.03	-6.04	-6.05	-6.1
0.125 to 0.0625	-6.04	-6.14	-6.12	-6.04	-6.09	-6.01	-5.97
0.0625 to 0.03125	-5.98	-5.71	-5.94	-6.04	-6.02	-6.16	-5.92

Power vs Frequency for various Amplitudes
(Single Tone Signal, RF 2450MHz, LO 2493.75MHz)

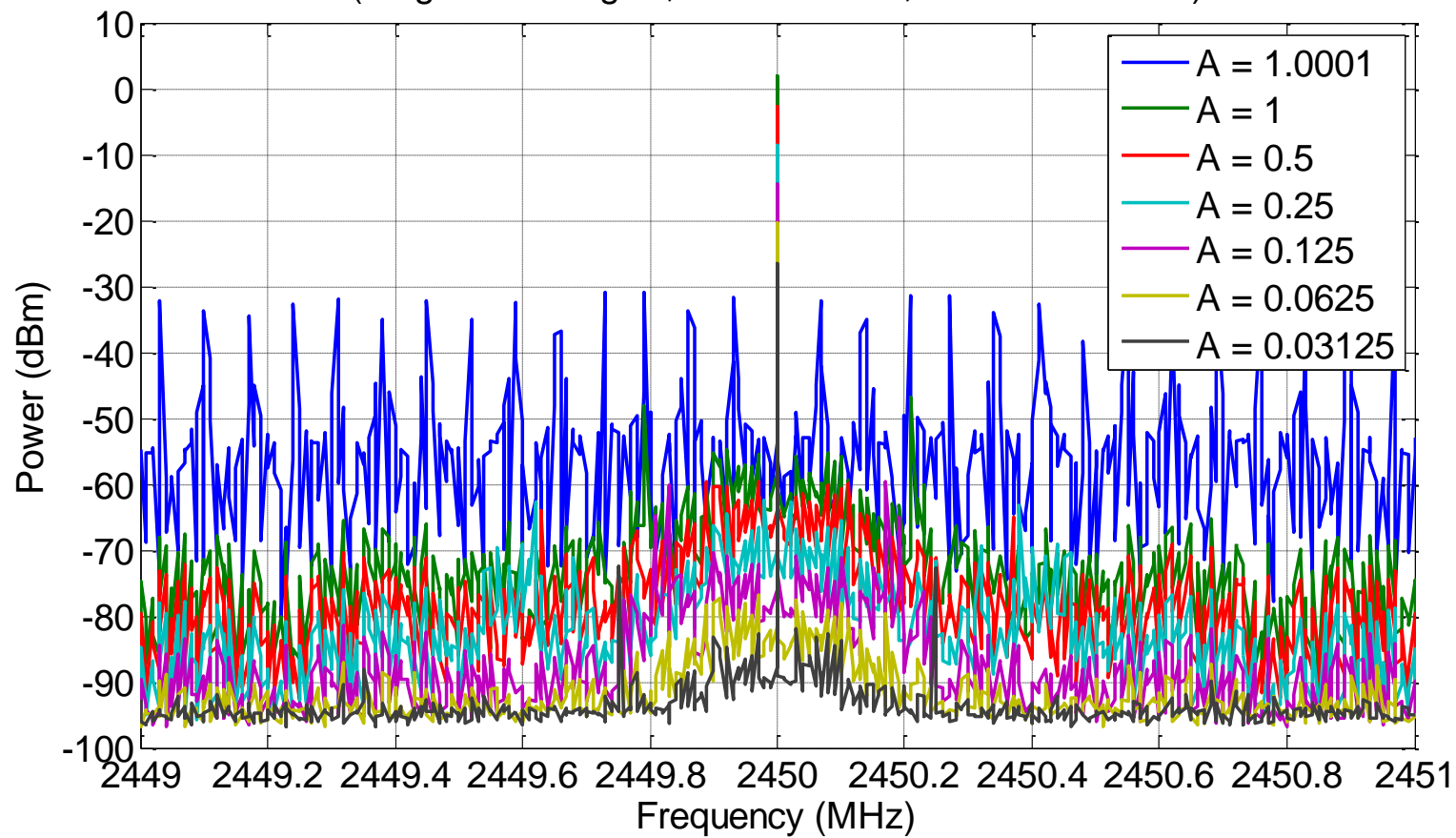


Figure 25: Single tone waveform response to various amplitude values (low band)

Power vs Frequency for various Amplitudes
(Single Tone Signal, RF = 5400MHz, LO = 5393.75MHz)

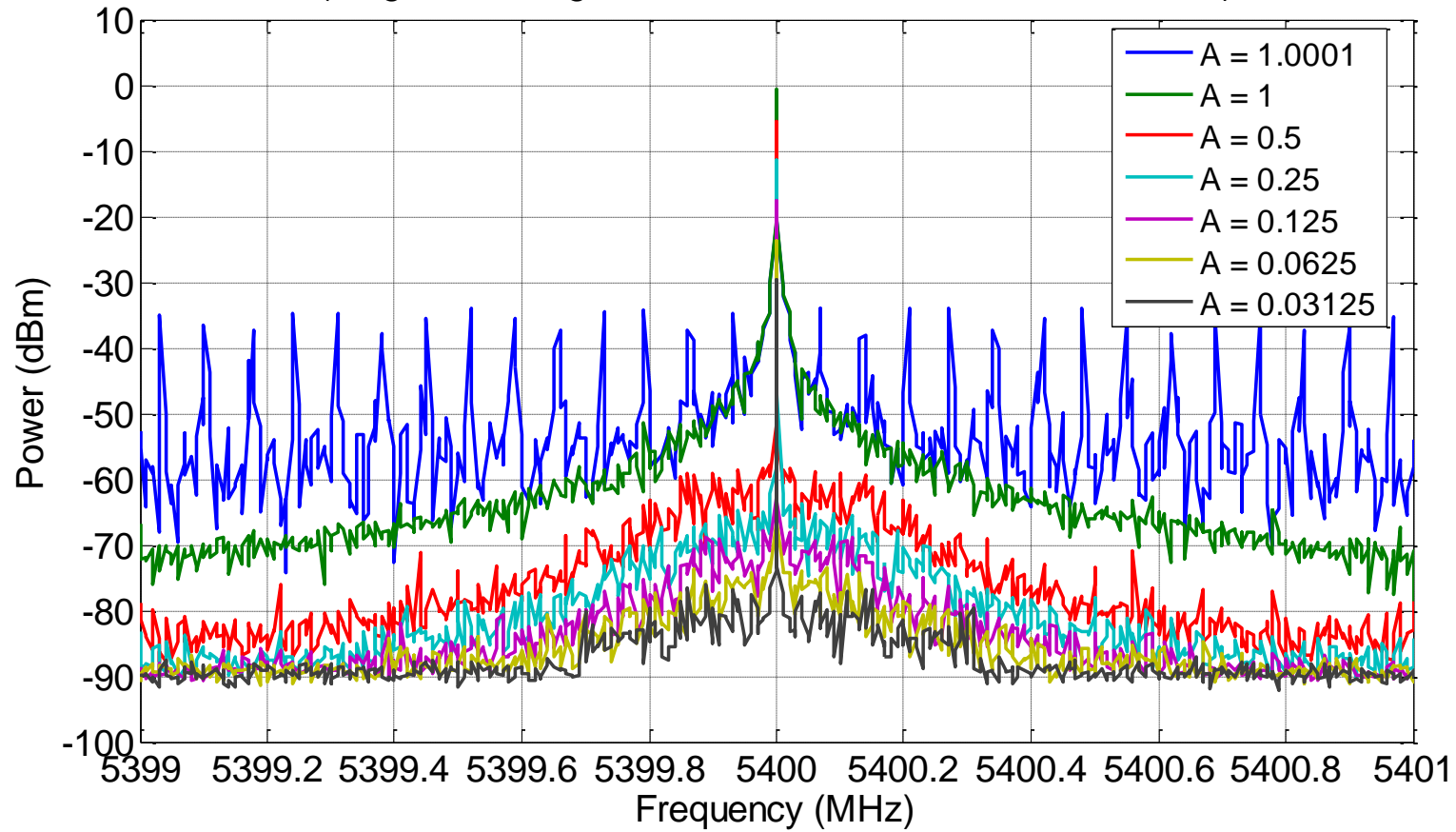


Figure 26: Single tone waveform response to various amplitude values (high band)

Two Tone Tests

Additional tests were conducted in the centre of the low and high bands using the two tone test waveform. As with the single tone test results the change in output power remained at approximately -6 dB each time the amplitude value was halved, as shown in Table 20 and Table 21.

The notable difference observed in the two-tone test signal is that the amplitude threshold for distortion appeared to be 0.5 as shown in Figure 27 and Figure 28. As the maximum amplitude of the two-tone test signal is the summation of the 0.5 amplitudes of the two individual tones¹² this threshold is still consistent with the expected maximum amplitude of 1. For amplitudes of 0.51 or above the intermittent flashes of noise appeared across the spectrum analyser raising the noise floor by approximately 25 dB. The presence of the intermittent noise flashes appeared more prominently for increasing amplitude values above 0.51. This is attributed to the fact the summation of the sinusoidal amplitudes exceeds 1 on a more frequent basis for higher amplitude values. A spot check was conducted using a summation of 3 test tones. Flashes of noise appeared for amplitude values of 0.34 or higher, which is consistent with the theory that the flashes of noise are caused by superposition of the amplitudes periodically exceeding the maximum of 1.

Ideally during a two tone test, the power of inter-modulation products IM1 and IM2 will shift according to a linear 3:1 ratio, i.e. each 1dB shift in the input power should cause a 3 dB shift in power of IM1 and IM2 [37]. This linear response is expected when the power of the IM1 and IM2 are around 10 dB above the noise floor. Thus, in this region halving the amplitude should cause a -18 dB response¹³.

In the low band, the power response of IM1 and IM2 was roughly of a 3:1 ratio for amplitude shifts between 0.5 and 0.125. At lower amplitude values the power drop reduced below the linear 3:1 ratio. This is expected, given that at lower amplitude values, these tones had lowered close to the noise floor (Figure 27).

In the high band, IM1 and IM2 were highly suppressed, being close to the noise floor for amplitudes of 0.25 and beneath the noise floor at lower amplitudes (Figure 28). At the maximum useable amplitude of 0.5, IM1 and IM2 were 30 dB lower in the high band than they were in the low band.

As with single tone tests, observations show that the amplitude parameter should be kept at a value well below 0.5 for two-tone signals, with 0.25 appearing to be a suitable value. Additionally, the power amplifier in the high band path appears to generate lower inter-modulation products than the one in the low band path.

¹² Periodically the two peak signal amplitudes of 0.5 will combine to equal a peak of 1

¹³ As halving the amplitude should lower the input power by $-6.0206 \text{ dB} \times 3 = -18.0618 \text{ dB}$

Table 20 Amplitude reduction test results for a two tone waveform (low band)

Amplitude Reduction	RF Frequency (MHz)			
	IM1	F1	F2	IM2
	2453	2454	2455	2456
Step Change in Output Power (dB) with Amplitude Reduction				
1 to 0.5	-16.28	0.94	1.24	-16.98
0.5 to 0.25	-17.16	-5.09	-5.1	-17.83
0.25 to 0.125	-16.56	-5.8	-5.79	-20.83
0.125 to 0.0625	-13.9	-5.96	-5.96	-11.35
0.0625 to 0.03125	-3.14	-6.01	-6.01	-1.85

Table 21 Amplitude reduction test results for a two tone waveform (high band)

Amplitude Reduction	RF Frequency (MHz)			
	IM1	F1	F2	IM2
	5403	5404	5405	5406
Step Change in Output Power (dB) with Amplitude Reduction				
1 to 0.5	-39.05	7.64	7.89	-37.78
0.5 to 0.25	-12.33	-6.02	-5.51	-13.23
0.25 to 0.125	Noise Floor	-5.77	-6.76	Noise Floor
0.125 to 0.0625	Noise Floor	-6.1	-5.3	Noise Floor
0.0625 to 0.03125	Noise Floor	-6.13	-6.53	Noise Floor

Output Power vs Frequency for various Amplitudes
(Two Tone Signal, F1 = 2454MHz, F2 = 2455MHz, LO = 2450MHz)

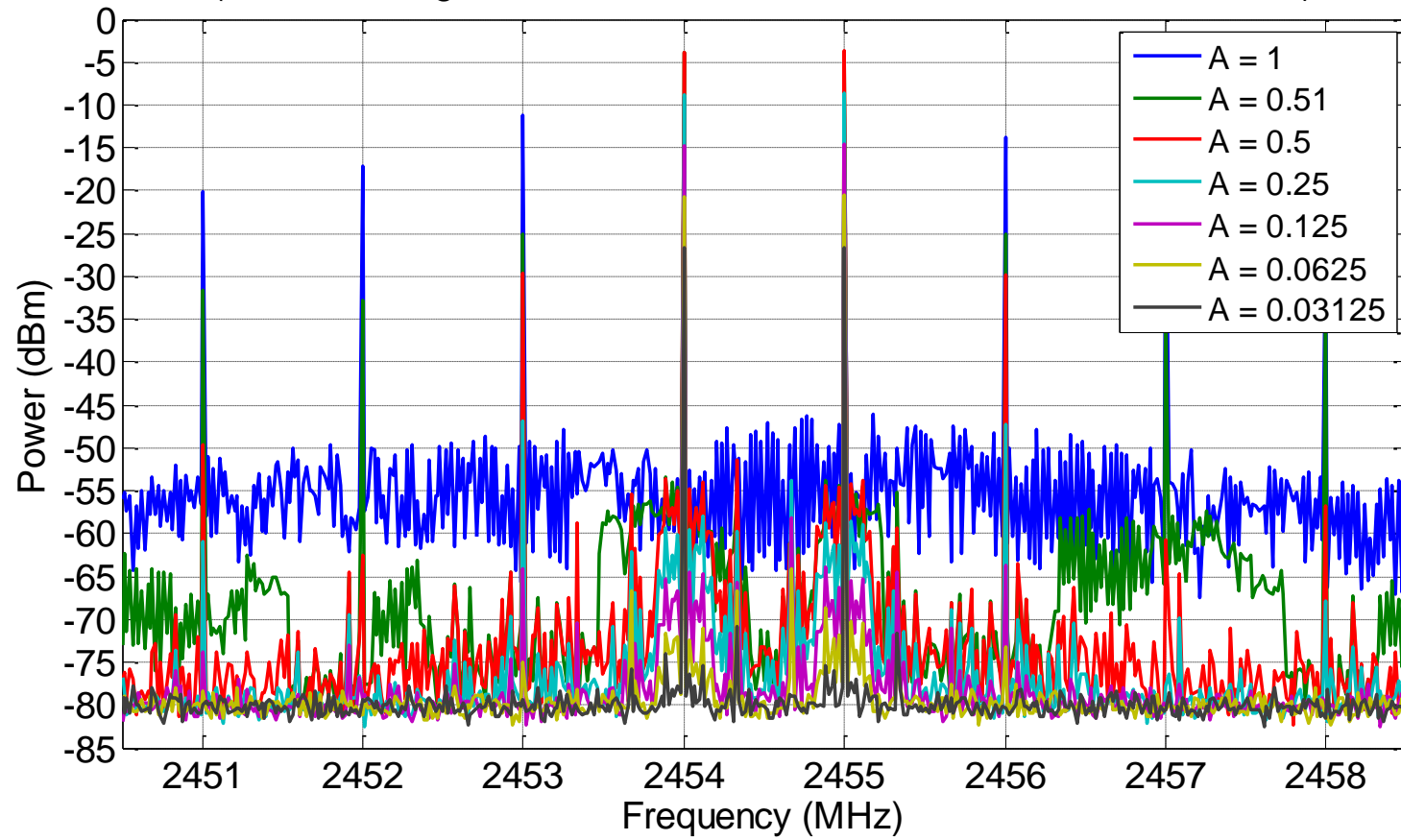


Figure 27: Two tone waveform response to various amplitude values (low band)

Output Power vs Frequency for various Amplitudes
(Two Tone Signal, F1 = 5404MHz, F2 = 5405MHz, LO = 5400MHz)

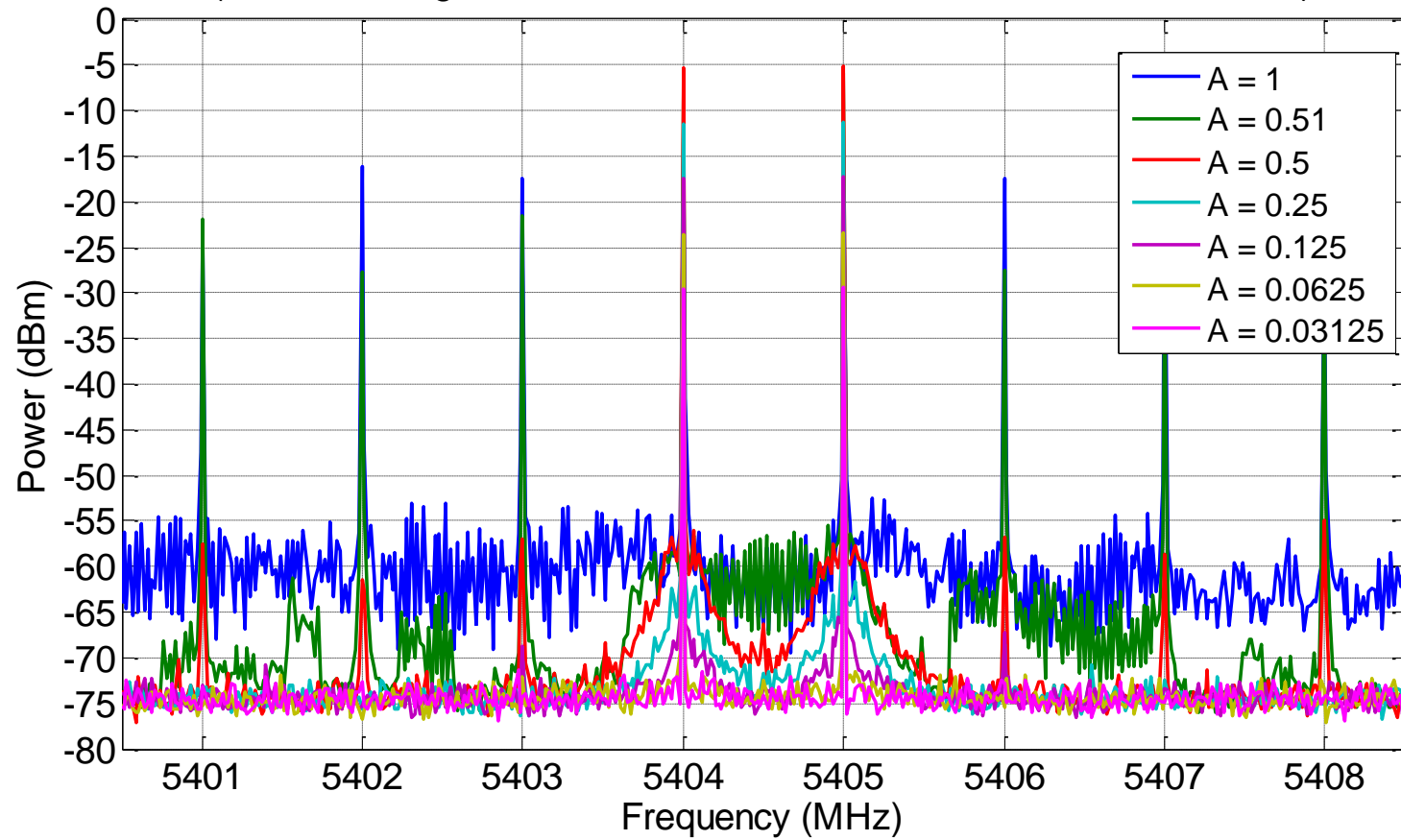


Figure 28: Two tone waveform response to various amplitude values (high band)

4.1.5 Effects of the Gain Request Variable

These tests aimed to observe the impact of the gain variable on the signal output, to observe any regions exhibiting non-linear behaviour and identify the maximum output power achievable. A maximum output power of 0.1 Watts (20 dBm) is expected, with compression (if any) occurring close to this region.

USRP Gain Control

As discussed earlier a 35 dB gain range is achieved by the MAX2829 transceiver component, which involves combining a 30 dB Voltage Gain Amplifier (VGA) gain and 5 dB baseband gain [34]. It is unclear how the GRC assigns a gain input request between these two gain sources. Examining the GNU Radio and UHD source code, along with information from the MAX2829 datasheet provides insight on what the gain responses from these two sources should look like, as shown in Figure 29. The 30 dB VGA gain is increased in 1dB steps, using 0.5 dB steps for values greater than 22.5 dB. The 5 dB baseband gain is implemented in gain step bins of 0 dB, 2 dB, 3.5 dB then 5 dB. These distinctions between the two may be distinguishable during testing.

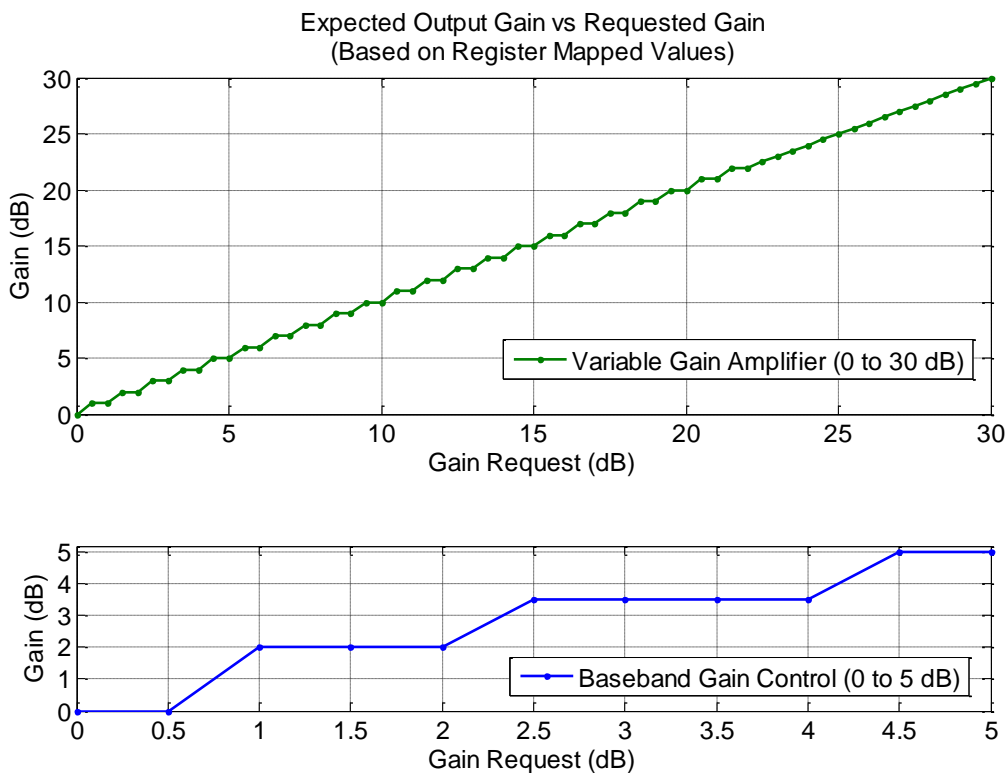


Figure 29: Expected gain response for the two individual gain sources in the XCVR2450

Stepped Gain Testing

For this set of tests the defined single tone waveform was used with the amplitude parameter set to 0.25 based upon the outcomes of the previous amplitude tests. Tests were conducted in the centre of the low and high bands, with the gain parameter varied from -5 dB to 38 dB in 0.5 dB steps. The maximum output power was measured for the desired RF, the LO frequency and the image frequency mirrored on the opposite side of the LO frequency. Although the gain response may differ for different frequencies in the each band, these tests will provide an understanding of what results to expect.

The low band gain test (Figure 30) showed a linear response that was consistent across the three frequencies measured. A change in output power only occurred for gain parameter inputs between 0 and 35 dB as expected, however the total output power only increased by a maximum of about 28.5 dB across this range.

As the gain parameter input was increased, changes in the output power were only observed every 1 dB, until reaching 22.5 dB at which point the output power responded to 0.5 dB increases, which is consistent with the stepping pattern observed for the VGA in Figure 29. As the gain parameter increased from 30 to 35 dB the step response appeared similar to those shown for the BB gain control (Figure 29). This shows that the gain requests are implemented using the VGA first, with the baseband gain control used to achieve values greater than 30 dB. The maximum output power achieved was 20 dBm and is consistent with the quoted value for the RF daughterboard (e.g. 0.1 W).

The high band gain test produced a similarly linear response for the three measured frequencies as the gain parameter increased to 23 dB (Figure 31). The power of the RF signal continued to increase as the gain parameter increased further, but the response became non-linear, approaching an asymptote limit at 20 dBm. During this region, the power increase for the LO and the image signals plateau heavily, even lowering as the gain parameter exceeded 30 dB. The total output power across the gain parameter range increased by a maximum of about 31dB.

Comparing the response of the low band and high band tests highlights the following observations. In operation the USRP gain output received may not match the gain request, as shown in the low band testing. The maximum gain cannot be determined from this set of tests as the output power reaches the maximum before the full gain is applied¹⁴. Furthermore, non-linear behaviour may be observed as the output power approaches the 20 dBm (0.1 W) maximum.

¹⁴Further testing in Section 4.1.6 will show that the maximum gain was measured at 28dB for the low band and 35dB for the high band.

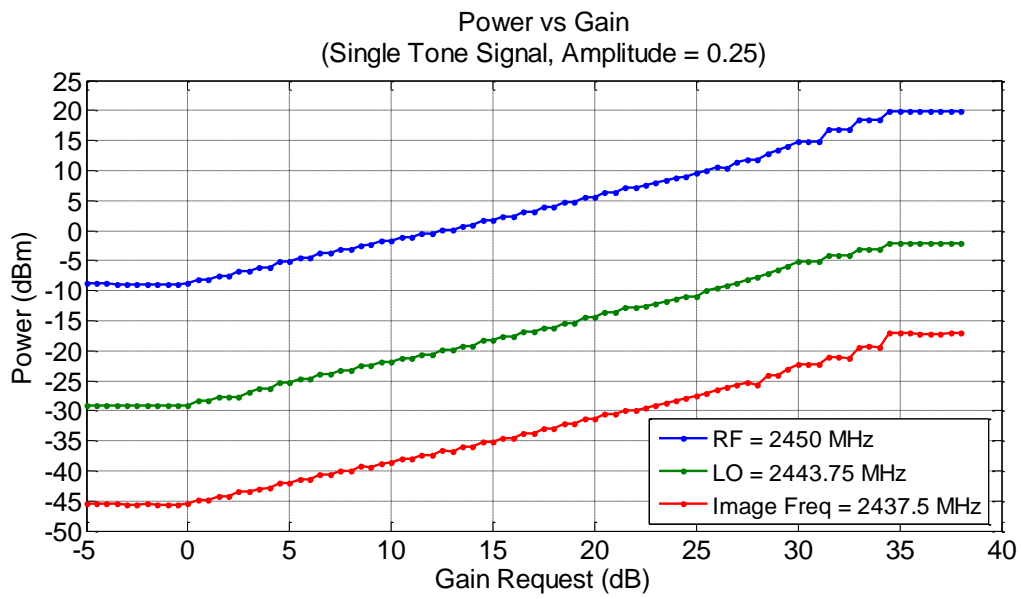


Figure 30: Stepped gain test results for a single tone waveform (low band)

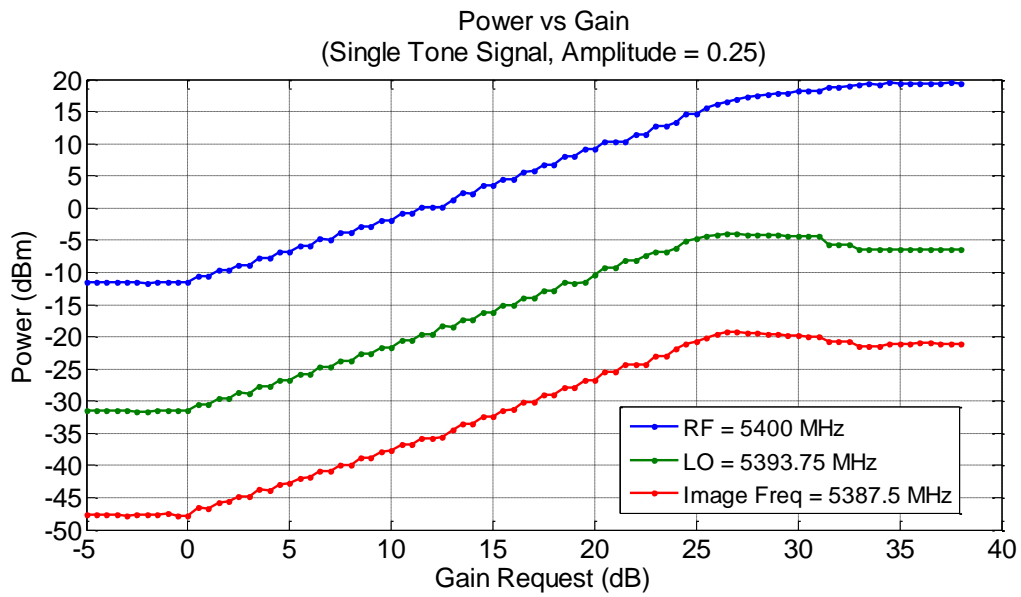


Figure 31: Stepped gain test results for a single tone waveform (high band)

Observations in the Frequency Spectrum

Data was recorded for the output of a single tone waveform across a 100 MHz span, for various gain values in the low band and high band. See Figure 32 and Figure 33 respectively. As observed in the previous set of tests, the RF, LO and image signal power values increase steadily as the gain increases. A large number of spurs are observed in both the low and high band spectrums. The larger spurs spaced at multiples of the baseband frequency (6.25 MHz) are harmonic frequencies¹⁵, and drop in power as they increase in distance from LO frequency. The other spurs appear to be inter-modulation products that can be seen increasing rapidly as the gain increases. More of these appear in the results for the low band, along with much wider noise skirting and side-lobes as the gain increases.

Distortion effects at higher gain values can be seen in the image frequencies (notably the largest spur to the right of the each RF signal). The rate, at which these spurs increase in size with gain, rises significantly at higher gain values suggesting that these are the result of intermodulation. This is seen for the gain increase from 30 dB to 35 dB in the low band results, and 25 dB to 30 dB in the high band results. This is consistent with the gain region where non-linear effects are observed previously in Figure 30 and Figure 31.

¹⁵ $f_{harmonic} = f_{RF} \pm n \times f_{BB}$, where n is an integer

Power vs Frequency for various Gains
(Single Tone Signal, RF = 2456.25MHz, LO = 2450MHz)

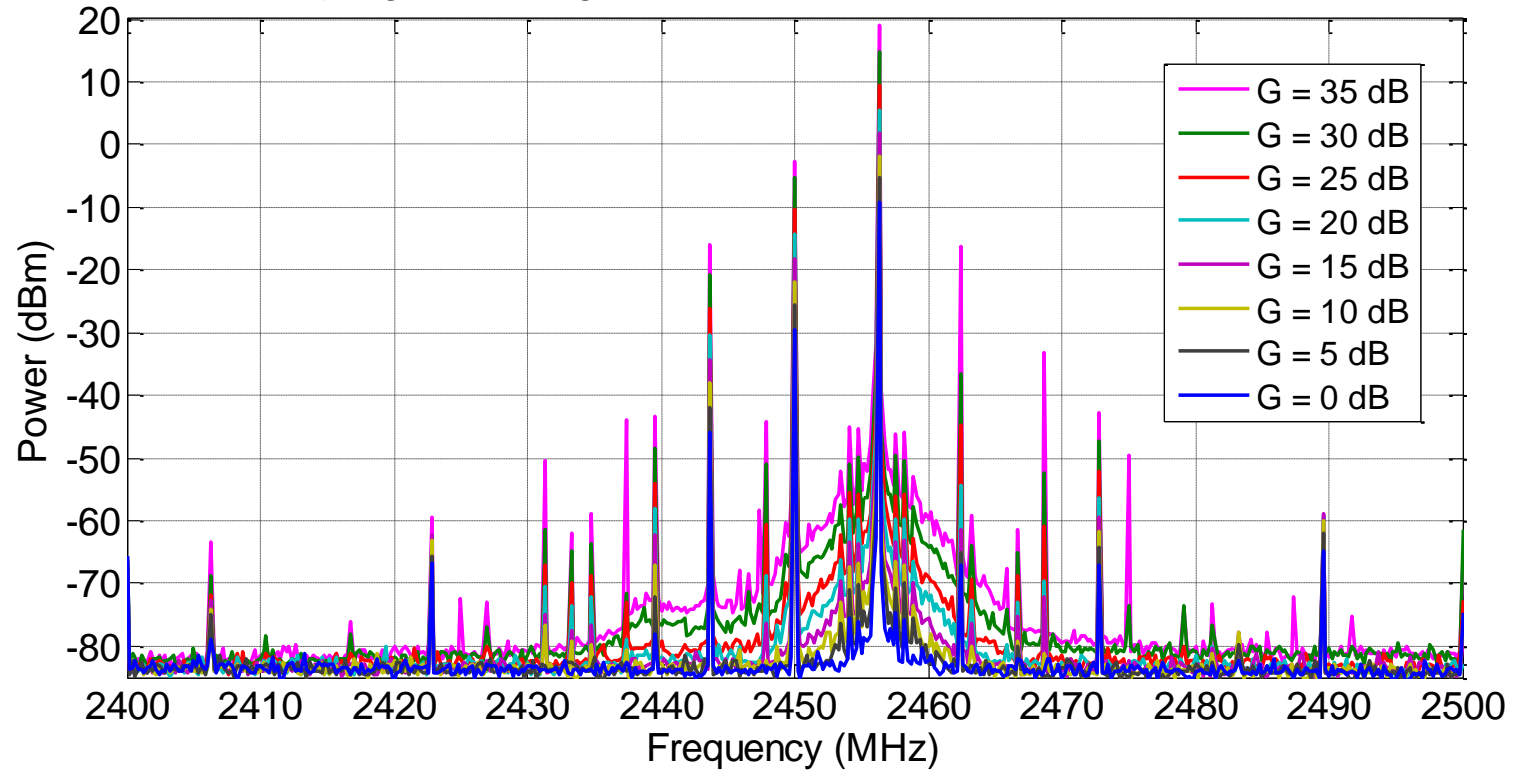


Figure 32: Single tone waveform response to various gain values (low band)

Power vs Frequency for varying Gains
(Single Tone Signal, RF = 5406.25MHz, LO = 5400MHz)

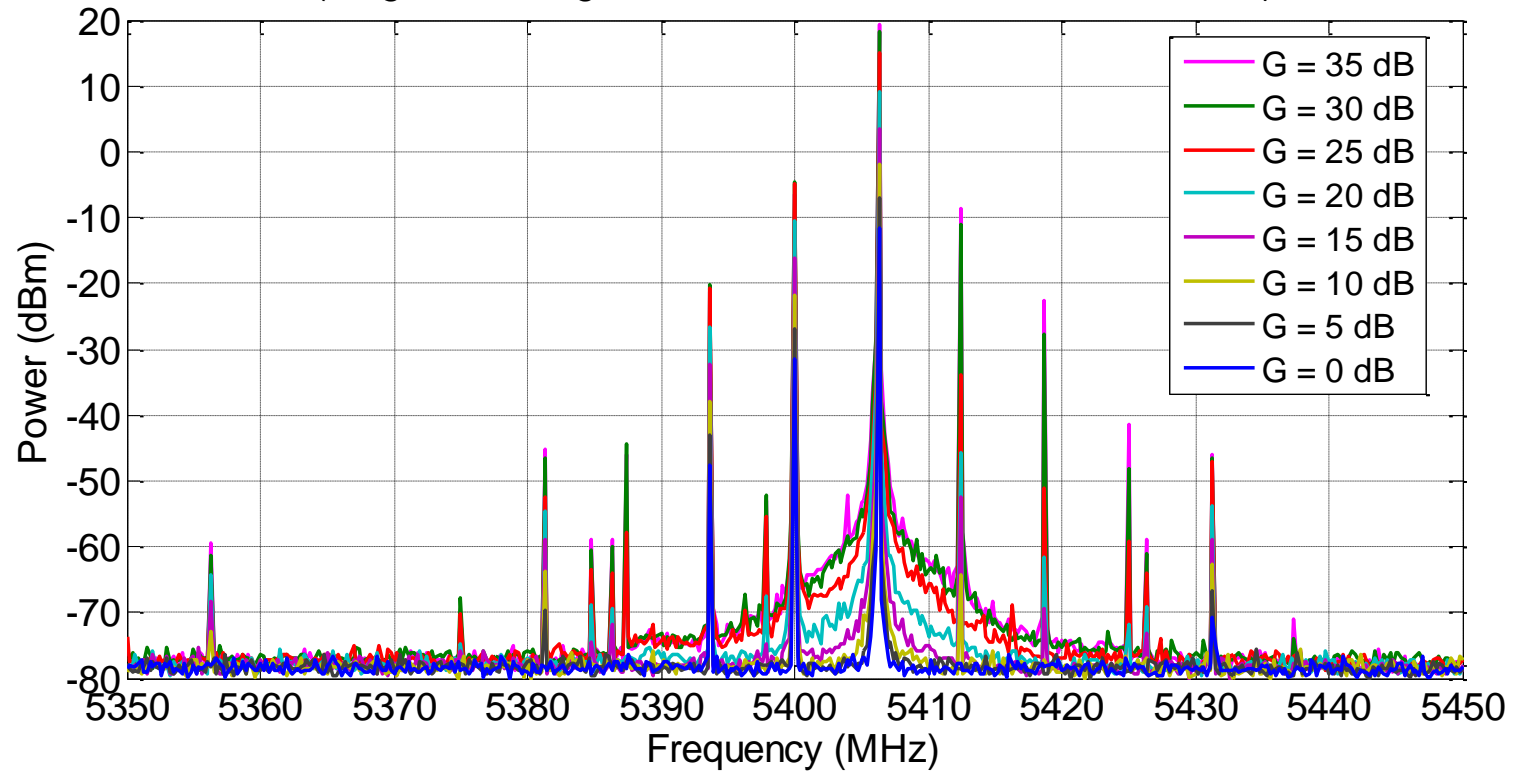


Figure 33: Single tone waveform response to various gain values (high band)

4.1.6 Power versus Gain Request and Amplitude Variables

The separate gain and amplitude tests showed the characteristic effects of these variables on the USRP output in isolation. They further demonstrated that the USRP output may be subject to non-linear behaviour if either of these variables is set too high.

This set of tests aims to observe the combined effects of these variables on the output power. It is believed that these variables operate independently to each other, and that the changing both of these variables will not result in any unexpected behaviour.

A single tone waveform was used in these tests with the RF signal placed at 2.45 GHz and 5.4 GHz as previously done in the individual gain and amplitude tests. This time the power of the RF signal is measured at gain steps of 5 dB, with the amplitude parameter progressively halved as before.

The results seen in Figure 34 and Figure 35 match the results obtained in isolated amplitude and gain tests. Firstly, the gain increased at the same linear rate regardless of the selected amplitude value. Secondly, each time the amplitude was halved, the output power reduced by 6 dB. As before, this change in power compressed to values of 4 or 5 dB for amplitudes closer to one. Thirdly, the output power did not exceed the stated 20dBm maximum for the device and the response became non-linear when increases in the amplitude and gain parameters caused the output to approach this limiting value. During these tests a maximum gain was observed of 28 dB for the low band and 35 dB for the high band.

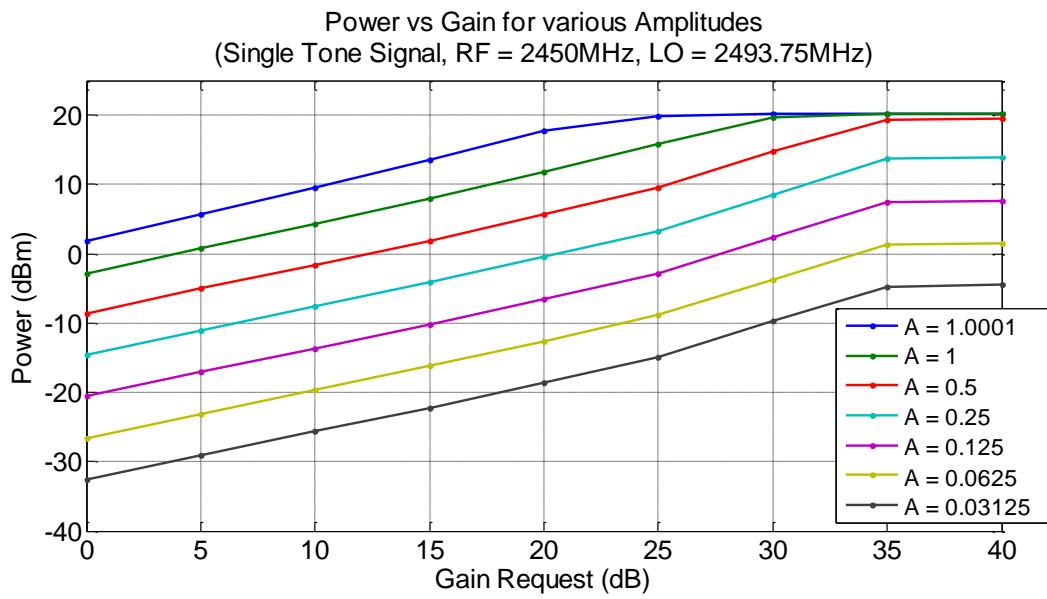


Figure 34: Gain and amplitude test results for a single tone waveform (low band)

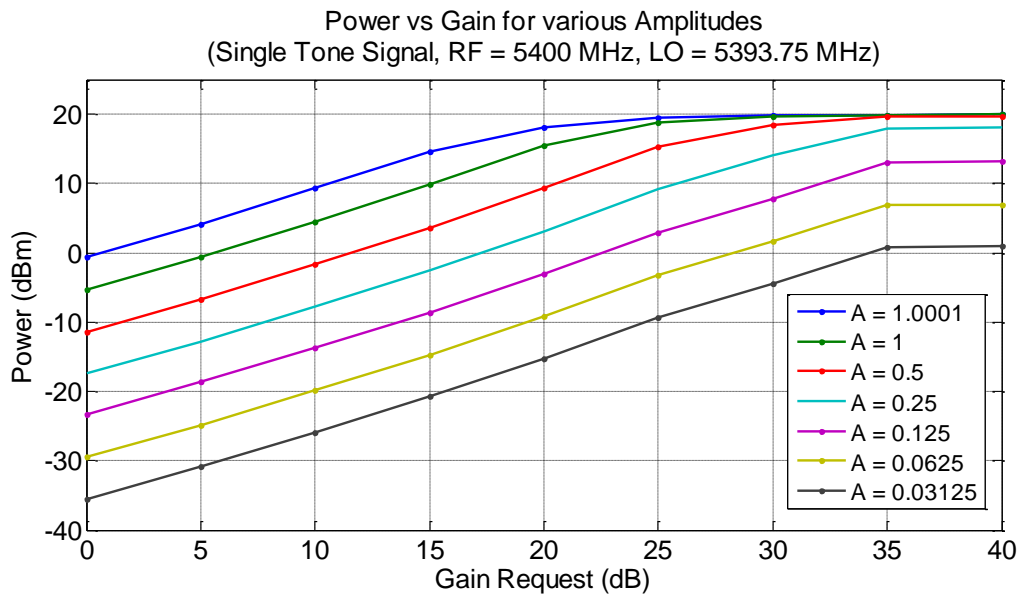


Figure 35: Gain and amplitude test results for a single tone waveform (high band)

4.1.7 Power versus RF Frequency

These tests were designed to examine how the output power of the USRP varied as a function of the waveform frequency in each band.

Examining the XCVR2450 schematic [38] shows that the two main components whose performance is expected to impact the transmit power in both bands, are the MAX2829 Transceiver and the subsequent IRM406U power amplifier.¹⁶

Figure 36 shows plots of the transmit power versus frequency obtained from the manufacturer datasheet for the MAX2829 Transceiver. These suggest that the power output in the low band will remain relatively consistent across the band, whereas a difference of up to 4dB is expected for the high band. The IRM406U data sheet does not provide info of its output power of the frequency bands, but indicates that the output may vary by 3dB between its minimum and typical values [39].

NOTE:
This figure has been removed due to copyright.
Alternatively, the item is available from the referenced links

Figure 36: Transmit power plots for the low band (left) and high band (right) from the MAX2829 Transceiver datasheet [39]

¹⁶ A single IRM406U amplifies signals in both bands despite being presented as two separate amplifiers in the Figure 5 block diagram.

Tests used the single tone waveform and involved shifting the placement of an RF signal at regular intervals across each frequency band. The gain and amplitude remained at 0 and 0.25 respectively.¹⁷

Low band results (see Figure 37) show the output power increased almost linearly by 4 dB across the band, whereas the response (at least from the MAX2829 component) was expected to be reasonably constant. For the high band (see Figure 38), the output power was typically consistent in the centre of the band (i.e. between the data points at 5350 and 5650 MHz). Beyond this region the power reducing linearly by about 8 or 8.5 dB at the band limits, rather than the 4dB shift expected.

Both sets of results show approximately a 4 dB maximum deviation from what was indicated in Figure 36. Assuming the potential variation in the power amplifier output accounts for 3dB, this leaves a 1 to 1.5 dB discrepancy, which is the ball park of a reasonable deviation from what the datasheets indicate. Nonetheless, the results indicate that other hardware components in the chain are causing losses and changes in performance across each frequency band, beyond what the datasheets for the main component indicate.

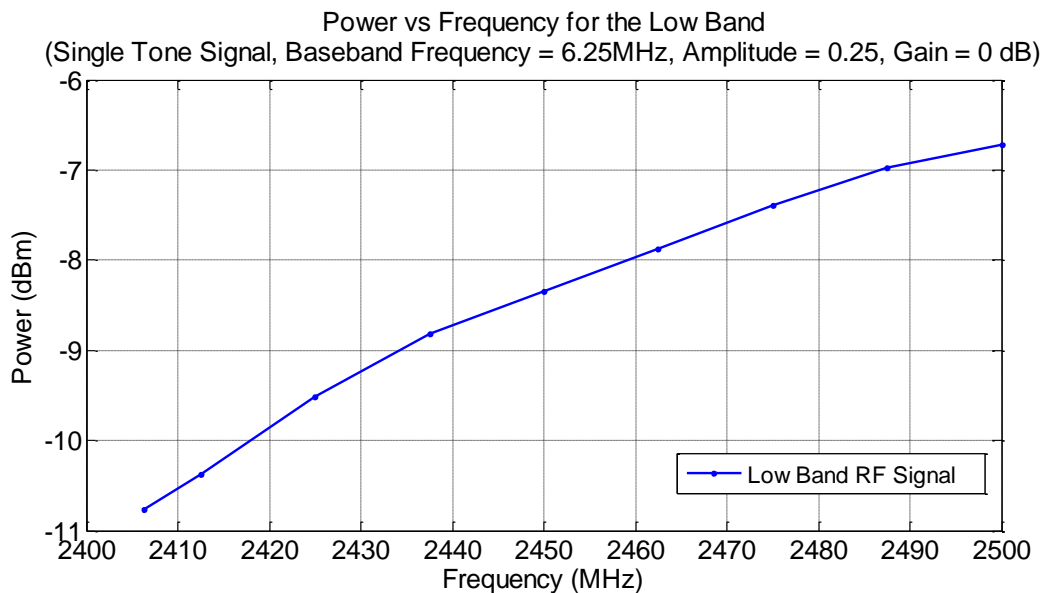


Figure 37: Peak power vs. frequency test results for a single tone waveform (low band)

¹⁷ Note: Measurements begin 6.25 MHz above the lower limit in each band since there is a +6.25 MHz offset between the LO and the RF, and the LO frequency cannot go below the lower band limits.

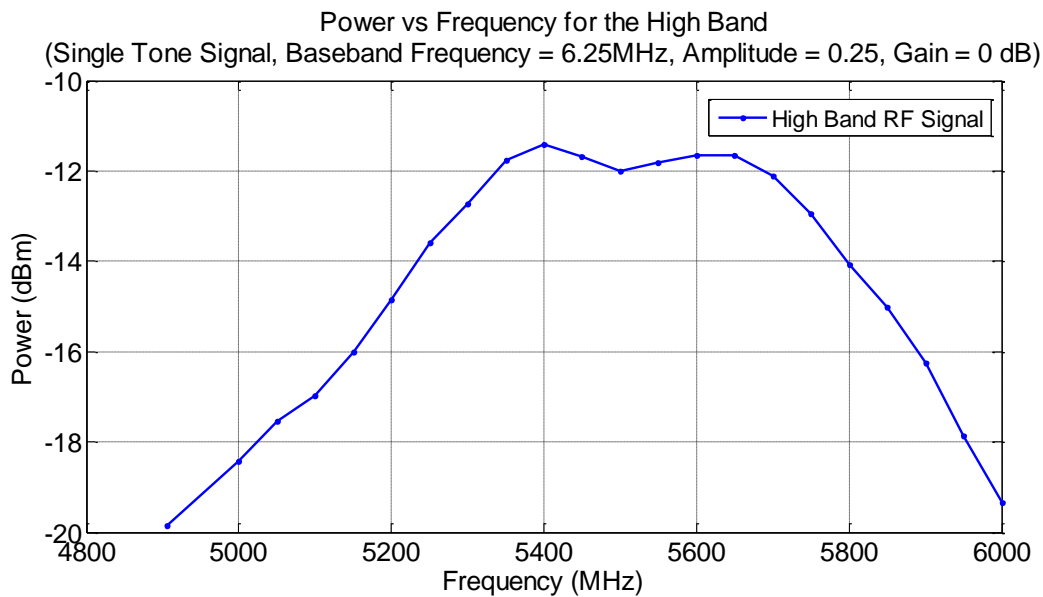


Figure 38: Peak power vs. frequency test results for a single tone waveform (high band)

4.1.8 Effects of the Baseband Filter

This set of tests aims to further characterise the extent to which the output power of a single tone waveform changes as a function of the baseband frequency offset. Additionally it examines how the output is impacted by both the selection of the MBW and also the size of the baseband filter.

The output power of the RF signal is expected to reduce the further it is offset from the LO frequency, and to drop quickly as it approaches the boundaries of the MBW. It is unclear as to what the shape of the power curve will be.

The baseband filter is a low-pass filter implemented in the MAX2829 transceiver. It is a half band Finite Impulse Response (FIR) filter. According to the datasheet [34, p.10], the filter sizes of 24 MHz, 36 MHz and 48 MHz available during transmission refer to 3 dB band-pass filter ranges, centred at a baseband frequency of 0 MHz. As such it is expected that as the RF signal approaches these boundaries it will drop by 3 dB.

Note: Tests in this section focus on the signal at the desired RF. In many cases, measurements are taken beyond the boundaries of the MBW or filter, to obtain an understanding of the effects of these variables. It is important to highlight that in practice, frequencies beyond these boundaries cannot be used due to the presence of strong image signals, or folded RF / image signals that are not the focus of this test section.

Unfiltered¹⁸ Output Response

Initial tests were conducted in the low band with the local oscillator tuned to 2443.75 MHz for consistency with previous testing. The baseband frequency was varied from 0 to the MBW limits and beyond, with the signal power measured at the RF. The sample size remained at 8-bit complex for most tests so that higher bandwidths of up to 50MSps could be explored. The filter size was maximised to 48 MHz so that the output response could be observed without interference from the baseband filter. An amplitude of 0.25 and a gain of 0 dB were used for all tests.

Tests were conducted for MBW values of 5, 15, 20, 25 and 33 MHz as shown in Figure 39. The power curve for each MBW had a parabolic shape, including a noticeable reduction in the RF signal power well before the baseband frequency had approached the boundaries of the MBW. In most cases the shape of the parabola became wider with a greater plateau response as the MBW increased. The exception to this applied to the 25 MHz MBW, which resulted in a plateau response with a very sharp roll-off at the edges.

Filtered Output Response

To examine the impact of the filter on the output signal, further tests were conducted where the filter was set to sizes smaller than that of the MBW. These results are provided in Figure 40. The impact of the 24, 36 and 48 MHz filter can be clearly seen creating a sharp tent shaped roll-off to the plateau response from the 50 MHz MBW power curve. The 3 dB cut off bandwidth frequencies were measured as 23, 33 and 42 MHz respectively.

Comparing the unfiltered 25 MHz MBW curve to the 24 MHz filtered version, showed very similar responses since the filter boundaries are close to those of the MBW. Comparing the unfiltered 33 MHz MBW curve to the 24 MHz filtered version, shows distinctly different responses. The filtered version has a parabolic shape for frequencies between ± 11 MHz, before undergoing a sharp tent shaped roll-off for frequencies beyond these bounds. The unfiltered version of this signal, maintains its parabolic shape until reaching ± 16.666 MHz, at which point it undergoes a sudden change in parabolic shaped rolls off due to exceeding the boundaries of the MBW.

¹⁸ Unfiltered, in this context implies that the filter was set to a 48 MHz size, considerably larger than the modulation bandwidth of the signal so that it ideally does not interfere with the signal output.

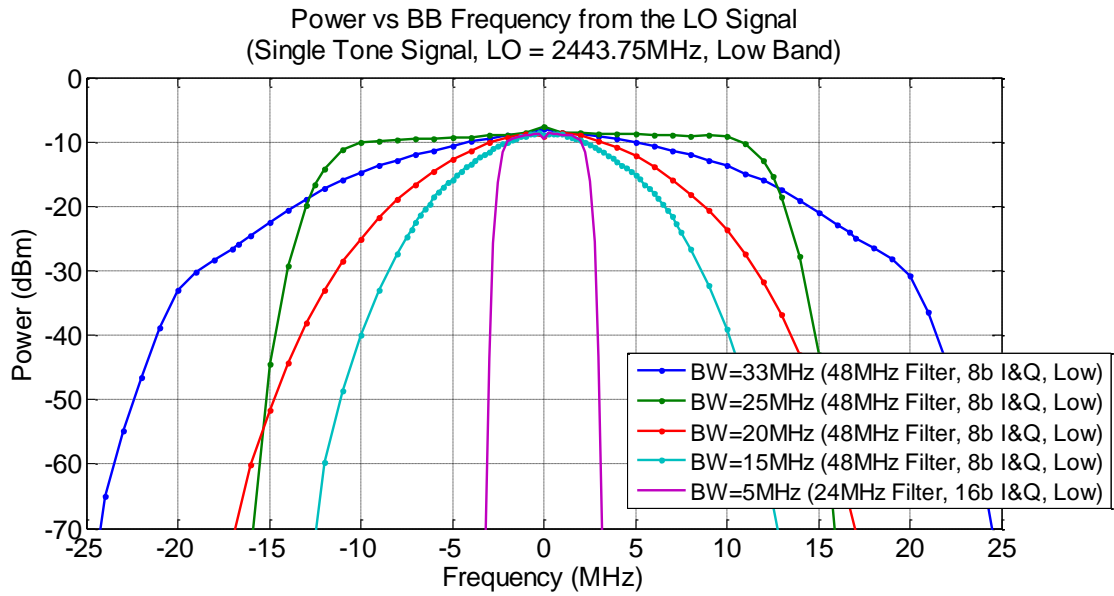


Figure 39: Baseband frequency offset test results – Response of unfiltered single tone waveforms (low band)

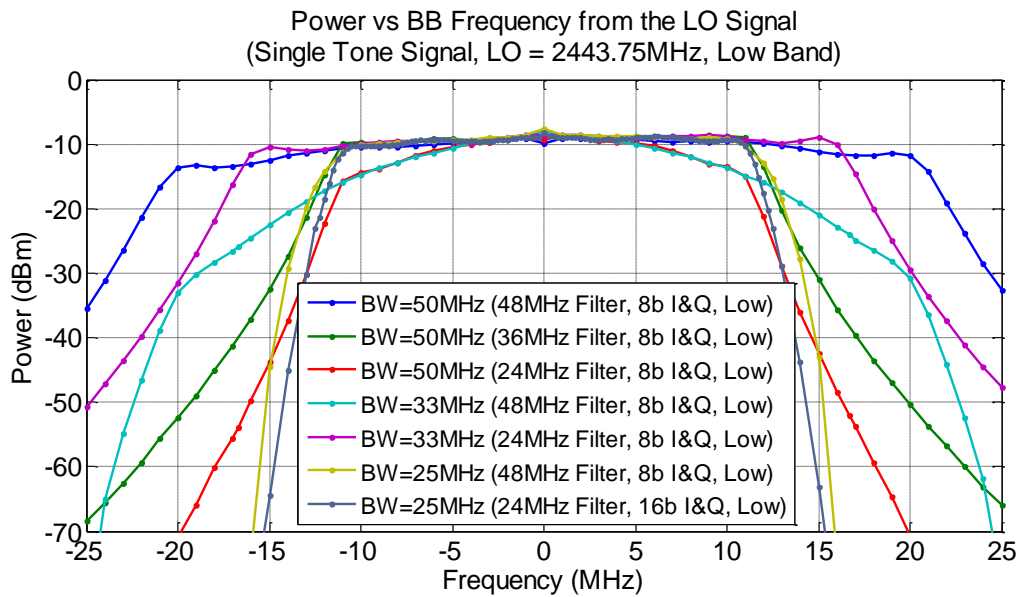


Figure 40: Baseband frequency offset test results – Response of filtered and unfiltered single tone waveforms (low band)

Low vs. High Band Response

Some brief testing was performed with the LO tuned to 5393.75 MHz to verify that similar behaviour was observed in the high band and the low band. The results are shown in Figure 41 and Figure 42. The observed behaviour was the same in both bands except that the output power for low band results was generally 3 dB higher than that in the high band. The noise floor remained consistent throughout all tests remaining at around -80 dB for high band tests, and -85 dB for low band tests.

Throughout the various tests, it was noticed that some ripples were observed in the pass-band of the filtered power curve. This was particularly apparent in Figure 41, and can be observed at baseband frequency offsets of 0, where the signal occasionally peaked or dropped by 1dB. These are believed to be side effects of the half band filter.

Noise Output Response

Wide band Gaussian noise (as previously defined) was generated across the frequency spectrum as an alternate method of observing how the filter size shapes the output.

Results are shown in Figure 43, but are believed to be limited in applicability to noise only, and not to tone signals. The noise power curve takes a parabolic shape and drop off sharply at frequencies approaching the filter limits of $\pm f_{baseband\ filter}/2$, however the reduction observed was much larger than 3 dB approaching these values. Another key observation from this test is the presence of spurs observed at frequency values offset from the LO frequency by ± 25 MHz, ± 33.33 MHz and ± 50 MHz, which appeared at up to 20 dB above the noise floor.

It is unknown as to why these spurs appear, however they occur at frequency offsets twice that of some of the MBW limits identified earlier¹⁹. As such, these noise spurs are believed to be harmonics likely to be observed at multiples of the available MBW limits. Additionally, these appear beyond the limits of the baseband filter, thus could potentially interfere with out of band receivers.

¹⁹ Test results shown in Table 17 earlier, identified that some of the achievable sampling rates for the USRP include values of 25 MHz, 33.33 MHz and 50 MHz, which would generate modulation bandwidth limits at frequency values of ± 12.5 MHz, ± 16.66 MHz and ± 25 MHz respectively.

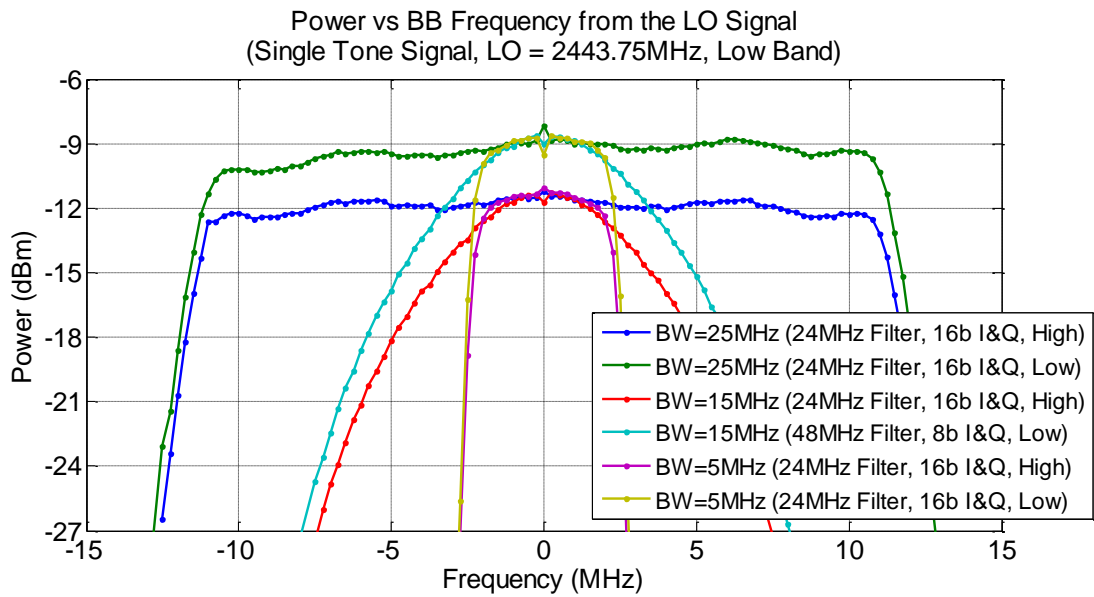


Figure 41: Baseband frequency offset test results - Comparison of low band and high band single tone responses for offsets up to 25 MHz

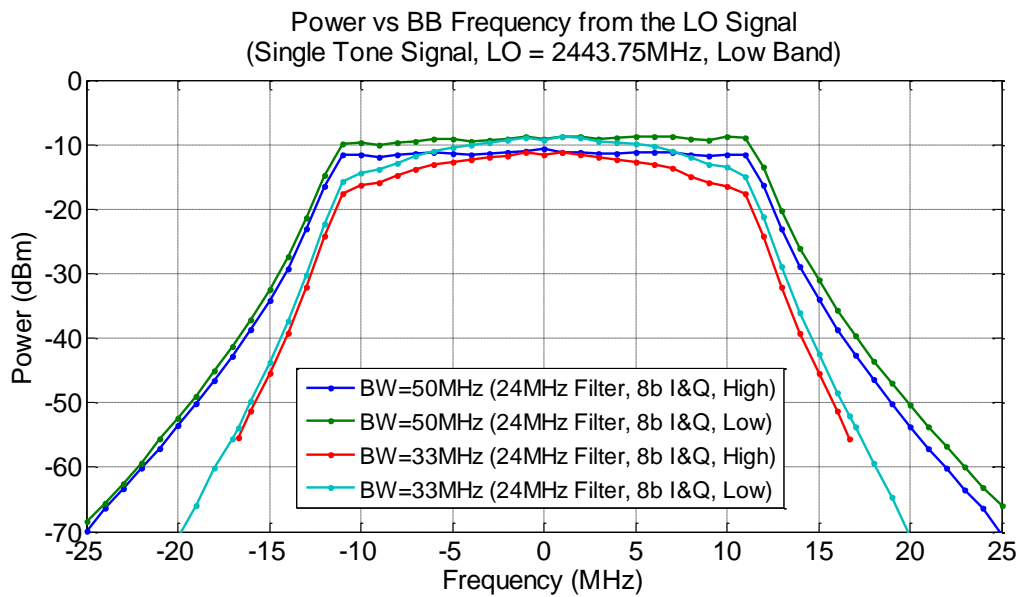


Figure 42: Baseband frequency offset test results - Comparison of low band and high band responses for offsets over 25 MHz

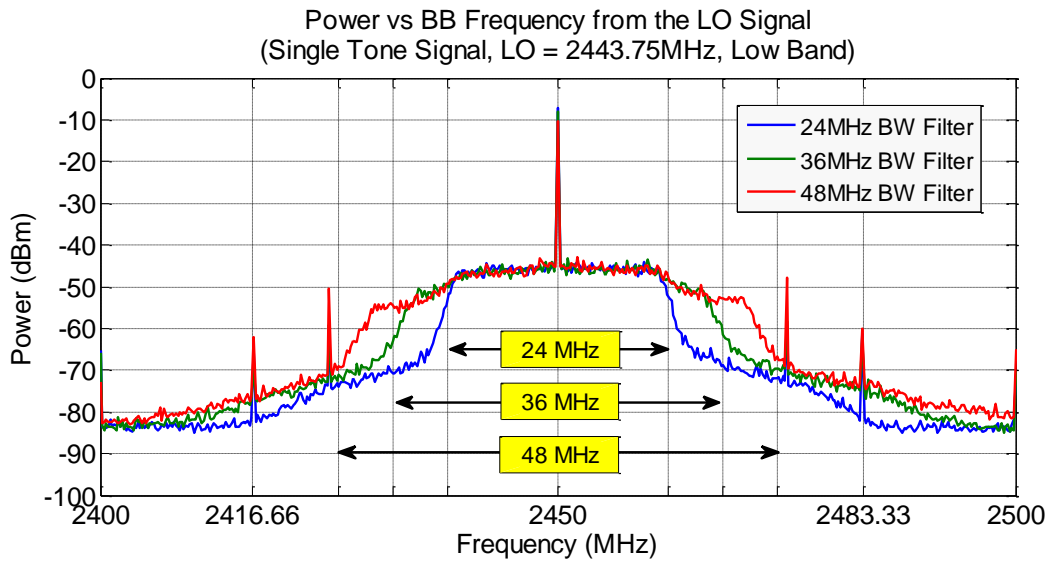


Figure 43: Baseband frequency offset test results – Response of wideband Gaussian noise (low band)

Baseband Filter Observations

Key observations from these tests are that the power of the signal output is visibly affected by the choice of MBW and baseband filter size. Frequency modulated signals will provide a more uniform power output if implemented using 25 MHz or 50 MHz sampling rates, since these offer wider plateau regions in the power curve response with wide 3 dB cut-off bandwidths. This is further illustrated in Table 22 below, which summarises the approximate 3 dB bandwidth frequencies and roll-off factor²⁰ beta from test data.

Table 22 Characteristics of unfiltered power curves for various modulation bandwidths

Modulation Bandwidth (MHz)	3 dB Modulation Bandwidth Cutoff (MHz)	Roll-Off Factor Beta
50	42*	n/a
33	12	1.5151
25	22	1.36
20	10	1.8
15	7	1.86666
5	5	1.3
*Data for this 50 MHz curve was taken from a test using a 48 MHz filter.		

Wide band noise testing showed that spurs (harmonic or otherwise) may be generated at frequencies beyond the baseband filter limits. This highlights a limitation in the radar transmitter's ability to generate band focussed or band limited noise, since significant spurs will be created at out of band frequencies that may affect out of band receivers.

²⁰ Roll-Off Factors Beta = Excess Bandwidth / Modulation Bandwidth

4.1.9 Third Order Output Intercept Point

The aim of this test was to obtain a measure of the transmitter's non-linearity, by determining the third order output intercept point (OIP3).

Two methods for determining the OIP3 were used, both involved transmitting the two tone test waveform²¹ then obtaining power measurements of the inter-modulation tones (IM1 and IM2) and the fundamental tones (F1 and F2) so that the OIP3 could be determined [37].

Three criteria must be met to obtain an accurate measure of the inter-modulation tones.

- The IM tones measured should be at least 10 dB above the noise floor.
- Measurements should be taken at lower power levels in the linear response region. As identified during earlier two tone waveform tests in Section 4.1.4, an amplitude of 0.25 appears to produce the desired linear 3:1 response from the IM1 and IM2.
- In the case of the USRP, the amplitude of each signal should remain below 0.5 to avoid DAC saturation (as discussed in Section 4.1.4).

No information was found on what to expect for the OIP3 of the XCVR2450 during transmission. However, available data for the WBX daughterboard in receive, showed IIP3 values typically between 0 dBm and 15 dBm. In the absence of other information this provides a ball park figure of what to expect from the XCVR2450 daughterboard.

²¹ Details regarding the IM1, IM2, F1 and F2 are described under the two tone test waveform Section 3.2.2 and are illustrated in Figure 12.

Method 1: Graphical Determination of the OIP3

This method of determining the OIP3, involved plotting the output power vs. input power (in dB) of both a fundamental tone and an inter-modulation tone. Ideally the response of both tones would be linear with a 1:1 response for the fundamental tone, and a 3:1 response for the inter-modulation tone; that is, prior to both tones experiencing compression at higher input powers as illustrated in Figure 44.

NOTE:
This figure has been removed due to copyright.
Alternatively, the item is available from the referenced links

Figure 44: Representation of the OIP3 [40]

As discussed earlier the change in voltage and hence power is directly proportional to the change in amplitude. The formula below expresses the normalised input power for each amplitude, where 0 dB is the input power for an amplitude of 1.

$$\text{Normalised Input Power (dB)} = 20\log(\text{Amplitude})$$

Given that the exact input power at each amplitude value is unknown, the amplitude input has been normalised and expressed as a power in dB relative to 0 dB (e.g. at an amplitude of 1.) The fundamental and inter-modulation curves were then plotted as shown in Figure 45 and Figure 46. The OIP3 was determined from these plots by identifying the hypothetical point where straight lines extended through the ideal linear regions of each curve would intersect²².

Microsoft Excel was used to create trend-lines based on data points that met the three criteria for accurate measurements discussed above. Formulas for these trend-lines were provided in Microsoft Excel, and used to determine the intersecting point at which the OIP3 exists.

²² Two lines of the form: $y_1 = m_1x + c_1$ and $y_2 = m_2x + c_2$, will intersect when $y_1 = y_2$. This will occur at a point (x, y) where $x = (c_2 - c_1)/(m_1 - m_2)$ and $y = (c_1m_2 - c_2m_1)/(m_2 - m_1)$

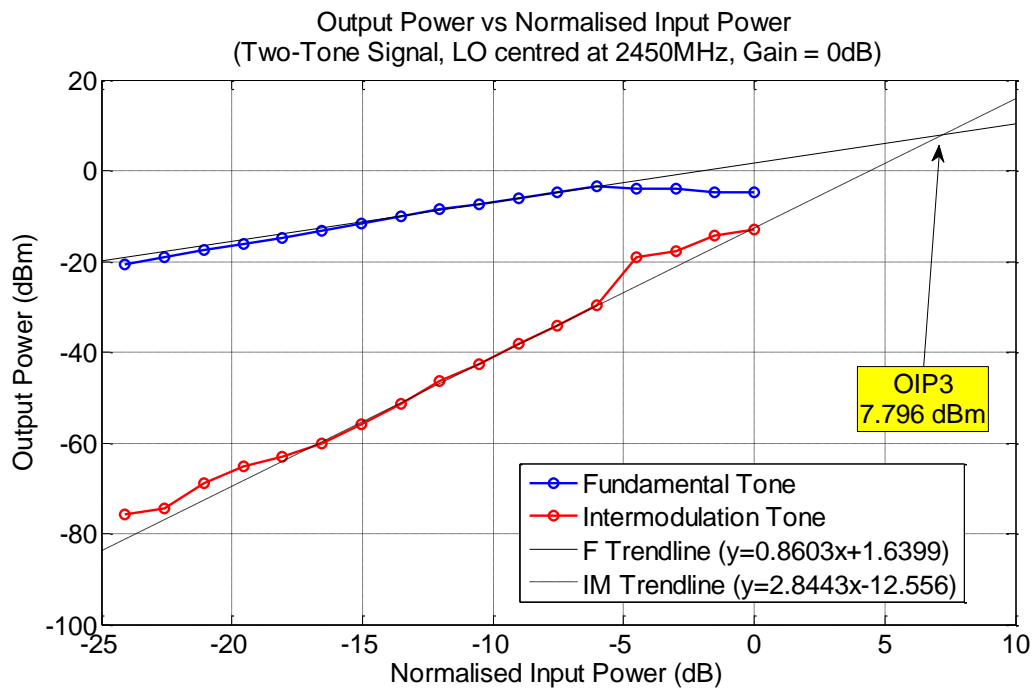


Figure 45: OIP3 results using the graphical method at 2450 MHz

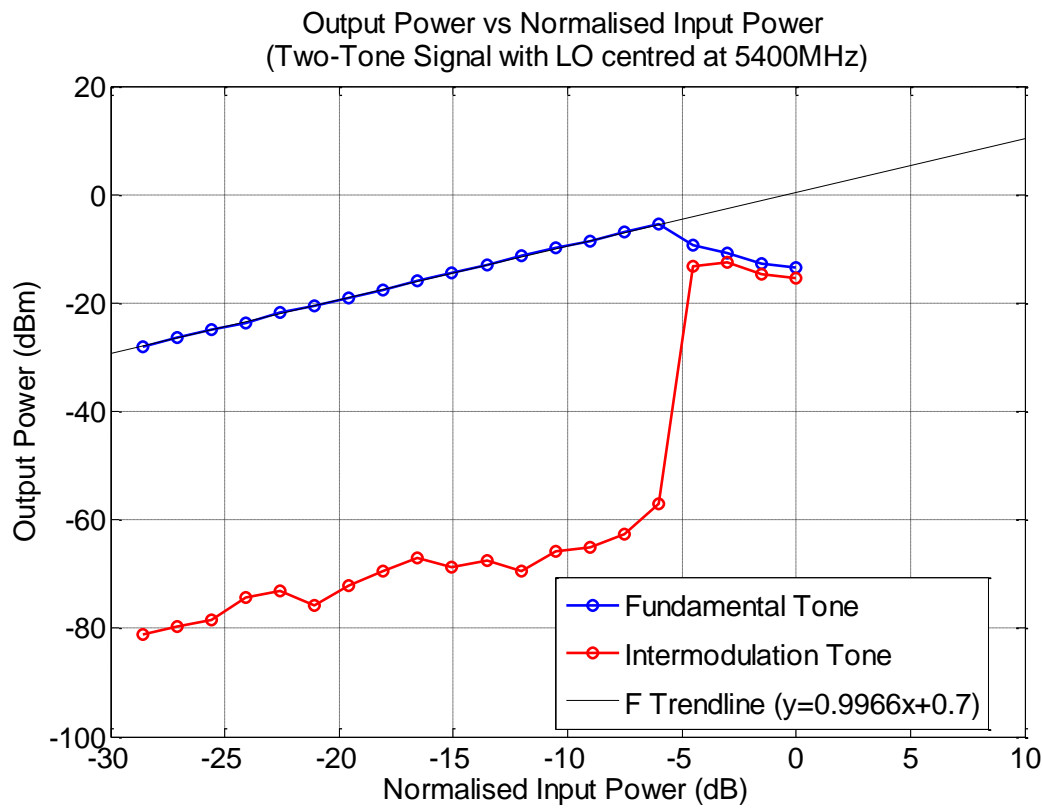


Figure 46: OIP3 results using the graphical method at 5400 MHz

As identified in earlier amplitude tests involving two tone waveforms, the high band path highly suppresses inter-modulation products. Thus very few IM measurements obtained in the high band were both above the noise floor, and beneath the 0.5 amplitude limit at which DAC saturation occurs in the high band. Out of the measurements in this range, few data points demonstrated behaviour close to a linear 3:1 response to an increase in the input power. As such a clear OIP3 value could not be identified line from the high band data using this method. This problem did not arise in the low band case and an adequate line matching the data was obtained, that was close to a slope of 3. As indicated on the plot the OIP3 values obtained for a gain of 0 dB was around 8 dBm at 2450 MHz.

Method 2: Rapid Calculation of the OIP3

This method for determining the OIP3 required only taking measurements of the fundamental tones F1, F2 and a single inter-modulation tone; either IM1 or IM2. The following formula [41] can then be used to obtain a value for the OIP3 that is 'faster and more accurate than the traditional (graphical) approach.'

$$\text{OIP3} = \text{Power}_{F1} + 0.5 \times (\text{Power}_{F2} - \text{Power}_{IM1}) = \text{Power}_{F2} + 0.5 \times (\text{Power}_{F1} - \text{Power}_{IM2})$$

This second method was applied to verify that the first set of calculations for the low band data appeared reasonable, and to obtain an OIP3 value for the high band. Additionally, since this method only requires a single measurement of 3 data points to determine the OIP3, this approach was used to rapidly extend the OIP3 calculations. Calculations were made for each gain step, covering frequencies at the start, centre and end of both frequency bands.

Results for the low band and high band are shown in Figure 47 and Figure 48 respectively, which show the OIP3 changing as a function of gain, for a fixed input power i.e. corresponding to a fixed amplitude value of 0.25.

Note: this is not a traditional 'Input Power versus Output Power' plot of fundamental / inter-modulation frequencies where a 3:1 ratio would be expected.

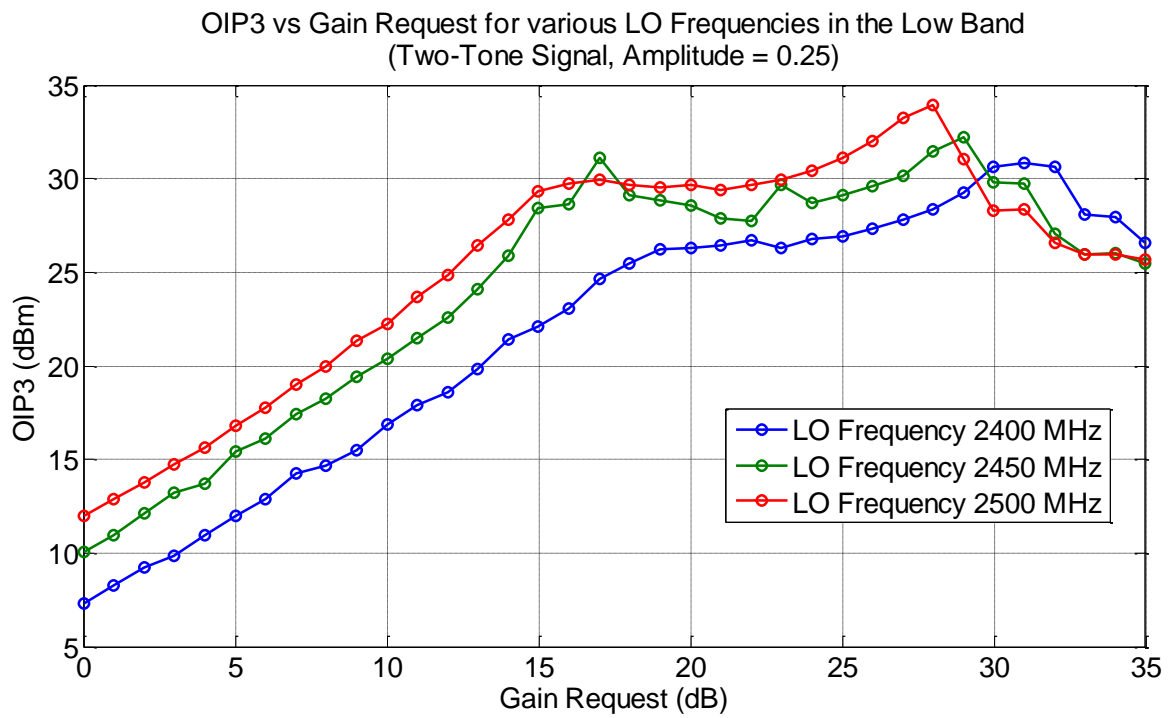


Figure 47: OIP3 results using the rapid calculation method for selected low band frequencies

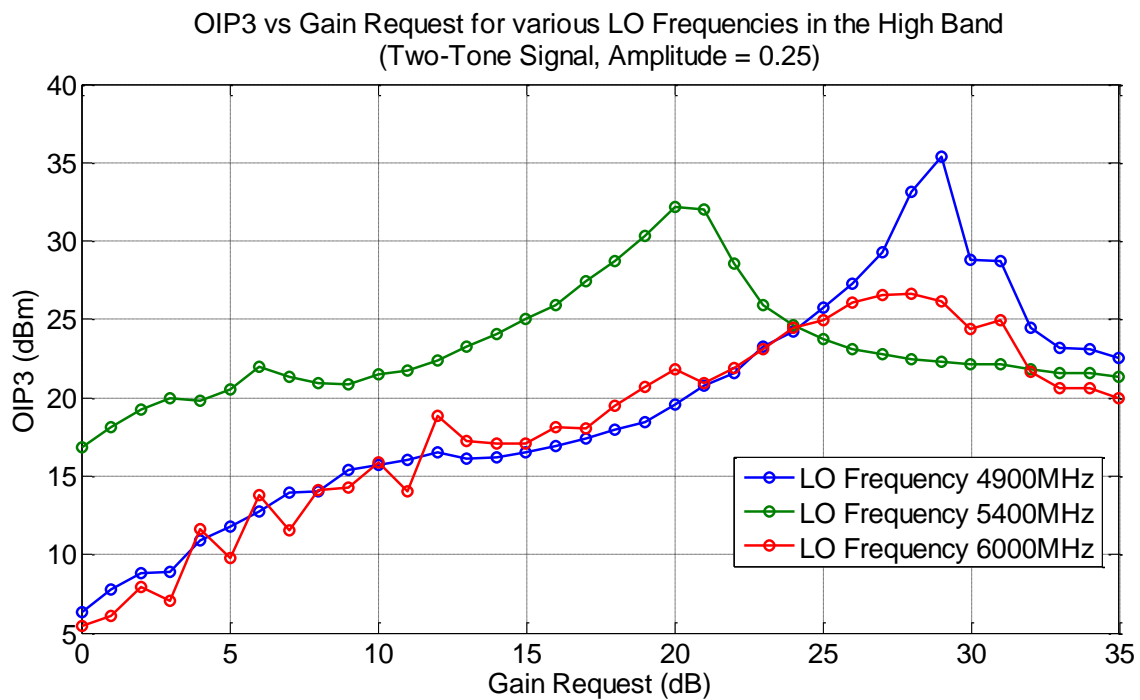


Figure 48: OIP3 results using the rapid calculation method for selected high band frequencies

Comparing results from each method for a gain of 0 dB, at 2450 MHz and 5400 MHz; method 1 produced OIP3 values of 8 dBm and an inconclusive result, whereas method 2 produced values of 10 dBm and 17 dBm. These low band values match within ~2 dB and thus indicate that both methods have been applied correctly to the low band and provide consistent results.

Examining the low band and high band results showed changes in the OIP3 for different LO frequencies. In the low band the OIP3 was observed to increase as the LO frequency changed from 2400 MHz to 2450 MHz and then to 2500 MHz. At 2500 MHz the OIP3 had increased by 5 dB, which is consistent with the 5 dB increase in output power observed during power versus frequency tests shown earlier in Figure 37. Examining the high band results (see Figure 48) showed similar behaviour. The approximately 10 dB increase in the OIP3 observed when the LO frequency was placed in the centre of the band, is consistent with the observations observed in earlier testing (see Figure 38).

In all low band test cases the OIP3 increased linearly with gain as expected²³. A similar, somewhat linear response occurred in the high band. It is theorised that the erratic behaviour of the OIP3 at 6000 MHz in this 'linear region' may be the result of operating at the upper frequency limit of the USRP device, with the two tones offset to the right past this limit might have impacted or suppressed the IM frequencies further, thus leading to erratic measurements, but further testing would be required to determine this.

At higher gain values the response of the OIP3 curves began to plateau. It is believed that at this stage the inter-modulation products and / or the fundamental tones have left their linear regions of behaviour and are thus causing variations in the OIP3. Further investigation would be required to verify this.

The OIP3 values observed across all tests cases were at a minimum of 5dB in each band.

²³ OIP3 = IIP3 + Gain, where IIP3 refers to the third order input intercept point

4.1.10 Local Oscillator Suppression

The LO signal (or the image signal) may potentially be the strongest undesired signal output from a transmitter, and may affect receivers out of the desired frequency band of operation. The LO suppression is the difference between the power of the RF signal and the LO signal. The image suppression is calculated in the same way, as shown in the formulas below. These provide measures as to how much these signals may interfere with a receiver.

$$LO_{suppression} = RF_{power} - LO_{power}$$

$$IMAGE_{suppression} = RF_{power} - IMAGE_{power}$$

No dedicated testing has been performed to examine the LO or image suppression, however LO data collected during the ‘Power vs. Gain and Amplitude’ tests and Power vs. Baseband Frequency’ tests showed several observations regarding the LO signal behaviour that provide an understanding of the LO suppression when transmitting a single tone:

During the detailed gain tests discussed in Section 4.1.5 the LO signals placed at 5393.75 MHz and 2393.75 MHz began at -31.5 dBm and -29 dBm respectively for a 0 dB gain input. As the gain was increased from 0 dB to 23 dB (i.e. remaining in the linear region of operation), the LO signal power increased by the same amount that the RF signal increased. Thus the LO suppression remained near 21 dBm in both bands as summarised in Table 23. Data applies to the linear region, defined as 0dB to 23dB.

Table 23 LO and Image Suppression Summary for a Single Tone Test

Parameter	Low Band Testing	High Band Testing
RF Frequency	2450 MHz	5400 MHz
LO Suppression	20 to 21dB	18.5 to 21dB
Image Suppression	36.5 to 37 dB	35.5 to 36.5 dB

During the ‘Power vs. Baseband Frequency’ tests discussed in Section 4.1.8, which were conducted with a gain input of 0 dBm, the power of the LO remained at the minimum values of -31.5 dBm and -29 dBm respectively regardless of the RF signal power, frequency or bandwidth.

Thus without extending the tests conducted earlier, we still have an understanding of the LO suppression. Since changes in gain increase both the LO and RF signal powers by the same amount, the LO suppression will remain constant for gain values in the linear region of operation for that band, and based upon the limited data collected in this study, the LO suppression is likely to remain around 20 dB, although this is expected to shift depending upon the LO frequency used. If the RF signal is offset sufficiently from the LO signal that a reduction in power occurs²⁴ the LO suppression will reduce by this amount.

²⁴ As shown in Section 4.1.2, this will be a factor of the baseband frequency and sampling rate.

4.1.11 Phase Noise Measurements

Local oscillator noise can have a significant impact on the output of any transmitter, since this noise will also be subject to following amplification stages along with the desired signal, and thus be present when the waveform is transmitted from the device.

The aim of these was to measure the phase noise in the low and high band to obtain a gauge of the expected performance. This involved transmitting the single tone test waveform to a signal analyser, equipped with a mode specifically for measuring the phase noise, referenced to the phase noise of the signal analyser. Measurements were taken of the RF signal at various frequencies covering the low and high bands. The gain and amplitude was also adjusted to observe any impact on the phase noise.

An indication of the expected results is provided in Figure 49, which shows phase noise measurements available in the datasheet of the MAX2829 transceiver, which provides the local oscillators and mixing functions of the RF daughterboard. Details regarding the test conditions and reference signal for this data are not provided thus this data serves only as a ball park expectation of what results will be obtained and are not suitable for a detailed comparison.

NOTE:
This figure has been removed due to copyright.
Alternatively, the item is available from the referenced links

Figure 49: Phase noise plots from the MAX2829 Transceiver datasheet [34]

The following discussions will focus on the core of the information which is presented in plots of the phase noise spectrum. However, tables summarising the full set of tabulated data from these tests is available in the Appendix, Section 6.2 for the interested reader. These tables include other measures such as jitter, residual phase modulation and residual frequency modulation.

Phase Noise Response to variations in the Gain and Amplitude Parameters

The test matrix for varying the gain and amplitude values encompassed all combinations of the following values.

- Amplitudes: 1.1, 1, 0.5, 0.25, 0.125, and 0.0625
- Gains: 0, 10, 20 and 35 dB

Typical phase noise plots measured at the centre of each band are shown in Figure 50 and Figure 51. The low band case (2450MHz) shows phase noise values typically around -90dBc/Hz at 2450MHz, with negligible spurs. The high band case (5400MHz) shows phase noise typically around -85dBc/Hz at 5400MHz, with spurs extending up to 35 dB above the main curve of the phase noise signal. These spurs are not reflected in the manufacturer data sheets.

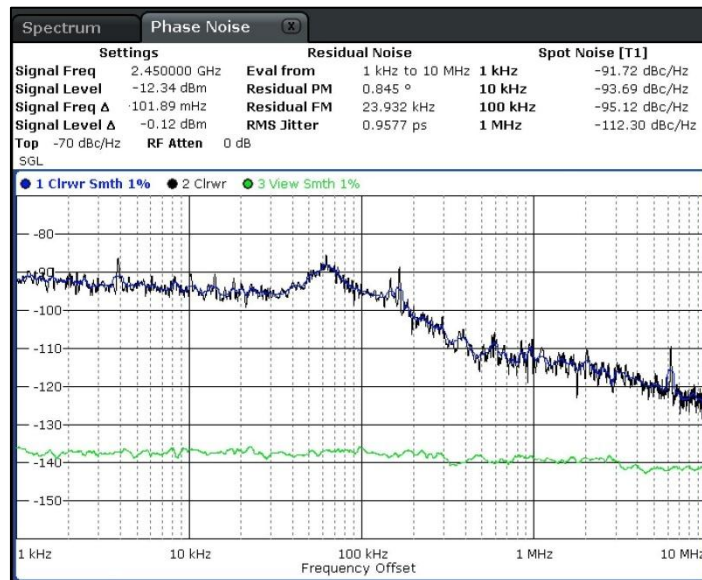


Figure 50: Phase noise plot for a single tone at 2450 MHz (Gain = 0 dB, Amplitude = 0.25)

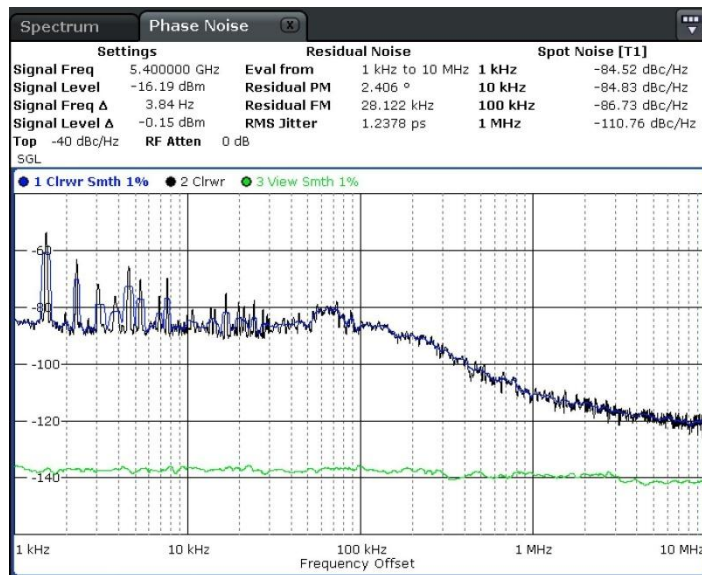


Figure 51: Phase noise plot for a single tone at 5400MHz (Gain = 0 dB, Amplitude = 0.25)

Adjusting the gain did not cause any noticeable change in the phase noise spectrum as shown in Figure 52. Increases were observed in the residual noise measurements such as jitter (see top of figure) when the gain was set to 35dB. The rising spur observed in Figure 52 at an offset of 6.5MHz on the right is the LO signal, which has risen by the gain input of 35dB as expected.

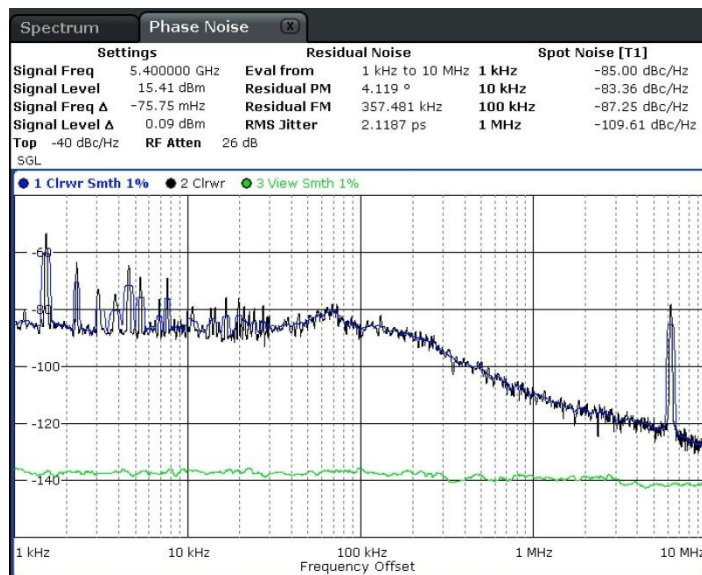


Figure 52: Phase noise plot for a single tone at 5400 MHz (Gain = 35 dB, Amplitude = 0.25)

Adjusting the amplitude did not have any significant impact on the phase noise in the cases tested, except when amplitudes of 1 or greater are used. An amplitude value of 1 caused the phase noise to increase at offsets up to 30 kHz (see Figure 53). This is possibly caused by saturation of the DACs, despite typically occurring at values greater than 1 as observed in most tests. This noise spread across the spectrum more significant at an amplitude value of 1.1.

Changing the amplitude (at useable values below 1) did result in notable changes to the residual noise measurements and the RMS jitter (which varied between 0.73 and 2.33 ps.) These values were at a minimum when the amplitude was set to 0.5.

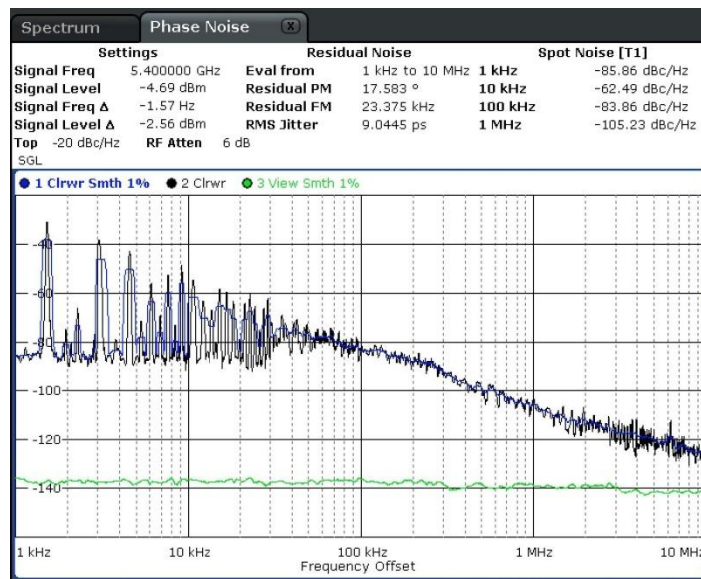


Figure 53: Phase noise plot for a single tone at 5400 MHz (Gain = 0 dB, Amplitude = 1)

Phase Noise Response to variations in the RF Frequency

The phase noise responses at various RF frequencies stepped across the low and high bands are presented in Figure 54 and Figure 55. Data lines reflect different frequency offsets at which the spot noise measurements occurred. In the low band test cases, the phase noise measurements were reasonably consistent with minor fluctuations occurring by around 2dBc/Hz. The exception applied to the measurement of the 10 kHz offset which increased significantly by around 12dB when the RF signal was at 2475MHz.

In the high band test cases, the phase noise at the 10 kHz and 100kHz offsets varied by 5 to 10dB depending upon the RF frequency. These values were at their minimum for frequencies of 5100 and 5600 MHz. RMS jitter varied throughout testing depending upon the RF frequency but remained beneath 1.4 ps when using an amplitude value of 0.25 which has been recommended throughout this thesis.

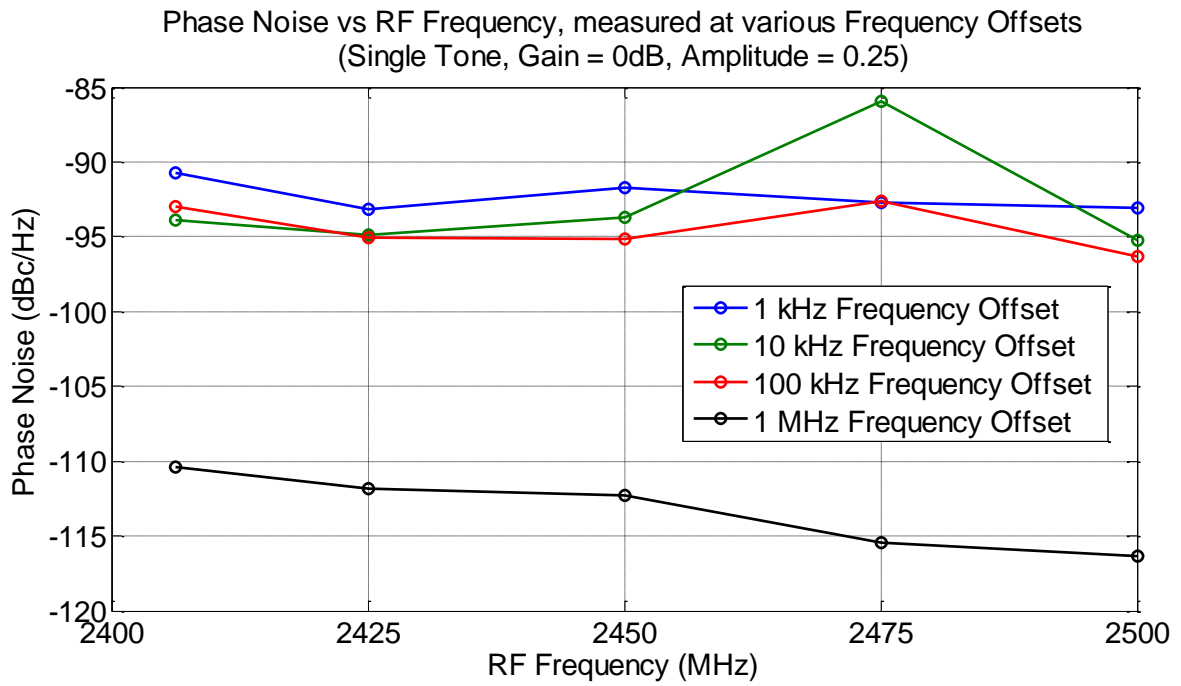


Figure 54: Phase noise measurements at various low band frequencies

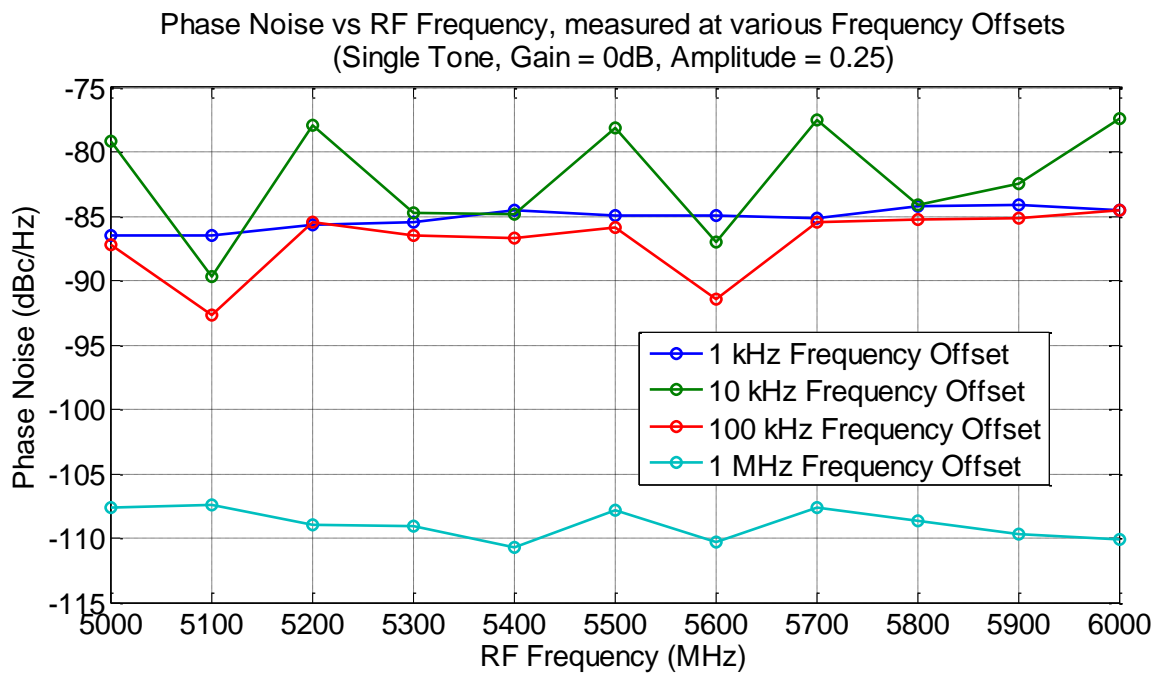


Figure 55: Phase noise measurements at various high band frequencies

4.2 Waveform Verification Testing

The aim of this section of testing was to assess the accuracy of waveforms output by the radar transmitter. Unlike the characterisation testing that focused on the limits of the USRP performance to identify unexpected behaviour and regions where it occurred, the waveform testing focused on the performance of the USRP under ideal conditions to examine how accurately it can produce radar waveforms.

This involved transmitting the set of waveforms defined earlier in Section 3.3 then:

- Recording the signal output in the time domain using the oscilloscope, to compare to the input data in the time domain from GNU Radio.
- Recording the signal output in the frequency domain using the spectrum analyser, to compare to a model of the expected frequency domain response.

The modelled results were based upon time domain data of the transmitted signal from GNU Radio, which was converted to the frequency domain using a FFT in Matlab.

The RF waveform output from the USRP, will (ideally) share the same timing characteristics and power spectrum around the LO frequency to that of the BB signal input passed to the USRP from GNU Radio.

4.2.1 Continuous Waveform

The continuous waveform consisted of a cosine wave. This serves as simple baseline for testing. A scope plot of the recorded CW data input to the USRP is shown in Figure 56. (Due to the 4 samples per period minimum used in these tests, the figure appears more like triangle wave.) The model of the expected power spectrum relative to the LO is shown in Figure 57. This plot shows the power of the RF tone beginning to spread at -400 dB which is a highly idealised case. In reality it is expected that this will occur at a much higher level, and close to the noise floor, which will likely be around -65 to -70 dB based upon observations in earlier testing.

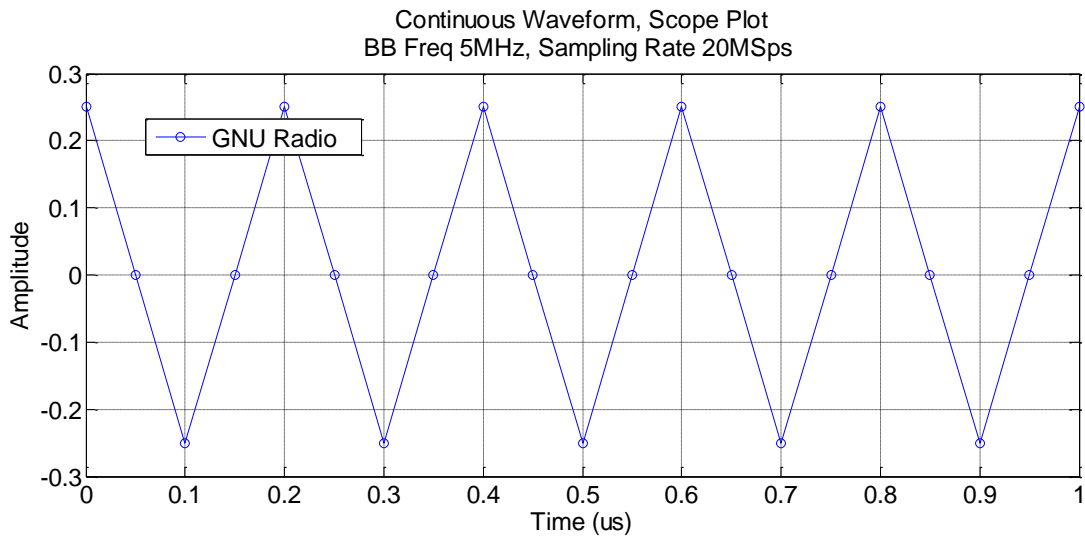


Figure 56: Time scope plot of the baseband CW input to the USRP

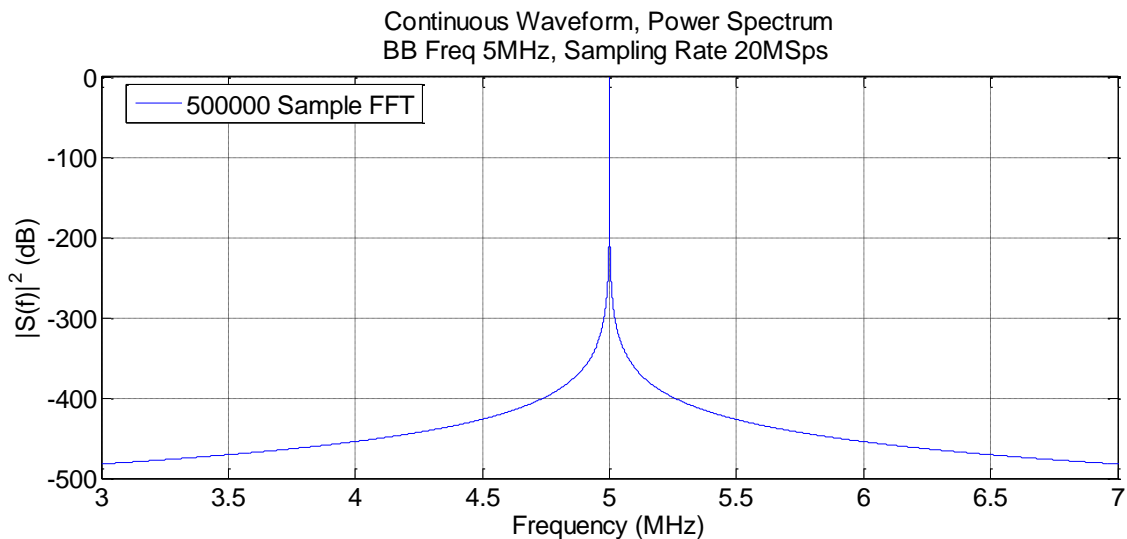


Figure 57: Modelled normalised power spectrum of the baseband CW input to the USRP

The output signal recorded by the spectrum analyser is shown in Figure 58. The RF, LO, image signal were placed at the frequencies expected. The only distortion visible was a signal at 5805MHz, which may be a harmonic of the BB frequency, or a product of reciprocal mixing. The peak power was 2 dBm. SNR was 64 dB²⁵ and SFDR was 16 dB.²⁶

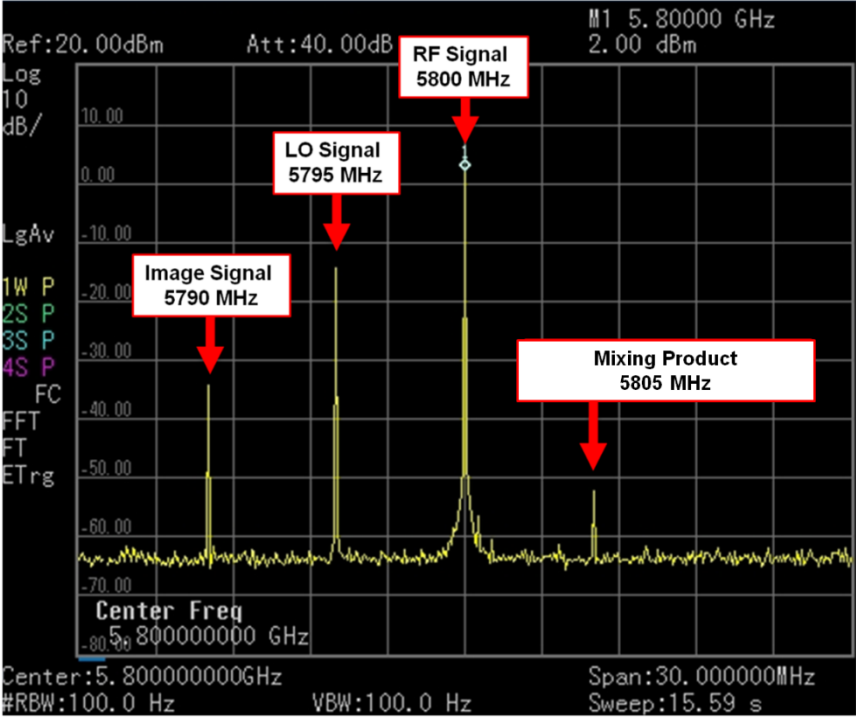


Figure 58: Measured power spectrum of the CW output from the USRP

The output signal recorded by the oscilloscope is shown in Figure 59 (non-interpolated data) and Figure 60 (interpolated data). The non-interpolated data shows four samples per period as expected. As the signal has been mixed with the LO output, samples will appear at different points in each period of the waveform unlike what is shown in the baseband waveform from Figure 56. Observing the data using the interpolation feature was necessary to enable the auto-measurement function to be used in this test. Measurements showed a mean frequency of 5.80277 GHz (which equates to a frequency deviation of 2.77 MHz). Given that this does not match the measurement from the spectrum analyser, it is believed that the interpolation feature of the oscilloscope has (in reconstructing the waveform) changed the location at which the waveform crosses the centre line at which measurements occur. Ideally this would still result in an average frequency of 5.8GHz nonetheless. Further measurements would need to be taken using a CW waveform with a higher number of samples per period to verify this. The frequency measurement taken from the spectrum analyser is thus considered the more accurate measurement of the two.

²⁵ SNR = 2 dBm - (-62 dBm) = 64 dB
²⁶ SFDR = 2 dBm - (-14 dBm) = 16 dB

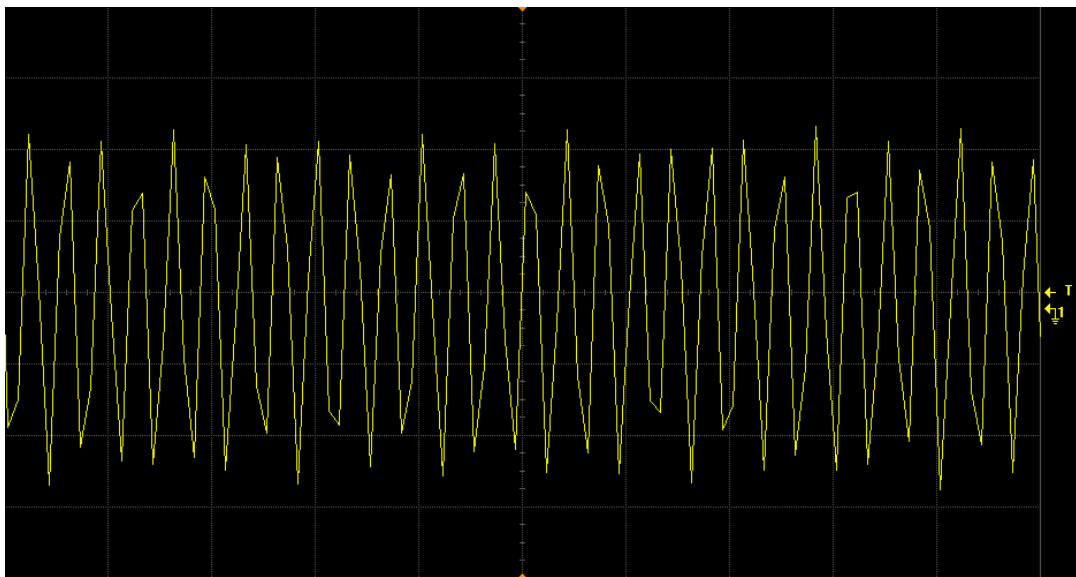


Figure 59: Measured time scope plot of the non-interpolated CW output from the USRP (500 ps/div, 5 ns span)

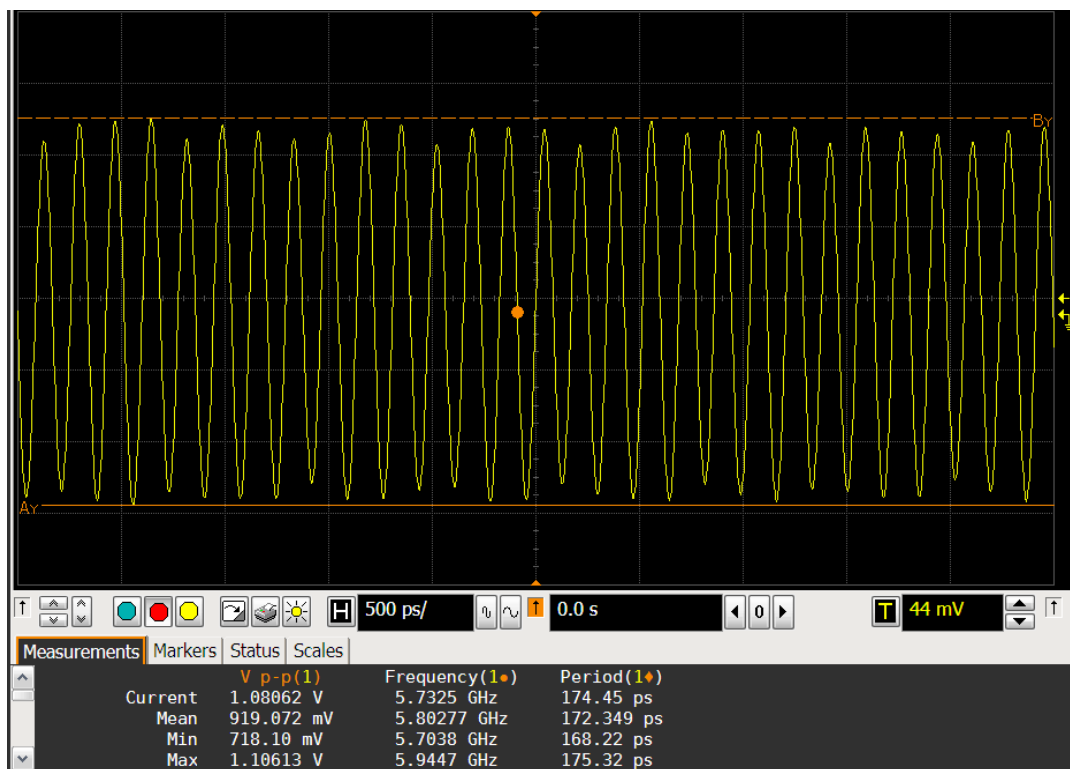


Figure 60: Measured time scope plot of the interpolated CW output from the USRP (500 ps/div, 5 ns span)

4.2.2 Pulsed Waveform

The pulsed waveform consisted of the continuous waveform used in the previous test, with a duty cycle of 10% applied to divide it into 1 μs pulses, repeating at 10 μs intervals. A scope plot of the recorded CW data input to the USRP is shown in Figure 61.

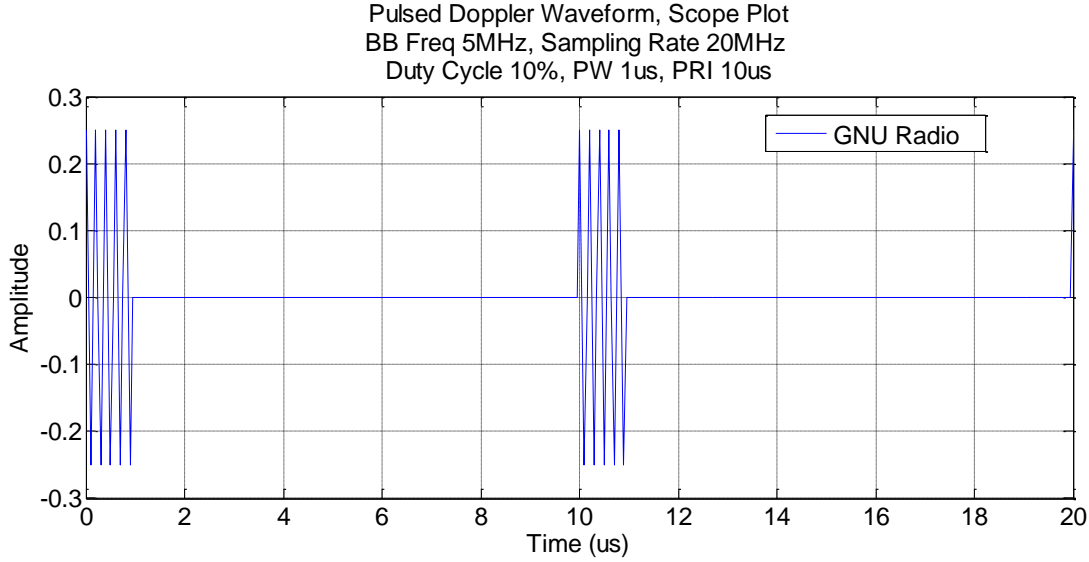


Figure 61: Time scope plot of the baseband pulsed waveform input to the USRP

The model of the expected power spectrum relative to the LO is shown in Figure 62 and Figure 63. Several key waveform characteristics can be determined [42] from this plot, which are expected to be visible in the USRP output.

- The PRI can be identified by observing the spectral line spacing, and using the formula below. As the spectral lines are spaced at 100 kHz (PRF) intervals, this confirms the PRI of 10 μs .

$$PRI = \frac{1}{PRF} = \frac{1}{\text{Spectral Line Spacing}}$$

- The PW can be identified by observing the width of each side lobe. These occur at 1 MHz intervals which confirm the PW of 1 μs .

$$PW = \frac{1}{\text{Lobe Width}}$$

- The duty cycle of 10% can then be calculated from the above values.

$$\text{Duty Cycle} = \frac{\text{Spectral Line Spacing}}{\text{Lobe Width}} = PRF \times PW$$

The theoretical desensitization factor can be determined using the following formula by substituting a duty cycle value of 10% (e.g. 0.1) into the following equation. This provides a desensitisation value of α_L equals -20 dB. This is not reflected in the normalised power spectrum shown in Figure 62, however when comparing the measured peak pulse power of the output pulsed waveform and the non-pulsed CW observed previously, a power reduction of -20 dB should be visible.

$$\alpha_L = 20 \times \text{Log}(\text{Duty Cycle})$$

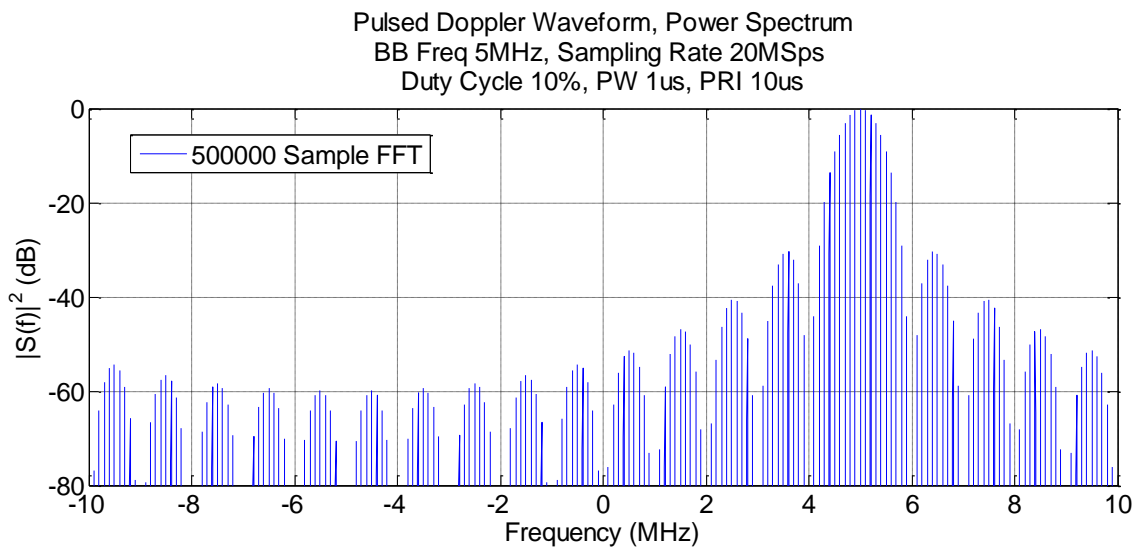


Figure 62: Modelled normalised power spectrum of the baseband pulsed waveform input to the USRP

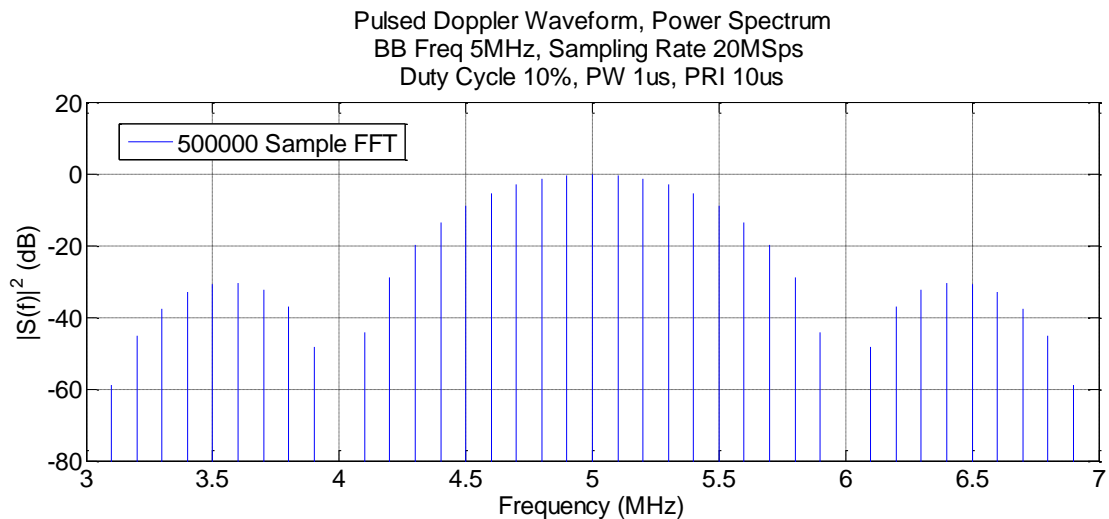


Figure 63: Modelled normalised power spectrum (close up view) of the baseband pulsed waveform input to the USRP

The output signal recorded by the spectrum analyser is shown in Figure 64. The expected characteristics described earlier are observed. The main lobe is centred at 5800 MHz (+5 MHz relative to the LO frequency). As shown clearer in Figure 65 the width of the sidelobes and spectral line spacing are 1 MHz and 100 kHz respectively, thus confirming the PRI, PW, and duty cycle calculated earlier. The peak pulse power is -18.79 dBm as shown in the top right corner of Figure 64. When compared to the 2 dBm peak power of the CW signal from Figure 58 earlier, this produces a desensitisation factor of -20.79 dB²⁷ which adequately matches the theoretical value of -20 dB. This reduction lowers the power of the main RF signal around 4 dB beneath that of the LO signal which may interfere with receivers near the LO frequency.

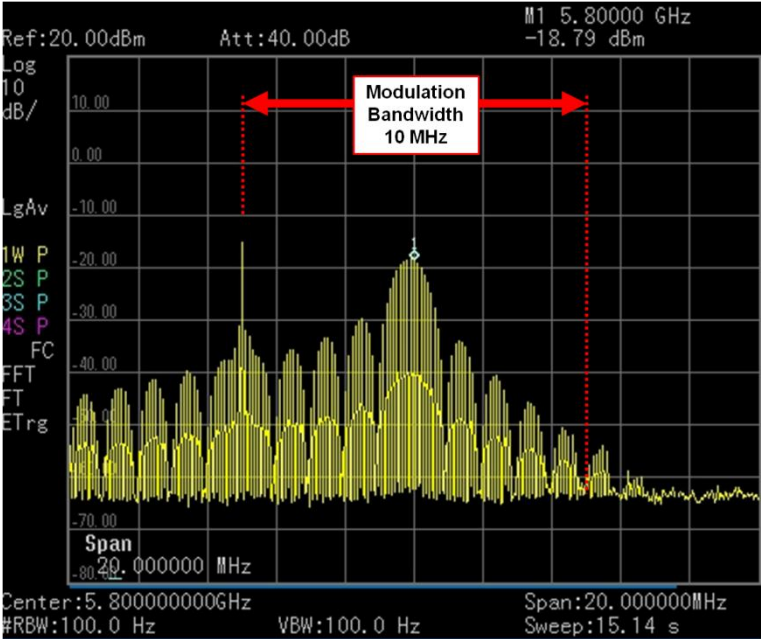


Figure 64: Measured power spectrum of the pulsed waveform output from the USRP

²⁷ Measured Desensitisation Factor = (-18.79 dBm) - (2 dBm) = -20.79 dB

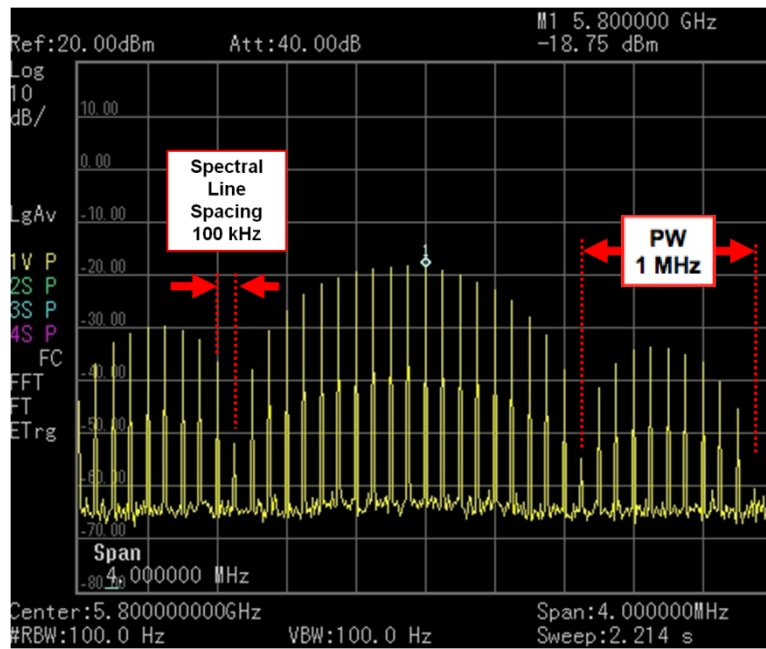


Figure 65: Measured power spectrum of the pulsed waveform output from the USRP

The oscilloscope output is shown in Figure 66. Visual inspection further confirms that the PRI is approximately 10 μs . This was verified in several tests, and matches the observations on the spectrum analyser. However, the auto measurement function measured a mean period of $\sim 9.04 \mu\text{s}$, as shown at the bottom of this figure. Given that would imply a 10% error, it is believed that there was an error in the trigger settings for this test. The auto measurement appears to be measuring the time difference between the trailing edge of one pulse to the leading edge of the next, thus triggering a 9 μs period measurement. Assuming this is the case, the measurement matches the 9 μs off time between pulses. Converting the four auto-measured frequency values into the time domain produces four period values differing from the four auto-measured period values displayed. This produces eight off-time measurements. Compared to a 9 μs off time, the maximum deviation is 0.14 μs which provides some bounds on the timing accuracy of the pulses generated by the radar transmitter.

A close up view of a pulse is shown in Figure 67, which shows 200 ns divisions equating to a span of 2 μs . The PW signal appears to be slightly wider than the target 1 μs PW. The part of the signal that exceeds the start and end of the pulse is less than the 50 ns²⁸ time per sample, thus is interpreted as an expected artefact of the USRP voltage ramping up or down to during the start and end of the 'on' period, and thus triggering the auto-measurement function at different times, rather than due to a mistiming or error in sample transmission. This would account for the 0.14 μs deviation in the pulse timing.

²⁸ Time per sample = 1 / Sampling Rate = 1 / 20 MSps = 50 ns

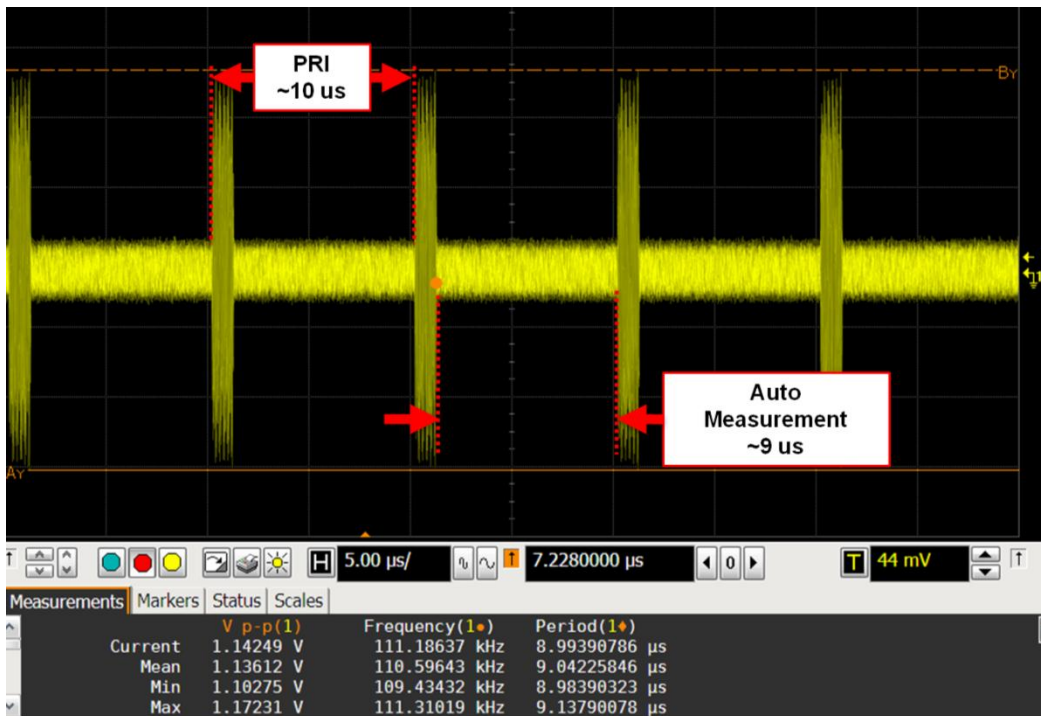


Figure 66: Measured time scope plot of the non-interpolated pulsed waveform output from the USRP (5 $\mu\text{s}/\text{div}$, 50 μs span)

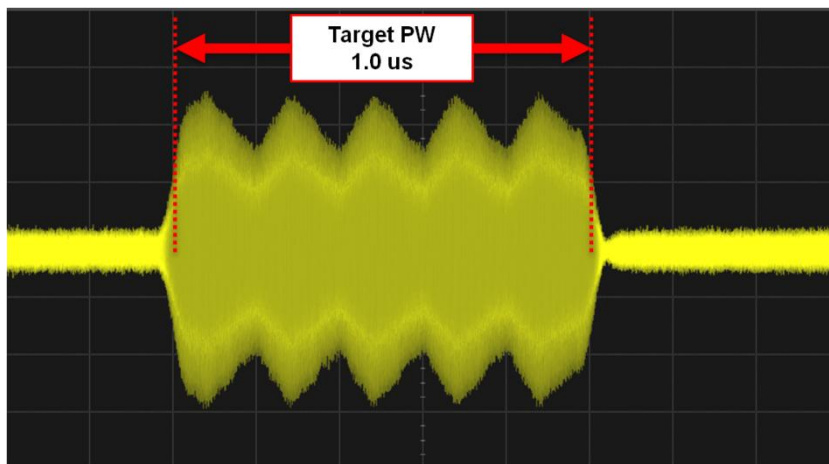


Figure 67: Measured time scope plot of the non-interpolated pulsed waveform output from the USRP (200 ns/div, 2 μs span)

4.2.3 Frequency Modulated Continuous Waveform

The FMCW consisted of the CW used in the first test, with two-way frequency modulation sweeps applied over a 20 μs time frame (e.g. 10 μs from the start to the maximum frequency deviation, then 10 μs to return to the start frequency.) The RF signal was placed at 5800 MHz, with the LO located at 5805 MHz.

Scope plots of the recorded FMCW data input to the USRP are presented for selected frequency sweeps in Figure 68, Figure 69 and Figure 70. It should be noted as the complex baseband frequency begins at a negative value then sweeps towards zero, although the mixed RF signal will be of a higher frequency, the magnitude of the complex baseband frequency reduces. Hence for the 10 MHz sweep shown in Figure 70 which is swept through the zero region, the signal appears to reduce in frequency as it moves from -5 MHz towards zero, increases in frequency as it approaches +5 MHz, then on the return sweep reduces in frequency as it moves from +5 MHz to zero, then increases again as it approaches -5 MHz.

Measured output in the time domain appears in Figure 71, Figure 72 and Figure 73, which correspond to the FM sweeps shown in Figure 68, Figure 69 and Figure 70 respectively. Due to the presence of the 5805 MHz LO frequency mixed in with the baseband signal, increases and decreases in the frequency modulation must be determined by regions of increased and decreased fluctuations in the amplitude. Comparing the scope plots of the FMCW input to their corresponding measured output show that frequency modulation over the 20 μs ramp time appeared as expected.

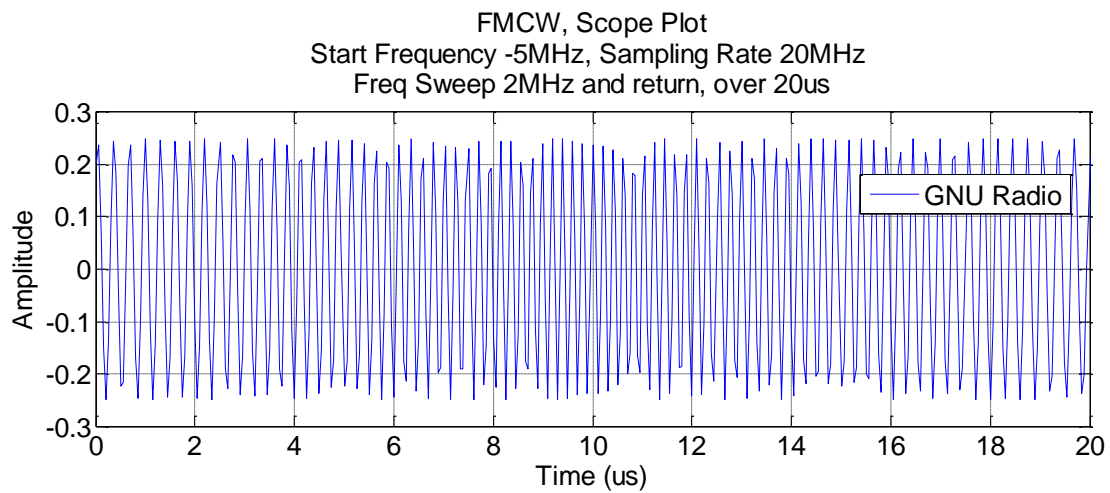


Figure 68: Time scope plot of the 2 MHz sweep FMCW input to the USRP

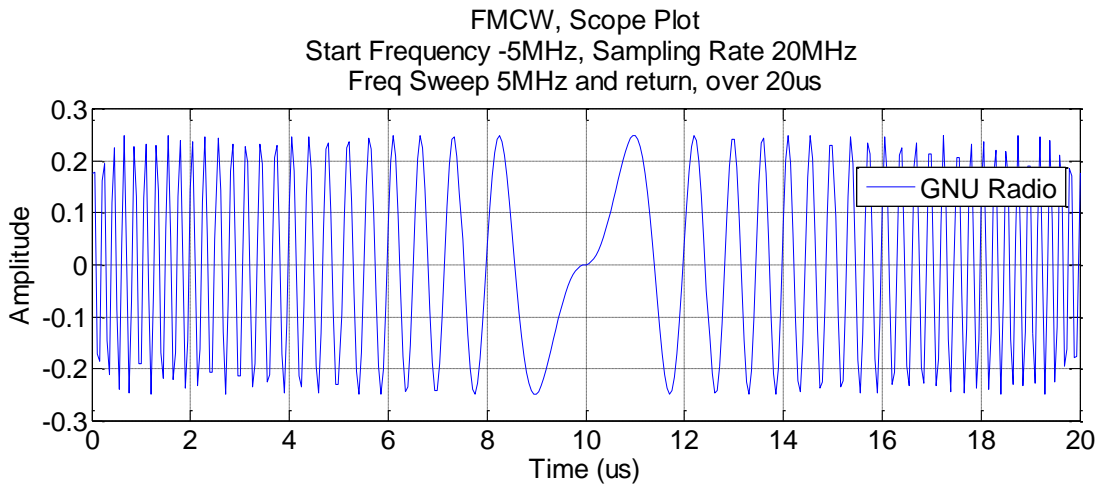


Figure 69: Time scope plot of the 5 MHz sweep FMCW input to the USRP

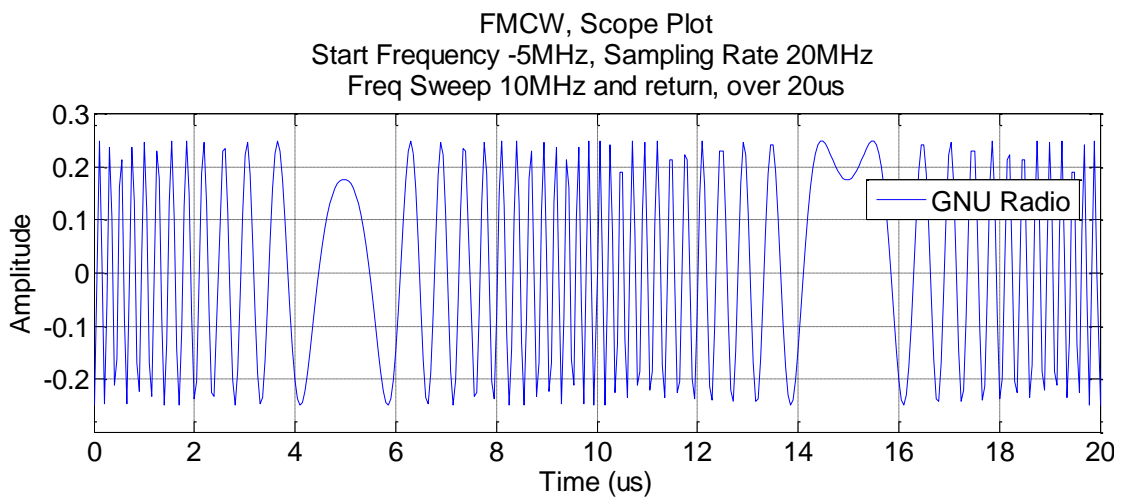


Figure 70: Time scope plot of the 10 MHz sweep FMCW input to the USRP

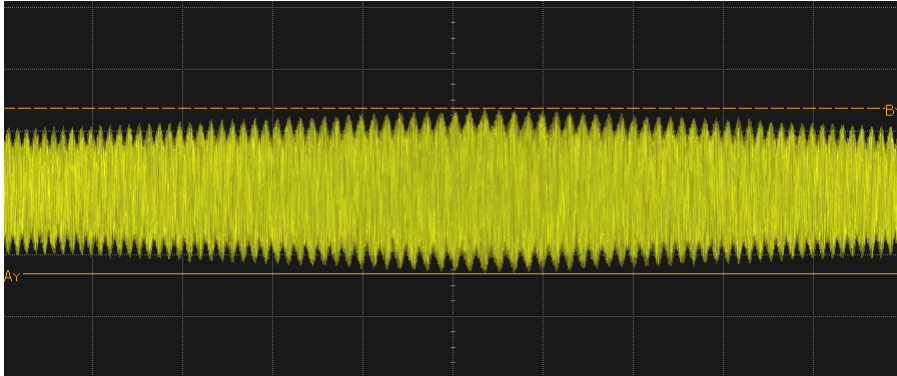


Figure 71: Measured time scope plot of the 2 MHz sweep FMCW output from the USRP (2 $\mu\text{s}/\text{div}$, 20 μs span)

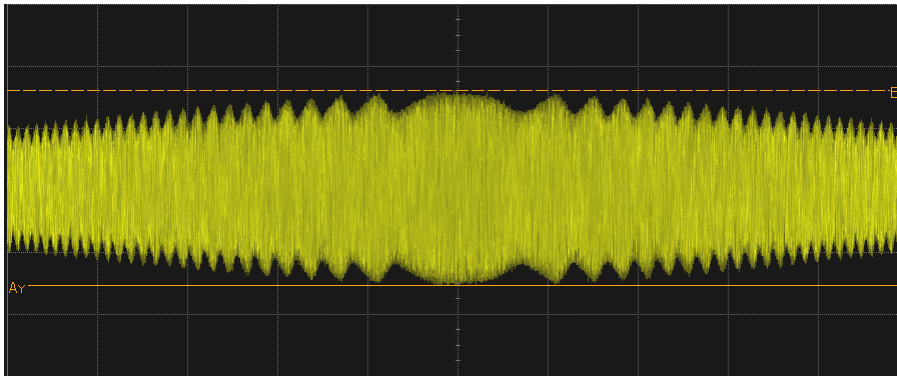


Figure 72: Measured time scope plot of the 5 MHz sweep FMCW output from the USRP (2 ns/div, 20 μs span)

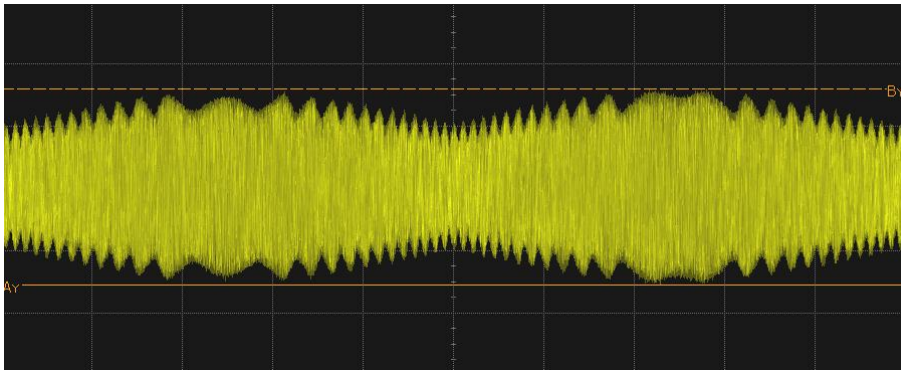


Figure 73: Measured time scope plot of the 10 MHz sweep FMCW output from the USRP (2 ns/div, 20 μs span)

Models of the expected power spectrum for these cases (relative to the LO) are shown in Figure 74, Figure 75, and Figure 76. These provide an indication of what the signal response is expected to look like based upon the change in frequency sweep size.

Since each frequency sweep repeats every 20 μ s, we thus see spectral lines on these three plots every 0.05 MHz. The spectral lines were not observed in the measured results, since the measured data shows the spectrum of a single repeating pulse and not a pulse train.

The power spectrums for several FMCWs output from the USRP are shown in Figure 77 and Figure 78. These show the response for a range of different frequency sweeps at 20MSps and 50MSps respectively. The frequency modulation sweeps across the range intended in each case, and the shape of the power spectrum appears as expected. An image of the FM sweep is observed starting 30 dB below the main signal at 5810 MHz, along with a harmonic of the FM sweep beginning at 5820 MHz.

As the frequency modulation increased, the power was reduced to spread over a wider bandwidth. The peak power of the LO remained at the same power level in each plot regardless of the frequency modulation (although this is difficult to see since the LO signal overlaps for each data curve

This indicates that due to poor LO suppression (up to -20 dB for a 25MHz sweep), large FM sweeps (i.e. greater than 10MHz) will reduce the RF power beneath the LO signal as seen in Figure 78.

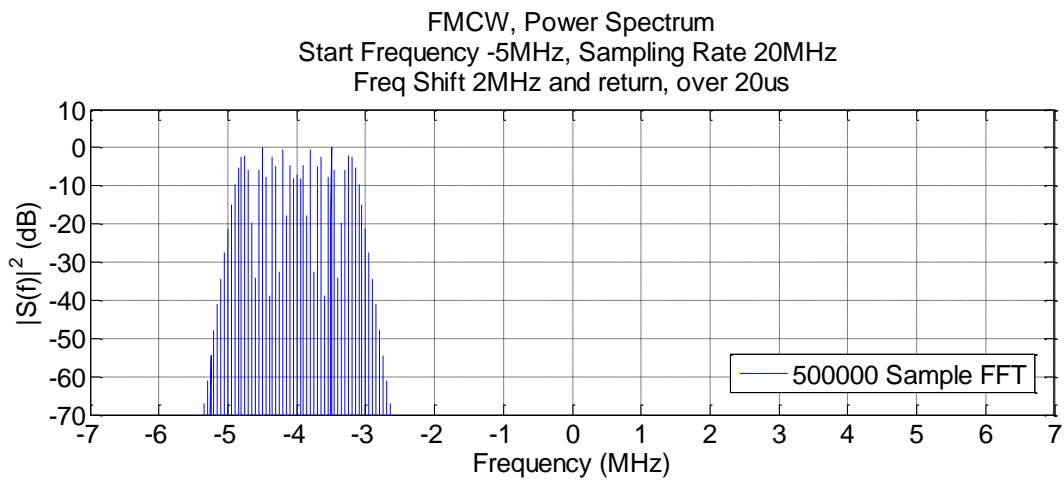


Figure 74: Modelled normalised power spectrum of the 2 MHz sweep FMCW input to the USRP

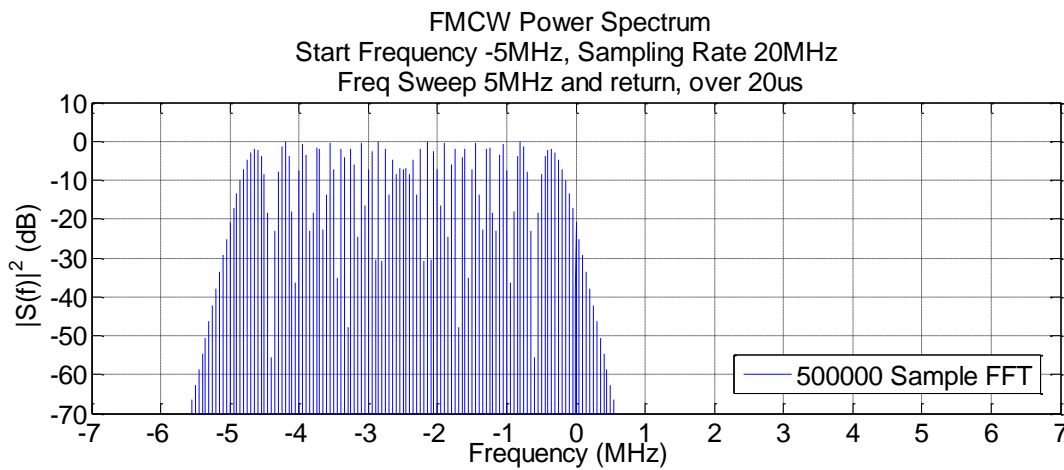


Figure 75: Modelled normalised power spectrum of the 5 MHz sweep FMCW input to the USRP

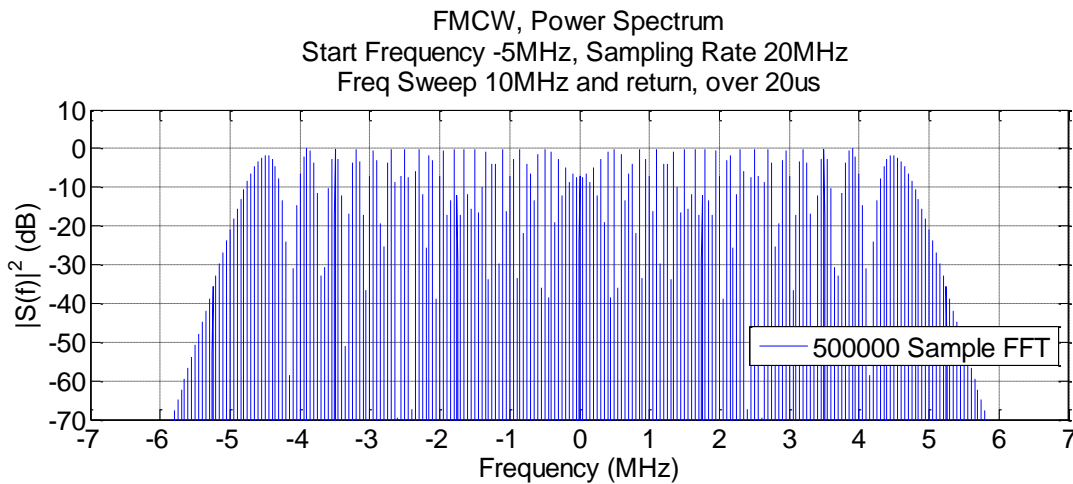


Figure 76: Modelled normalised power spectrum of the 10 MHz sweep FMCW input to the USRP

FMCW, Power Spectrum
Sampling Rate 25MSps, LO Freq 5805 MHz, Start RF 5800MHz
FM Sweeps of 0MHz / 0.5MHz / 2MHz / 5MHz / 10MHz

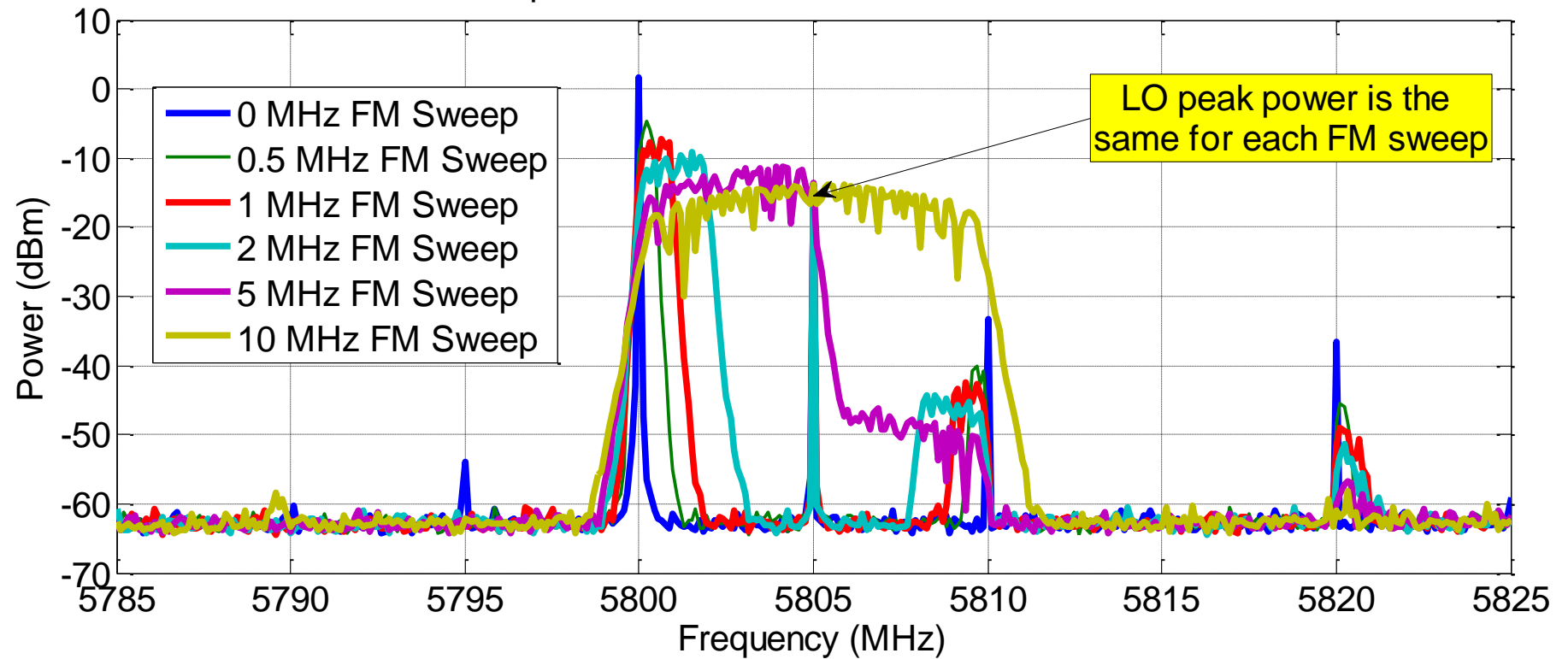


Figure 77: Measured power spectrum of the FMCW output from the USRP, for a range of Triangular FM sweeps at 20 MSps

FMCW, Power Spectrum
Sampling Rate 50MSps, LO Freq 5805 MHz, Start RF 5792.5MHz
20us Triangular FM Sweeps of 12.5MHz / 25MHz

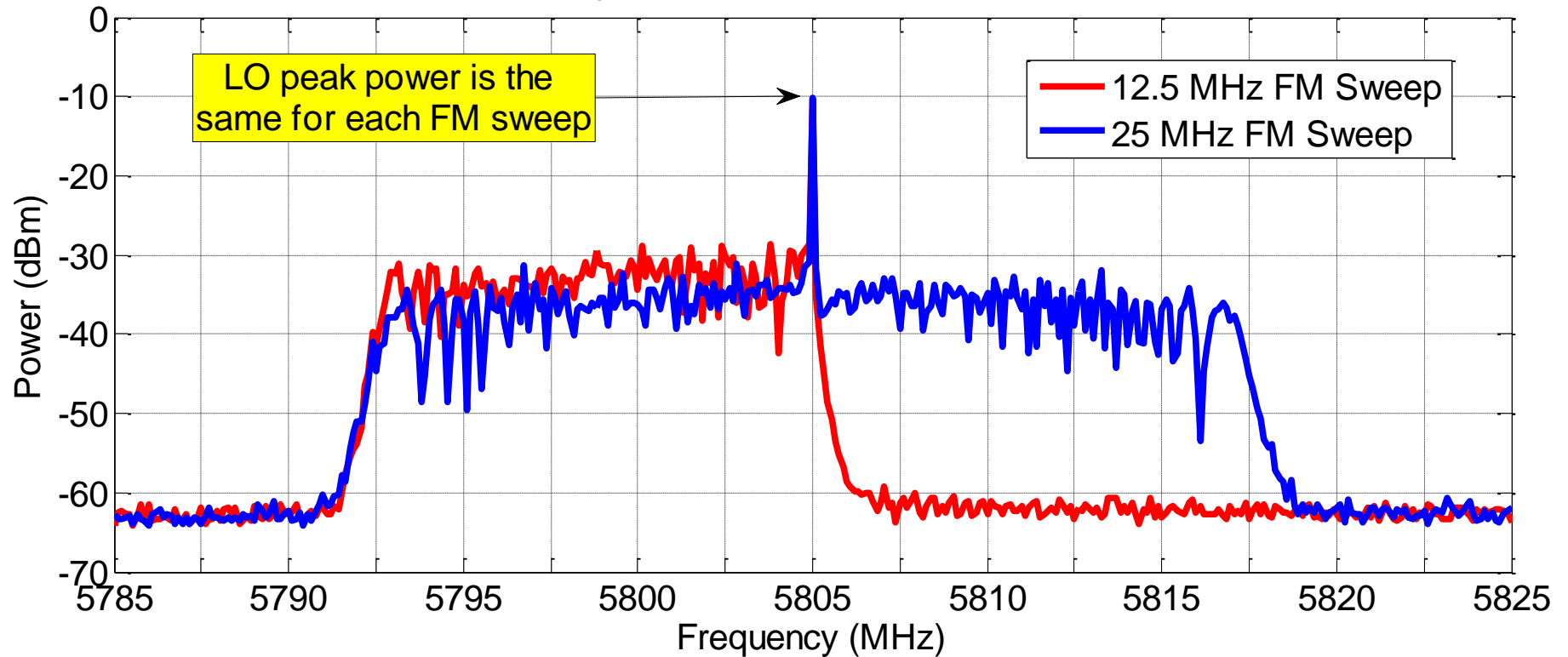


Figure 78: Measured power spectrum of the FMCW output from the USRP, for a range of Triangular FM sweeps at 50 MSps.²⁹

²⁹ Due to an input error, the LO signal was placed at 5805 MHz for this test instead of 5812.5 MHz. Thus the test is centred at a different frequency. Other parameters were correct. This change will not have any impact on the results.

4.3 Experimentation Summary

The characterisation testing and waveform verification tests were conducted successfully with test results consistent when compared across tests.

Test Outcomes

The characterisation tests investigated and verified limitations of the USRP performance, and identified others that were unknown at the time or did not match expected values.

The waveform verification test results showed that the SDR transmitter produced pulsed waveforms with accurate timing and performed frequency modulation accurately over various sweep ranges achievable by the USRP device.

Observations on Host Computer Processor Performance

As stated earlier the host computer performance (see Section 2.2.5) met the minimum requirements recommended (see Section 1.4.3). Nonetheless, the host computer's processing power was not sufficient to generate / transmit signals and also display the signals simultaneously on the GNU Radio GUI visualisers. In doing so, the packet under-run flags began to appear in the GNU Radio output and the system occasionally stalled or stopped if attempting to transmit pulsed waveforms or frequency modulated waveforms.

Turning off the GUI visualisers removed this problem. The system still accumulated packet under-run flags over a long period of time; however this quantity was infrequent enough to be considered negligible and did not impact testing.

This highlights the processor intensive requirements of running a GNU Radio and USRP based SDR (transmitter only) even as a using a host computer with comparatively high processing performance.

Summary of Findings

A summary of the main findings is provided in the followings tables: Table 24, Table 25, Table 26 and Table 27. However, the full extent of the findings including detailed values are captured in the figures, tables and discussions presented in each test section of this thesis.

Table 24 Summary of characterisation test findings (Part A)

Characterisation Test Findings (Part A)	
Sample Rate Testing	<p>Restrictions exist on the sample rates achievable.</p> <p>Unachievable sample rate requests are corrected to the nearest achievable sample rate.</p> <p>If sample rates > 25 MSps are selected using 16-bit complex samples, the device will experience packet underruns and / or cease operation.</p>
Modulation Bandwidth Limit Testing	<p>The MBW is equal to half the sample rate as expected, and thus the BB frequency is limited to a maximum frequency deviation of 25 MHz using 8-bit samples, or 12.5 MHz using 16-bit samples.</p> <p>Limits of 12.5 and 6.25MHz will need to be observed for these sample sizes to maintain a minimum of 4 samples per period.</p> <p>Signals modulated beyond these limits undergo aliasing as expected.</p>
Frequency Limit Testing	<p>The LO frequency ranges for this device are 2.4 to 2.5 GHz and 4.9 to 6 GHz.</p> <p>RF frequencies beyond these ranges are achievable through modulation.</p>
Effects of the Amplitude Variable	<p>The amplitude variable directly influences the voltage of the system, thus halving the amplitude changes the output power by about -6dB.</p> <p>Signals with a combined amplitude value of greater than 1 cause the DAC to saturate, generating significant noise across the transmit spectrum.</p> <p>Amplitude values should be kept at around 0.25 to ensure the amplifier response is in the linear region.</p> <p>Intermodulation products are significantly more suppressed in the high band than the low band. Testing showed up 30dB additional suppression at an amplitude value of 0.5</p>
Effects of the Gain Request Variable	<p>The maximum output power of the USRP is 20 dBm.</p> <p>The system appears to demonstrate some signs of a non-linear response at gain request values above 23 dB in the high band.</p>

Table 25 Summary of characterisation test findings (Part B)

Characterisation Test Findings (Part B)	
Power versus Gain and Amplitude Variables	<p>The full range of the measured output gain was +28 dB for the low band and +35 dB for the high band.</p> <p>The system appears to demonstrate a non-linear response at gain request values above 23 dB in the high band. Thus a 20dB limit is recommended.</p>
Power versus LO Frequency	<p>Output power increased in a near linear manner by about 4dB as the LO shifted from 2400 to 2500 MHz.</p> <p>Output power increased by around 10dB as the LO shifted from the edges at frequencies of 4900 MHz and 6000 MHz towards the region between 5400 MHz and 5600 MHz.</p>
Effects of the Baseband Filter	<p>The baseband filters cause the signals to cut off sharply close to the filter limits (24MHz, 36MHz and 48 MHz), by amounts much larger than 3dB.</p> <p>Unexpected spurs were visible at offsets from the LO at multiples of the sampling rate frequencies, when transmitting Gaussian noise.</p>
Third Order Output Intercept Point	<p>The OIP3 at the centre of the low band was 8 to 10 dBm. The OIP3 at the centre of the high band was around 17 dBm.</p> <p>Minimum OIP3 values were around 5dBm in each band.</p> <p>OIP3 values were higher at frequencies corresponding to higher power values, as shown in the Power vs. RF Frequency Tests.</p>
Local Oscillator Suppression	<p>LO suppression was approximately 21dBm as measured at the centre of each band for a single tone signal. This reduced to values of up to -20dB for FM signals as shown in later testing.</p>
Phase Noise Measurements	<p>Low band phase noise was relatively stable at around -90dBc/Hz measured at 2450MHz, but measurements at 10kHz offsets increased by around 12dB when the RF was set to 2475 MHz.</p> <p>High band phase noise varied by around 5 to 10 dB for 10 and 100kHz offsets but were minimised when the RF was at 5100 or 5600 MHz. High band phase noise was worse at offsets close to the RF signal, with spikes of up to 15dB occurring.</p> <p>Phase noise was largely insensitive to the selection of gain and amplitude values, unless an amplitude value of 1 or greater was selected at which point saturation effects appeared to occur.</p> <p>RMS jitter and other residual noise measures were notably affected by the selected amplitude, but minimised for an amplitude value of 0.5.</p> <p>RMS jitter varied throughout testing depending upon the RF frequency but remained beneath 1.4 ps when using an amplitude value of 0.25 which has been recommended throughout this thesis.</p>

Table 26 Summary of waveform verification test findings

Waveform Verification Test Findings	
CW Testing	<p>Continuous Waveform values closely matched the target signal, with the target frequency of 5800 MHz achieved as measured by the spectrum analyser.</p> <p>Results from the oscilloscope showed a mean deviation of 2.77MHz, but this is attributed to oscilloscope causes changes in the shape of the reconstructed signal.</p>
Pulsed Waveform Testing	<p>Pulsed waveform, accurate but some fluctuation by up to 0.15 μs was observed. This was attributed to power changes during the pulse ramping high and low.</p>
FMCW Testing	<p>The power spectrum of modulated signals appeared as expected.</p> <p>Frequency modulation was accurate and occurred over the desired frequency range.</p> <p>Unexpected spectral lines appeared in the model of the FFT based on sample data, but identified as being caused by the FFT algorithm used.</p> <p>The LO signal is likely to cause interference at high FM sweeps (e.g. at 25MHz or above).</p>

Table 27 Summary of general test findings

General Test Findings	
Host Computer Processor Speed	<p>The literature review identified that the host computer should meet the following processor specification at a minimum:</p> <ul style="list-style-type: none"> • Intel Core 2 Duo, @ 3 GHz <p>The host computer used in this SDR transmitter had the following processor specifications:</p> <ul style="list-style-type: none"> • Intel Core 2 Quad, @ 3GHz <p>The CPU was unable to maintain the desired sample rate with the GNU Radio visualisers active. Turning the visualisers off allowed the SDR transmitter to operate effectively.</p>

5. Conclusions

GNU Radio and the USRP can be effectively combined to create a software-defined radar transmitter, as measured by the accuracy with which the output waveforms matched the set of target waveforms defined.

This thesis has detailed the system design of a SDR transmitter that has been developed using these tools and used in experimentation to support this thesis.

Characterisation tests investigated and verified limitations of the USRP performance, and identified others that were unknown at the time or did not match expected values. The majority of test results are explainable in the context of the hardware device's subcomponents and datasheets. The USRP exhibited notable variations in transmit power and phase noise across the flexible operating domain achievable. Additionally, the SDR generated low noise spurs during low band testing that were between 5 to 18dB above the noise floor at full scale. IM products were well suppressed in the high band compared to the low band, by up to 30dB in some cases. The low band spurs and IM products may be unacceptable for some radar transmission applications, and would require filtering.

The cause of some noise spurs observed in testing are not yet identified. The characterisation test results highlight behavioural aspects of fundamental importance to radar designers considering using these tools to produce a radar transmitter.

Waveform verification test results produced 1 μ s pulsed waveforms with accurate timing and performed frequency modulation accurately over sweep ranges from 0.5 to 25MHz. The transmitted waveforms were not without imperfections. Poor LO suppression meant that for FM sweeps above 10MHz the power of the RF signal was below that of the LO signal.

Furthermore, it is recommended that future work with these tools incorporate a host computer with higher processing power than the one used in this study. This will further ensure the sample rate required by the USRP is maintained, preventing packet under-runs that will degrade the integrity of the transmitted signal.

6. Appendix

6.1 Appendix A - Matlab FFT Function from GNU Radio

```
%
% Copyright 2001 Free Software Foundation, Inc.
%
% This file is part of GNU Radio
%
% GNU Radio is free software; you can redistribute it and/or modify
% it under the terms of the GNU General Public License as published by
% the Free Software Foundation; either version 3, or (at your option)
% any later version.
%
% GNU Radio is distributed in the hope that it will be useful,
% but WITHOUT ANY WARRANTY; without even the implied warranty of
% MERCHANTABILITY or FITNESS FOR A PARTICULAR PURPOSE. See the
% GNU General Public License for more details.
%
% You should have received a copy of the GNU General Public License
% along with GNU Radio; see the file COPYING. If not, write to
% the Free Software Foundation, Inc., 51 Franklin Street,
% Boston, MA 02110-1301, USA.
%
function [f_graph] = plotfft (data, sample_rate)

    if (nargin == 1)
        sample_rate = 1.0;
    end;

    %if ((m == nargchk (1,2,nargin)))
    % usage (m);
    %end;

    len = length(data);
    s = fft (data.*kaiser(len, 5),len);
    fft_data = abs(fftshift(s))/len; %added /len

    incr = sample_rate/len;
    min_x = -sample_rate/2;
    max_x = sample_rate/2 - incr;

    f_graph = plot([min_x:incr:max_x]/10^6, fft_data);
    xlabel('Frequency (MHz)'); %Added Code
    ylabel('Amplitude'); %Added Code
    hleg1 = legend([num2str(len), ' Sample FFT']); %Added Code
    set(hleg1,'Location','NorthWest') %Added Code
    grid; %Added Code

end %function
```

6.2 Appendix B - Tabulated Phase Noise Measurements

Table 28 Single tone waveform response to various amplitude values with gain values of 0 and 10dB (high band)

RF Freq (MHz)	Gain (dB)	Amplitude (Scalar)	Normalised Amplitude (dB)	Signal Level (dBm)	Signal Freq Delta (Hz)	Signal Level Delta (dBm)	Residual PM (deg)	Residual FM (kHz)	RMS Jitter (ps)	Spot Noise			
										1 kHz (dBc/Hz)	10 kHz (dBc/Hz)	100 kHz (dBc/Hz)	1 MHz (dBc/Hz)
5400	0	1.1	0.41	-4.41	0.36	-0.65	18.28	321.95	9.40	-86.46	-63.19	-82.59	-88.98
5400	0	1	0.00	-4.69	-1.57	-2.56	17.58	23.38	9.04	-85.86	-62.49	-83.86	-105.23
5400	0	0.707	-1.51	-7.17	-1.20	0.04	3.31	19.89	1.70	-85.42	-83.51	-84.11	-109.00
5400	0	0.5	-3.01	-10.17	-1.09	0.04	2.17	20.41	1.12	-86.35	-82.33	-85.60	-110.30
5400	0	0.35355	-4.52	-13.20	-4.36	-0.11	3.17	23.43	1.63	-85.53	-81.95	-86.05	-110.34
5400	0	0.25	-6.02	-16.57	2.05	0.11	2.49	31.78	1.26	-84.98	-78.19	-85.90	-107.84
5400	0	0.125	-9.03	-22.32	0.72	-0.02	2.74	49.13	1.41	-84.91	-83.61	-85.10	-108.88
5400	0	0.0625	-12.04	-28.35	-2.26	0.01	3.11	88.87	1.60	-85.60	-82.77	-84.18	-106.14
5400	10	1.1	0.41	5.53	0.66	-1.37	18.55	399.44	9.52	-87.16	-63.26	-84.26	-86.58
5400	10	1	0.00	3.07	-3.40	1.34	22.80	28.57	11.73	-85.73	-60.20	-81.69	-105.55
5400	10	0.5	-3.01	-0.33	1.61	-0.02	2.25	20.01	1.16	-84.94	-82.26	-85.73	-111.21
5400	10	0.25	-6.02	-6.48	1.97	-0.02	2.35	22.65	1.21	-86.06	-83.76	-86.11	-111.65
5400	10	0.125	-9.03	-12.53	1.04	-0.18	2.65	31.47	1.36	-85.73	-84.45	-84.87	-110.46
5400	10	0.0625	-12.04	-18.70	-3.41	-0.03	3.08	58.57	1.59	-84.88	-83.44	-83.95	-108.60

Table 29 Single tone waveform response to various amplitude values with gain values of 20 and 35dB (high band)

RF Freq	Gain	Amplitude	Normalised Amplitude	Signal Level	Signal Freq Delta	Signal Level Delta	Residual PM	Residual FM	RMS Jitter	Spot Noise			
										1 kHz	10 kHz	100 kHz	1 MHz
(MHz)	(dB)	(Scalar)	(dB)	(dBm)	(Hz)	(dBm)	(deg)	(kHz)	(ps)	(dBc/Hz)	(MHz)	(dB)	(Scalar)
5400	20	1.1	0.41	14.41	5.37	0.08	17.31	362.60	8.91	-86.39	-63.97	-82.75	-87.61
5400	20	1	0.00	12.15	0.44	2.62	20.39	98.05	10.49	-85.85	-61.22	-79.35	-105.77
5400	20	0.5	-3.01	10.64	3.43	0.11	2.20	21.27	1.13	-84.81	-82.41	-85.70	-108.61
5400	20	0.25	-6.02	4.52	-1.13	-0.01	2.35	29.57	1.21	-85.64	-84.19	-85.24	-110.01
5400	20	0.125	-9.03	-1.71	0.56	0.01	2.72	41.01	1.40	-85.61	-84.34	-85.13	-110.38
5400	20	0.0625	-12.04	-7.81	-1.37	0.00	3.03	50.42	1.56	-86.53	-83.30	-84.66	-109.23
5400	35	1.1	0.41	15.51	0.22	-0.32	14.82	327.02	7.63	-87.07	-65.30	-82.05	-86.77
5400	35	1	0.00	15.51	0.28	0.19	12.57	95.78	6.47	-85.26	-65.01	-82.56	-108.44
5400	35	0.5	-3.01	15.84	1.24	-0.03	2.94	196.73	1.51	-86.40	-82.14	-85.09	-110.20
5400	35	0.25	-6.02	15.41	-0.08	0.09	4.12	357.48	2.12	-85.00	-83.36	-87.25	-109.61
5400	35	0.125	-9.03	13.65	1.77	0.00	4.53	391.07	2.33	-86.05	-84.03	-83.77	-109.97
5400	35	0.0625	-12.04	8.27	2.07	0.01	3.13	76.74	1.61	-85.51	-83.20	-83.56	-109.49

Table 30 Single tone response to stepped changes in the RF signal frequency across the low and high bands

RF Freq	Gain	Amplitude	Normalised Amplitude	Signal Level	Signal Freq Delta	Signal Level Delta	Residual PM	Residual FM	RMS Jitter	Spot Noise			
										1 kHz	10 kHz	100 kHz	1 MHz
(MHz)	(dB)	(Scalar)	(dB)	(dBm)	(Hz)	(dBm)	(deg)	(kHz)	(ps)	(dBc/Hz)	(MHz)	(dB)	(Scalar)
2406.25	0	0.25	-6.02	-14.14	0.00	-0.09	1.00	25.81	1.15	-90.69	-93.89	-92.96	-110.36
2425	0	0.25	-6.02	-13.12	-1.40	-0.09	0.85	24.13	0.98	-93.12	-94.90	-95.04	-111.86
2450	0	0.25	-6.02	-12.34	0.10	-0.12	0.85	23.93	0.96	-91.72	-93.69	-95.12	-112.30
2475	0	0.25	-6.02	-11.57	2.51	-0.12	1.18	22.20	1.32	-92.67	-85.99	-92.61	-115.43
2500	0	0.25	-6.02	-10.42	0.74	-0.03	0.78	19.62	0.86	-93.03	-95.25	-96.28	-116.32
5000	0	0.25	-6.02	-23.02	3.09	-0.01	2.17	40.27	1.20	-86.46	-79.13	-87.21	-107.60
5100	0	0.25	-6.02	-20.68	-1.26	-0.04	1.68	37.41	0.92	-86.50	-89.66	-92.71	-107.38
5200	0	0.25	-6.02	-18.94	-1.62	-0.10	2.30	31.13	1.23	-85.65	-77.89	-85.45	-108.99
5300	0	0.25	-6.02	-17.62	0.76	-0.06	2.22	29.83	1.16	-85.49	-84.78	-86.52	-109.11
5400	0	0.25	-6.02	-16.19	3.84	-0.16	2.41	28.12	1.24	-84.52	-84.83	-86.73	-110.76
5500	0	0.25	-6.02	-16.57	2.05	0.11	2.49	31.78	1.26	-84.98	-78.19	-85.90	-107.84
5600	0	0.25	-6.02	-17.59	0.66	0.06	1.47	29.90	0.73	-85.00	-87.02	-91.45	-110.30
5700	0	0.25	-6.02	-17.50	4.88	-0.18	2.55	29.74	1.24	-85.11	-77.52	-85.51	-107.59
5800	0	0.25	-6.02	-19.28	0.57	0.01	2.43	28.85	1.16	-84.20	-84.17	-85.29	-108.68
5900	0	0.25	-6.02	-21.39	2.70	0.01	2.57	30.45	1.21	-84.12	-82.52	-85.14	-109.65
6000	0	0.25	-6.02	-24.57	-1.94	0.22	2.56	34.03	1.18	-84.51	-77.43	-84.58	-110.08

7. References

1. *Application Note: Selecting a USRP Device*. [cited March, 2012]; Available from: http://www.ettus.com/content/files/kb/application_note_selecting_a_usrp.pdf.
2. Patton, L.K., *A GNU Radio Based Software-Defined Radar*, in *Department of Electrical Engineering 2007*, Wright State University: USA.
3. Fernandes, V.N., *Implementation of a Radar System using Matlab and the USRP*, in *Electrical Engineering 2012*, California State University, Northridge: USA.
4. Williams, L., *Low Cost Radar and Sonar using Open Source Hardware and Software*, 2008, University of Cape Town: South Africa.
5. Volkwin, A., *Suitability of a Commercial Software Defined Radio System for Passive Coherent Location*, in *Department of Electrical Engineering*, 2008, University of Cape Town: South Africa.
6. Szlachetko, B.L., A. and J. Zarzycki, *Application of the Software Defined Radio in a Passive Radar*, in *Military Communications and Information Systems Conference*, 2009, Wroclaw University of Technology, Poland: Czech Republic.
7. Prabaswara, A., A. Munir, and A.B. Suksmono, *GNU Radio Based Software-Defined FMCW Radar for Weather Surveillance Application*, in *The 6th International Conference on Telecommunication Systems, Services and Applications*, 2011, IEEE.
8. Debatty, *Software Defined RADAR a State of the Art*, in *2nd International Workshop on Cognitive Information Processing*, IEEE, June 2010, Royal Military Academy of Brussels: Italy.
9. *Definitions of Software Defined Radio and Cognitive Radio System*, 2009, p.3: International Telecommunications Union.
10. *What are the advantages of Software Defined Radio?*, July 2002: Software Defined Radio Working Group of the ARRL. p. 1.
11. Smith, S., *The Scientist and Engineer's Guide to Digital Signal Processing*. 1997: California Technical Publishing.
12. *Welcome to GNU Radio*. [cited March, 2012]; Available from: <http://gnuradio.org/redmine/projects/gnuradio/wiki>.
13. *Ettus Research Website*. [cited March, 2012]; Available from: <https://www.ettus.com/>.
14. Corgan, J., *GNU Radio in Action (Conference Overview)*, September 2011, Corgan Enterprises: GNU Radio Conference 2011.
15. Capria, A.C., M. Petri, D. Martorella, M. Berizzi, F. Mese, E. D. Soleti, R. Carulli, V., *Ship Detection with DVB-T Software Defined Passive Radar*, 2010, RaSS Centre CNIT, University of Pisa, Italian Navy CSSN ITE.
16. Godana, B., *Human Movement Characterization in Indoor Environment using GNU Radio based Radar*, 2009, Delft University of Technology: Netherlands.
17. Lambert, J.C., *A Radar Interrogator for Wireless Passive Temperature Sensing*, 2008, University of Central Florida: USA.
18. *USRP Technical Documentation*. [cited April, 2012]; Available from: <http://code.ettus.com/redmine/ettus/projects/public/documents>.
19. *XCVR2450 Subcomponent Specification Sheets Archive*. [cited June, 2012]; Available from: <http://code.google.com/p/microembedded/downloads/list?q=label:XCVR2450>.
20. Hamza, F.A. *The USRP under the 1.5X Magnifying Lens!* June 2008.

21. Balister, P.R., J., *USRP Hardware and Software Description*, June 2006, Virginia Polytechnical Institute & State University.
22. Shen, D., *Tutorial 1: GNU Radio Installation Guide Step by Step (10 Tutorials)*, May, 2005.
23. (Forum: GNU Radio) *Understanding USRP2 Flow Control*. July 2010 [cited May, 2012]; Available from: <http://www.ruby-forum.com/topic/213352>.
24. Prasetiadi, A., *A Simple Delay Compensation System in Software-Defined Frequency Modulated Continuous (FMCW) Radar*, in *European Wireless 2012* 2012, VDE VERLAG MBH: Poland.
25. Standert, R., *Software Model of a Radar Receiver*, 2002, Royal Institute of Technology, Stockholm: Sweden.
26. *Frequency Modulated Continuous Wave Radar*. [cited July, 2012]; Available from: <http://demonstrations.wolfram.com/FrequencyModulatedContinuousWaveFMCWRadar/>.
27. Frasier, S.J., T. Ince, and F.J. Lopez-Dekker, *Performance of S-Band FMCW Radar for Boundary Layer Observation*, in *15th Conference on Boundary Layer and Turbulence* 2002.
28. Stimson, *Introduction to Airborne Radar*. 2nd ed. 1998: SciTech Publishing Inc.
29. *Application Note: Selecting a RF Daughterboard*. [cited March, 2012]; Available from: http://www.ettus.com/content/files/kb/Selecting_an_RF_Daughterboard.pdf.
30. *NI USRP-2921 Block Diagram*, August 2011, National Instruments. Available from: http://zone.ni.com/reference/en-XX/help/373380A-01/usrphelp/2921_block_diagram
31. *NI USRP-2920, NI USRP-2921 Universal Software Peripheral Datasheet*. [June 2012]; Available from: <http://sine.ni.com/ds/app/doc/p/id/ds-355/lang/en>.
32. *USRP N210 Schematics*. [cited October, 2012]; Available from: <http://code.ettus.com/redmine/ettus/attachments/download/214/n210.pdf>.
33. *RF Daughterboard Notes*. [cited October, 2012]; Available from: http://files.ettus.com/uhd_docs/manual/html/dboards.html.
34. *MAX2829 Datasheet*. [cited November, 2012]; Available from: <http://datasheets.maximintegrated.com/en/ds/MAX2828-MAX2829.pdf>.
35. *Application Note: UHD Examples*. [cited March, 2012]; Available from: www.ettus.com/content/files/kb/application_note_uhd_examples.pdf.
36. *Australian Radiofrequency Spectrum Plan*, A.C.a.M. Authority, Editor January, 2009, Australian Government.
37. *Third Order Intercept Measurements*, 2001, Agilent Technologies.
38. *XCVR2450 Schematics*. [cited November, 2012]; Available from: http://code.ettus.com/redmine/ettus/attachments/download/210/xcvr2450_rev1.1.pdf.
39. Sharp Corporation, *IRM046U Target Specification Datasheet*. March 2009. <http://ses.sharpmicro.com/download/IRM046U-030918pdf>
40. Aniritsu Corporation, *Intermodulation Distortion (IMD) Measurements*. 2000; Available from: www.aniritsu.com
41. Kundert, K., *Accurate and Rapid Measurement of IP2 and IP3*. Designers Guide Community, May 2002.
42. *Spectrum Analyzer Measurements*. [cited October, 2012]; Available from: <http://www.microwaves101.com/encyclopedia/spectrumalyzer.cfm>.